QUASI-LOSSLESS DATA TRANSMISSION WITH ULTRA-LONG RAMAN FIBRE LASER BASED AMPLIFICATION

PAWEŁ ROSA

Doctor of Philosophy

ASTON UNIVERSITY

October 2013

Aston University

Quasi-Lossless Data Transmission with Ultra-Long Raman Fibre Laser Based Amplification

Paweł Rosa

Doctor of Philosophy

2013

The project consists of an experimental and numerical modelling study of the applications of ultra-long Raman fibre laser (URFL) based amplification techniques for high-speed multi-wavelength optical communications systems. The research is focused in telecommunications C-band 40 Gb/s transmission data rates with direct and coherent detection. The optical transmission performance of URFL based systems in terms of optical noise, gain bandwidth and gain flatness for different system configurations is evaluated. Systems with different overall span lengths, transmission fibre types and data modulation formats are investigated. Performance is compared with conventional Erbium doped fibre amplifier based system to evaluate system configurations where URFL based amplification provide performance or commercial advantages.

In loving memory of my partner

Anna Mitioucheva

1986 - 2011

"nothing is more real than nothing"

Samuel Beckett

Acknowledgements

I would like to thank my supervisor Dr Paul Harper for constant supervision and support and Dr Juan Diego Ania-Castañón who offered his help during my stay in Madrid while studying numerical modelling. Other thanks and credits need to be extended to Oclaro Inc. and EPSRC for providing me the financial opportunity to study the topic of my PhD and all staff of Aston University who had positive impact on my work.

Contents

List of Figures

List of Tables

Glossary

ADC Analog to Digital Converter

ASE Amplified Spontaneous Emission

ASK Amplitude Shift Keying

AWG Arrayed Waveguide Grating

AWGN Additive White Gaussian Noise

BER Bit-Error Rate

C-NRZ Chirped Non Return to Zero

CD Chromatic Dispersion

CMA Constant Modulus Algorithm

CO-OFDM Coherent Orthogonal Frequency Division Multiplexing

CR Clock Recovery

CRZ Chirped Return-to-Zero

CSRZ Carrier Suppressed Return to Zero

CW-DFB Continuous-Wave Distributed Feedback

DAC Digital to Analog Convertors

DCM Dispersion Compensation Modules

DLI Delay Line Interferometer

DML Directly Modulated Laser

DPSK Differential Phase Shift Keying

DQPSK Differential Quadrature Phase Shift Keying

DRA Distributed Raman Amplification

DRB Double Rayleigh Backscattering

DSP Digital Signal Processing

DWDM Dense Wavelength-Division Multiplexing

EAM Electro-Absorption Modulation

ECL External Cavity Laser

EDFA Erbium Doped Fibre Amplifier

FBG Fibre Bragg Grating

FEC Forward Error Correction

FWM Four-Wave Mixing

GVD Group Velocity Dispersion

IF Intermediate Frequency

ISI Inter Symbol Interference

ITU International Telecommunication Union

LD Laser Diode

LEAF Large Effective Area Fibre

LO Local Oscillator

M-ASK Multilevel Amplitude Shift Keying

MMF Multi Mode Fibre

MPI Multiple-Path Interference

MZM Mach-Zehnder Modulator

N-WDM Nyquist Wavelength Division Multiplexing

NF Noise Figure

NRZ Non-Return-to-Zero

NZ-DSF Non-Zero Dispersion Shifted Fibres

ODE Ordinary Differential Equations

ODE Ordinary Differential Equations

OOG Optical Comb Generator

OOK On-Off Keying

OSA Optical Spectrum Analyser

OSNR Optical Signal-To-Noise Ratio

OTDR Optical Time-Domain Reflectometer

PBS Polarisation Beam Splitter

PDM Polarisation-Division Multiplexed

PMD Polarisation-mode Dispersion

PRBS Pseudorandom Bit Sequences

PSK Phase Shift Keying

ROPA Remote Optical Pre-Amplifier

RRC Root Raised Cosine

RZ Return-to-Zero

SBS Stimulated Brillouin Scattering

SE Spectral Efficiency

SMF Single Mode Fibre

SNR Signal to Noise Ratio

SOA Semiconductor Amplifiers

SPM Self-Phase Modulation

SRS Stimulated Raman Scattering

TDCM Tuneable Dispersion Compensation Module

TOD Third-Order Dispersion

URFL Ultra-long Raman Fibre Laser

VOA Variable Optical Attenuator

WDM Wavelength-Division Multiplexing

XPM Cross-Phase Modulation

Chapter 1

Introduction

Information is a sequence of symbols that can be decoded and interpreted as a message which will change the current understanding of phenomena or lessen the uncertainty. The theory of information was developed in 20th century by Claude E Shannon. It defined the fundamental limits on signal processing operations and the maximum rate at which information can be transmitted in classical linear channel with an additive white Gaussian noise (AWGN) (1, 2). The information capacity in optical fibre channels is limited by fibre nonlinearity rather than Shannon's limit which was adequate for electromagnetic propagation over wires and cables (3). Recent studies have shown that nonlinear filters may increase transmission throughput beyond seminal Shannon limit for AWGN channel (4). It demonstrates new range of possibilities and potential of fibre optic communication. Careful design of nonlinear channel can satisfy the demand of exponentially growing data traffic as well as change the perception of nonlinearity itself.

In telecommunication information is transmitted by modulating data onto electromagnetic wave which act as a carrier. Number of complex techniques has been developed and implemented in radio frequencies, microwave as well as very high and ultra high frequencies. The amount of information which can be transmitted is directly related to the bandwidth. In theory the higher the carrier frequency the greater the bandwidth as the frequency extent is larger. However, in practice there are device and medium related limitations. In optical communication one of the leading factors which limits the transmission bandwidth is

wavelength dependent fibre loss and what follows need of an optical amplification. Although current technology allows the production of low attenuation fibres, amplification and regeneration of an optical signal in all available bandwidth of frequencies is still an issue.

In long-haul and unrepeatered links, distributed Raman amplification offers good noise performance and can be used to optimise the signal power evolution within the transmission span. In particular, higher-order pumping can reduce variations of the effective gain-loss coefficient along the span. A novel amplification scheme that uses fibre Bragg grating (FBG) to form an ultra-long Raman fibre laser (URFL) (5) along the transmission fibre allows to achieve 2^{nd} order pumping of the signal with a single pump wavelength only. Contrary to conventional 2^{nd} order Raman amplification, in URFL the gain profile can be modified by selecting appropriate FBGs (6). This can be used to realise a quasi-lossless span, approximating the optimal case for transmission performance (7).

Poor pump efficiency and nonavailability of high-power pump lasers essential for Raman amplification in late 1980s led to commercialisation of erbium doped fibre amplifiers (EDFA) and as a result most of the current optical transmission networks are based on EDFAs (8). Low noise figure, extended bandwidth and possibility of providing amplification practically at any wavelength resurged interest in distributed Raman amplifiers which are becoming more common in telecommunication systems (9).

1.1 Thesis Organisation

This thesis consists of 6 chapters. Second and third chapters provides theoretical introduction to fibre optic communication systems whereas the following chapters are experimentally oriented where brief theoretical introduction and references to the transmission methods used are given. Last chapter concludes the work presented in the thesis.

In chapter 2 the linear and nonlinear physical phenomena present in optical fibres are explained.

Chapter 3 is dedicated to optical amplification of light in fibres. Two most common optical amplification techniques are explained. EDFA is briefly intro-

duced, however, number of references are provided for detailed explanation on simulation and design proposals. Raman amplifier is described in detail. All equations and related references to simulation as well as experimental verification of novel amplification method is provided.

Chapter 4 experimentally and numerically characterise the ultra long Raman fibre laser based technique for long haul unrepeatered transmissions. The type of fibre and relevant components used in Raman amplification are tested with different span lengths and pump configuration. Optimisation method for the best performance in terms of on-off gain and optical signal to noise ratio is described. Last section compares the benefits of second order Raman amplification with lumped EDFA.

The procedure of characterisation and control of all components was automated with a software written in LabView. The software written in C and MatLab analysed the results.

Chapter 5 is dedicated to transmission experiments using amplitude and phase shift keying modulation with direct and coherent detection scheme. Amplitude and binary differential phase shift keying modulation is investigated in long unrepeatered transmission using direct detection only. In advanced coherent detection only quadrature phase shift keying modulation format is presented. Nyquist wave division multiplexing is also investigated and compared with EDFA and Raman amplification.

The bibliography is organised with full list of authors, title of the publication in bold font, the name of the journal in italic followed by volume, number in brackets, page numbers in the journal (if given), year of publication and finally the number of the page in thesis where the reference was used.

Chapter 2

Background

2.1 Optical Fibres

The medium used in optical communication is silica fibre. The first low loss optical fibre was developed in 1970s by the scientists Robert Maurer, Peter Schultz, and Donald Keck (10). They were first researches who explored possibilities of high-purity fused silica with attenuation low enough to enable data transmission experiments.

Depending on the number of supported transverse propagation modes, optical fibres can be categorised into multimode and single-mode. The limitations imposed on multimode fibres (MMF) due to intermodal dispersion which results in intersymbol interference (ISI) restricts the achievable distance and the data rates in telecommunication systems (11), however, the capacity limitations of a single mode fibres (SMF) and constantly growing internet traffic, directs research towards new technologies which would allow to exploit the potential of the MMF (11, 12).

Optical fibre consists of a core made of pure silica glass doped by germanium dioxide (GeO_2) or phosphorus pentoxide (P_2O_5) to increase refractive index and cladding which is doped with fluorine or boron trioxide (B_2O_3) in order to lower the refractivity (13). Dopants used in the production of fibre may vary depending on the application. The relative difference between core and cladding is described

as

$$\Delta = \frac{n_1 - n_c}{n_1}, \tag{2.1}$$

where n_1 and n_c is the refractive index of core and cladding layer respectively.

Manufacturing of optical fibres for long-haul transmission requires the ability to modify and control parameters such as attenuation, nonlinearities, chromatic dispersion (CD) and polarisation-mode dispersion (PMD). Optimisation of fibre parameters and properties led to development of wide range of fibre types (14, 15, 16). The choice of the fibre type in communication system design is application dependent.

2.1.1 Fibre Losses

An important parameter in optical system design is fibre loss which ultimately limits the distance of unrepeatered and long-haul transmission by attenuating the signal to level where it cannot be distinguished from the noise nor recovered.

In standard single mode silica fibre, the total transmitted power P_T over distance L is approximated by (17)

$$P_T = P_0 exp(-\alpha L), \tag{2.2}$$

where P_0 is the launch power and α is the attenuation constant of the fibre. The most significant loss mechanism which put fundamental limits on fibre attenuation is Rayleigh scattering which can be estimated by (13)

$$\alpha_R = C_R/\lambda^4, \tag{2.3}$$

with C_R in the range of 0.7 - 0.9 dB/(km-μm^4) depending on the fibre core. Wavelength dependent Rayleigh loss (dashed blue) and measured total loss (red) for SMF-28 fibre is plotted in Fig. 2.1.

Density fluctuations and impurity in form of OH ion with an absorption peak at ≈2.73 μm and also near 1.4 μm is an important limiting factor of the fibre

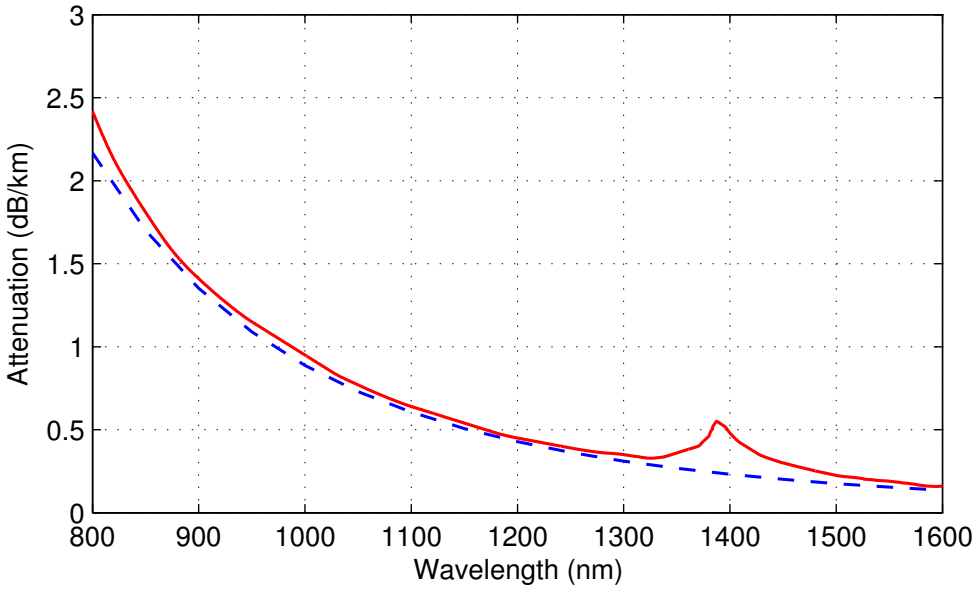

Figure 2.1: Wavelength dependent loss due to Rayleigh scattering (dashed blue) and measured attenuation (red) in silica SMF-28 fibre.

attenuation. This however can be reduced and removed completely during manufacturing process. The absorption peak at 1.4 μm in Fig. 2.1 is relevant to the SMF-28 fibre used in the experiments in the proceeding chapters only.

2.1.2 Chromatic Dispersion

Chromatic dispersion is a phenomenon in which the propagation velocity of an electromagnetic wave depends on the wavelength. Dispersion occurs because the various components of the radiation at different frequencies propagate at different speeds given by $c/n(\omega)$, where c is the speed of light and $n(\omega)$ is the refractive index at the frequency ω. By expanding mode propagation constant β in a Taylor series (13):

$$\beta(\omega) = n(\omega)\frac{\omega}{c} = \beta_0 + \beta_1(\omega - \omega_0) + \frac{1}{2}\beta_2(\omega - \omega_0)^2 + \cdots, \tag{2.4}$$

where

$$\beta_m = \left(\frac{d^m\beta}{d\omega^m}\right)_{\omega=\omega_0} \qquad (m = 0, 1, 2, \dots) \tag{2.5}$$

we can derive useful parameters. The group velocity is related to parameter β_1 and its derivative is

$$\beta_1 = \frac{1}{v_g} = \frac{n_g}{c} = \frac{1}{c}\left(n + \omega\frac{dn}{d\omega}\right), \tag{2.6}$$

where n_g is the group index and v_g is the group velocity. The group velocity mismatch of the closely spaced pulses propagating in the optical fibre may lead to *walk-off* effect where two pulses interact with each other. It is related to β_1 by the *walk-off parameter* d_{12} defined as (13)

$$d_{12} = \beta_1(\lambda_1) - \beta_1(\lambda_2) = v_g^{-1}(\lambda_1) - v_g^{-1}(\lambda_2), \tag{2.7}$$

where λ_1 and λ_2 are the wavelengths of the two pulses. The walk-off length L_W of the pulses of width T_0 is described as

$$L_W = T_0/|d_{12}| \tag{2.8}$$

The group velocity dispersion (GVD) parameter β_2 is responsible for pulse broadening. The wavelength dependent dispersion is quantified by the dispersion parameter D (13):

$$D = \frac{d\beta_1}{d\lambda} = -\frac{2\pi c}{\lambda^2}\beta_2 = -\frac{\lambda}{c}\frac{d^2n}{d\lambda^2}. \tag{2.9}$$

The measured dispersion slope for different fibre types is presented in Fig. 4.5 in Chapter 4.2.1.

In normal dispersion regime where fibre exhibits positive GVD ($\beta_2 > 0$) longer wavelengths move faster than the shorter. Opposite situation occurs when GVD is negative ($\beta_2 < 0$). The larger the GVD the grater impact on the pulse propagation it will have therefore it is important to quantify dispersion values for high speed communication links where optical pulses are short. The dispersion length L_D and nonlinear length L_{NL} parameters defined as (18):

$$L_D = \frac{T_0^2}{|\beta_2|} \tag{2.10}$$

$$L_{NL} = \frac{1}{\gamma P_0} \tag{2.11}$$

are great indicators of dispersive and nonlinear effects which become non negligible as fibre length L is close or larger than L_D or L_{NL}. If the condition

$$\frac{L_D}{L_{NL}} = \frac{\gamma P_0 T_0^2}{|\beta_2|} \ll 1, \tag{2.12}$$

is satisfied, the pulse will propagate in the linear dispersive regime. Although different types of fibres with shifted zero-dispersion wavelength have been developed to optimise dispersion in the C-band telecommunication window, direct detection links with data rates higher than 10 Gb/s require dispersion compensation modules (DCM) due to ultrashort optical pulses at high data rates. When the pulse width $T_0 < 1$ ps third-order dispersion (TOD) term β_3 can no longer be ignored and needs to be included as it will have an impact on GVD effect.

In the situation where

$$\frac{L_D}{L_{NL}} = \frac{\gamma P_0 T_0^2}{|\beta_2|} \gg 1, \tag{2.13}$$

nonlinear regime will be a dominating factor on pulse shaping (13).

2.1.3 Polarisation-Mode Dispersion

Polarisation-mode dispersion in optical fibres arises due to birefringence where propagation constant β changes with respect to two polarisation axes in x (fast) and y (slow) directions during propagation. Time delay ΔT between two polarisation components due to random changes in group velocities broadens the optical

pulse (13) and in case if ΔT is large enough so that stretched pulse overlaps with the neighbouring time slot it will cause inter-symbol interference.

$$\Delta T = \left| \frac{L}{v_{gx}} - \frac{L}{v_{gy}} \right| = L|\beta_{1x} - \beta_{1y}| = L(\Delta\beta_1), \tag{2.14}$$

where $\Delta\beta_1$ is related to group velocity mismatch and L is the fibre length. The degree of modal birefringence is quantified by (19)

$$\beta_m = \frac{|\beta_x - \beta_y|}{k_0} = |n_x - n_y|, \tag{2.15}$$

where $k_0 = 2\pi/\lambda$ is the core radius. The length of the full rotation of polarisation state is called beat length L_B and can be expressed as (19)

$$L_B = \frac{2\pi}{|\beta_x - \beta_y|} = \frac{\lambda}{Bm} \tag{2.16}$$

Refractive index asymmetry and birefringence varies along the span length therefore PMD should be estimated by averaged time delay:

$$\sigma_T^2 = \langle (\Delta T)^2 \rangle = 2(\Delta\beta_1 l_c)^2 [exp(-L/l_c) + L/l_c - 1], \tag{2.17}$$

where l_c is the length over which two polarisations are correlated (correlation length). With the assumption that correlation length is much smaller than the span length, Eq. 2.17 can be simplified to

$$\sigma_T \approx \Delta\beta_1 \sqrt{2 l_c L} \equiv D_p \sqrt{L} \tag{2.18}$$

where D_p is the PMD parameter used in fibre characterisation. PMD effect will have a relatively small impact on pulse broadening comparing with GVD. However, in high data rate communication systems operating near zero-dispersion wavelength PMD will degrade the transmission quality (20).

2.2 Nonlinear Effects

Nonlinearities originating from nonlinear refraction and stimulated inelastic scattering can have constructive and destructive impact on the transmission and play an important role in optical fibres. Intensity dependance of the refractive index puts the limit on the maximum optical power which can be used before destructive nonlinear effects will take place in the fibre and is defined as (13)

$$\tilde{n}(\omega, |E|^2) = n(\omega) + n_2|E|^2, \tag{2.19}$$

where $|E|^2$ is the optical intensity, $n(\omega)$ is the linear part approximated by the Sellmeier equation (21)

$$n^2(\omega) = 1 + \sum_{j=1}^{m} \frac{B_j \omega_j^2}{\omega_j^2 - \omega^2} \tag{2.20}$$

and n_2 is the nonlinear-index coefficient related to third-order susceptibility $\chi^{(3)}$ defined as (22)

$$n_2 = \frac{3}{8n} Re(\chi^{(3)}_{xxxx}), \tag{2.21}$$

High intensity optical power in the transmission fibres leads to nonlinear effects known as self-phase modulation (SPM) and cross-phase modulation (XPM).

The stimulated inelastic scattering of a photon to a lower energy photon where the energy difference is being absorbed by the nonlinear medium are the origin of stimulated Brillouin scattering (SBS) and stimulated Raman scattering (SRS). The difference between both is that acoustic phonons participate in SBS and can occur only in backward direction whereas optical phonons takes part in SRS where the light can be scatter in both, forward and backward directions. Due to broad gain spectrum of a Stokes shifted light in SRS the phenomena is used in optical amplification.

2.2.1 Self-Phase Modulation

The refractive index in nonlinear optical medium is dependent on the pulse intensity (23). It leads to self-focusing and phase modulation which may cause frequency broadening or, in some cases, optical pulse narrowing in the fibre (24). The spectral changes due to SPM are related to a time dependance of the nonlinear phase shift ϕ_{NL} and is referred as frequency chirping $\delta\omega$

$$\delta\omega(T) = -\frac{\partial\phi_{NL}}{\partial T} = -\left(\frac{L_{eff}}{L_{NL}}\right)\frac{\partial}{\partial T}|U(0,T)|^2, \tag{2.22}$$

where $U(0,T)$ is the field of the normalised amplitude $U(z,T)$ at $z = 0$.

For initially unchirped pulses new frequency components generated during pulse propagation will broaden (25) or narrow (26, 27) the spectrum. The chirp variations are directly dependent on the initial chirp and pulse shape and will change the received spectra with respect to distance considerably. Optical pulses with positive initial frequency chirp ($C > 0$) will exhibit longer frequency range with less pronounced peaks whereas opposite effect takes place for negatively chirped pulses ($C < 0$) where spectral narrowing occurs resulting in higher peak intensity at the output of the fibre (27).

The relation between dispersion length L_D and nonlinear length L_{NL} is described by the parameter N as (28)

$$N^2 = \frac{L_D}{L_{NL}} = \frac{\gamma P_0 T_0^2}{|\beta_2|}. \tag{2.23}$$

In the scenario where $N \ll 1$ pulse evolution along the fibre will be dominated by GVD. In normal dispersion regime ($\beta_2 > 0$) with nonlinear SPM effects dominating ($N \gg 1$) the pulse will be subject to optical wave breaking (29) where two different frequencies interfere with each other due to different speed propagations (30). This phenomenon can be also explained as four-wave mixing where two frequency components ω_1 and ω_2 of the same pulse creates new frequencies.

In anomalous-dispersion regime ($\beta_2 < 0$) where the effects of GVD and SPM cancel out each other ($N = 1$) chirp-free pulse might produce an optical soliton,

a phenomena which has a practical use in fibre optic communications due to its immunity to distortion over ultra-long distances (31, 32, 33, 34).

Higher-order nonlinear effects such as self-steeping and intrapulse Raman scattering should be included for ultrashort pulses where $T_0 < 1ps$ (28).

2.2.2 Cross-Phase Modulation

The effective refractive index is also influenced by the interaction of two or more optical fields copropagating in the fibre coupled together by cross-phase modulation. Modulation of refractive index by total optical power in non-dispersive medium will result in optical phase modulation only (22). In dispersive medium, phase modulation effect will directly translate into intensity fluctuations (35). XPM-induced modulation instability in anomalous GVD will have a negative impact on WDM transmission systems (36, 37, 38).

2.2.3 Stimulated Raman Scattering

Stimulated Raman scattering is a nonlinear process discovered by Sir Chandrasekhara Venkata Raman in 1928 (39). In Raman effect the power of an optical field is transferred to another field downshifted in frequency. The frequency difference between two fields $\Omega \equiv \omega_p - \omega_s$ as well as Raman-gain coefficient $g_R(\Omega)$ is medium dependent. In optical fibres the Raman gain is broad and may extend up to 40 THz. The initial growth of the shifted light is described by:

$$\frac{dP_s}{dz} = g_R P_p P_s, \tag{2.24}$$

where P_s and P_p refers to Stokes and pump intensity, respectively. This feature is used in optical amplification of light in silica fibres. The SRS process in optical fibres with losses at the Stokes (α_s) and pump frequencies (α_p) is well approximated by the set of two coupled equations (40):

$$\frac{dP_s}{dz} = g_R P_p P_s - \alpha_s P_s, \tag{2.25}$$

$$\frac{dP_p}{dz} = -\frac{\omega_p}{\omega_s} g_R P_p P_s - \alpha_p P_p, \tag{2.26}$$

The threshold condition for SRS to take place, valid when fibre loss at the Stokes α_s and pump frequencies α_p are similar is (40)

$$P_{s0}^{eff} exp(g_R P_0 L_{eff}/A_{eff}) = P_0, \tag{2.27}$$

where P_0 is the input pump power, A_{eff} is the effective core area defined as (22)

$$A_{eff} = \frac{(\int\int_{-\infty}^{\infty} |F(x,y)|^2 dxdy)^2}{\int\int_{-\infty}^{\infty} |F(x,y)|^4 dxdy} \tag{2.28}$$

and L_{eff} is the effective length over which the optical power is assumed to be constant:

$$L_{eff} = [1 - exp(-\alpha L)]/\alpha \tag{2.29}$$

The spectrum of Raman gain shift in standard single mode fibre SMF-28 is shown in Fig. 2.2.

Stimulated Raman scattering is used in several disciplines. In biomedicine SRS can be used in coherent Raman microscopy which allows highly sensitive optical imaging at video rate (41). Recently, this technology was used to detect the brain tumors which were previously undetectable under standard operative conditions (42). Photonics crystal fibres makes use of highly nonlinear holey fibre to generate Raman amplification and ultrafast signal modulation (43). Silicon waveguide technology uses SRS for on-chip amplification and coherent light generation in silicon integrated optics (44, 45).

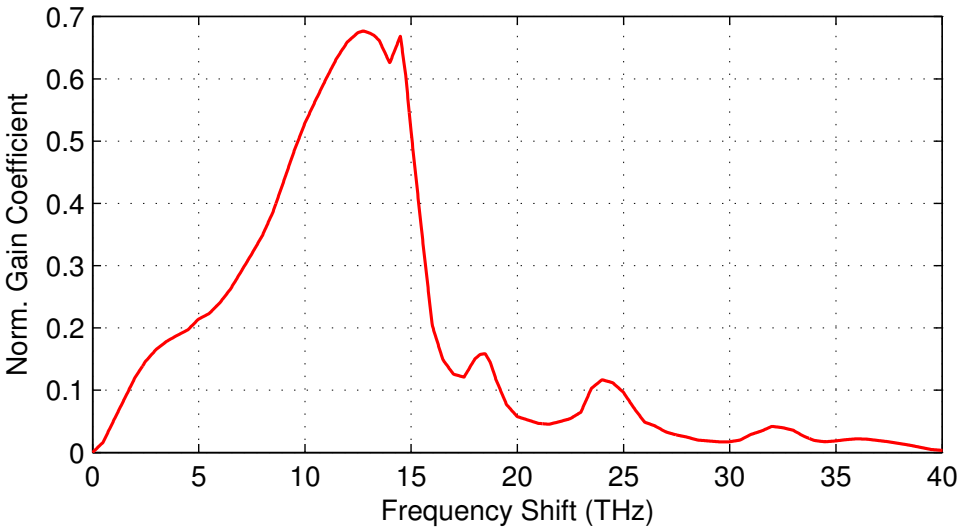

Figure 2.2: Raman gain spectrum in standard silica SMF-28 fibre.

Other application are optical sensing where backscattered light may be used to measure temperature (46), fibre-based Raman lasers (47) and Raman amplifiers (48, 49, 50, 51) which gained the main interest in high capacity optical communication systems where low noise amplification is crucial.

2.2.4 Four-Wave Mixing

Four-Wave Mixing (FWM) is a third-order nonlinear effect originating from dependance of refractive index on the intensity of the optical power. The efficiency of FWM is determined by frequency phase mismatch. Phase-matching condition differs FWM from SRS and SBS in the way that specific fibre parameters and input wavelengths are required for FWM to be effective. Three photons at the frequencies ω_1, ω_2 and ω_3 may transfer their energy to a new single photon at ω_4 (52) such that

$$\omega_4 = \omega_1 + \omega_2 + \omega_3 \tag{2.30}$$

In another case where ω_1 and ω_2 are annihilated, two new frequency components

are simultaneously created such that (52)

$$\omega_1 + \omega_2 = \omega_3 + \omega_4 \tag{2.31}$$

FWM can also be initiated with a single wavelength component where $\omega_1 = \omega_2 \equiv \omega_0$. In this case two equally spaced sidebands ω_3 and ω_4 will be created where one is downshifted and second upshifted with the reference to ω_0. (52)

The interaction between wavelengths have a negative impact on long-haul dense wavelength-division multiplexed (DWDM) optical communication systems and is known as an inter-channel crosstalk. Phase-matching condition decreases with higher chromatic dispersion (53, 54). This property can be used to reduce FWM effect. Increased and uneven channel spacing will further decrease the phenomena (54).

Chapter 3

Optical Amplification

The first work on optical amplification was done in the beginning of 1960s by Elias Snitzer and colleagues who demonstrated first optical fibre laser (55, 56, 57) and few years later developed world's first optical fibre amplifier (58). A decade later experiments on fibre-optic communications began. The innovation of the first low loss fibre (10, 59) enabled data transmission and triggered the research on optical amplifiers.

The basic characteristic of an optical amplifier is the operating gain which quantifies the signals amplification. This, however, is relevant to the optical input power, which will change considerably with the bandwidth of supported WDM channels. An important parameter for long-haul WDM transmission with the chain of inline amplifiers is the response to the dynamic changes in input powers due to channel add/drop which can affect the gain flatness. Finally the amplifier is characterised by its noise performance defined as a noise figure. All those factors led to development of different types of optical amplifiers.

The main optical amplifier technologies are doped fibre amplifiers, Raman amplifiers, semiconductor amplifiers (SOA), parametric amplifiers (FOPA) and Brillouin-fibre (SBS) amplifiers.

In doped-fibre amplifiers the stimulated emission in the gain medium amplifies the incoming light. They make use of rare-earth elements doped into fibre core which determine the operational wavelength and tuning range of the amplifier. The commonly used dopants, their pump and operating wavelengths and the operating ranges are listed in Table 3.1 (60, 61, 62).

Table 3.1: Rare-earth elements used in doped-fibre amplifiers

Element	Symbol	Pump Wavelength	Operating Wavelength	Tuning Range
Neodymium	Nd^{3+}	823 nm	1.09 μm	92 nm
Erbium	Er^{3+}	650 nm	1.55 μm	35 nm
		980 nm	1.55 μm	35 nm
		1480 nm	1.55 μm	35 nm
Praseodymium	Pr^{3+}	590 nm	1.06 μm	61 nm
Ytterbium	Yb^{3+}	910 nm	975 nm	3 nm
		910 nm	$\sim$1.05 μm	150 nm
		975 nm	$\sim$1.05 μm	150 nm
		1047 nm	$\sim$1.1 μm	100 nm

Semiconductor amplifiers (SOA) are based on the semiconductor gain medium (63) and pumped electronically via applied current. This allows for a potentially low cost production. However, high noise figure, low output power and low gain, cross-gain modulation that leads to crosstalk penalty for dense WDM input signals (64) makes SOA unsuitable for current communication networks.

Brillouin-fibre amplifiers are based on a nonlinear Stimulated Brillouin scattering (SBS) process which can generate a backward propagating Stokes wave shifted by an amount of the Brillouin shift which is about 11 GHz for the optical fibres. Due to limited bandwidth to about 100 MHz Brillouin amplifiers are not suitable for the WDM communication systems, however, they might be used for the selective amplification and narrowband optical filters (65).

The fibre-optic parametric amplification (FOPA) is based on nonlinear four-wave mixing (FWM) process (66). In the basic setup, few hundred of low-loss highly nonlinear fibre is used as a gain medium to design discrete amplifier. It may operate at any wavelength (67) and provide wide and flat gain bandwidth, which is an advantage over conventional EDFA. Due to phase-matching condition needed for effective FWM process, FOPA can be used in phase-sensitive

parametric amplification realising an ideal noise figure of 0 dB (68). This, however, requires the phase control of interacting light waves, which in turn may be realised with the use of a nonlinear Mach-Zehnder interferometer (69). Phase-insensitive FOPA, where two photons with random phases will amplify the signal and create the forth photon, so called idler, in the way that the phase difference between all will meet the phase-matching condition, offers high differential gain with relatively simple implementation and is investigated in high-speed optical communication systems (70).

Raman based amplifiers (49, 50, 51) relay on nonlinear Stimulated Raman Scattering (SRS) where light is downshifted in frequency. The first Raman amplifiers were demonstrated in 70s (48). They are classified as: discrete (lumped) where short length of high Raman gain fibre is used and distributed (DRA) where the transmission fibre itself serves as a gain medium. This feature, contrary to lumped amplifiers, prevents signal decay and allows for quasi-lossless gain distribution across the transmission span. Even though Raman amplification is technically very attractive as it offers improved noise figure (71) and broadband gain bandwidth (72), it did not succeed back in 1980s due to lack of high-power pump sources (73) as well as technical necessity due to the fact that EDFA offered noise figure low enough for binary modulation formats used at that time.

Each type of amplifier results from different phenomena and offers different qualities which may be desirable for specific application. In WDM communication systems Raman based amplifiers are attractive because of the flexibility in terms of the operating wavelength and the gain bandwidth which can be extended by coupling pumps at different wavelengths. In a single-wavelength pump regime EDFA, FOPA and Raman amplifiers can offer comparable gain bandwidth performance in a C-band telecommunication window, however, they differ with regards to noise figure (NF), gain and pump efficiency, excitation life time and an implementation ease. Phase-sensitive FOPA can go beyond the quantum limited NF of 3 dB and in principle provide ideal noiseless amplification (68) which would eliminate the nonlinear impairments and necessity of distributed Raman amplification. The practical difficulty imposed on phase control of light makes phase-sensitive FOPA a challenging task. The NF of EDFA, phase-insensitive FOPA and Raman amplifier offers high gain and can (in the ideal conditions)

reach the value close to the 3 dB quantum limit (74, 75, 76). Distributed amplification reduces NF of the span and allows for extension of the span length, which is what makes DRA an attractive candidate as an amplifier. This may also be achieved with FOPA, however, speciality dispersion-flattened fibre with fixed zero-dispersion slope is necessary whereas distributed Raman may operate with most of the current fibre types. One of the drawbacks of DRA is low pump efficiency, while EDFA and FOPA can offer excellent performance. Ultrafast excitation time of Raman and FOPA in a saturation mode may affect modulated signal as binary 0 will attract more amplification. It doesnt affect EDFA.

Currently majority of optical networks are based on EDFA, accounting for more than 90 % of all commercially deployed amplifiers (8), however, exponentially growing demand for higher data throughput over the internet forced the implementation of less noise resistant high level modulation formats and as a result by the early 2000s Raman amplification became main interest in optical communication (77), thanks to technological advancements which made it possible to achieve semiconductor lasers with satisfying pump power levels (78). Based on current statistics, EDFAs deployment will fall below 80 % by 2017 with Raman and hybrid-Raman-EDFAs sale increase (9). Low noise distributed amplifiers are great candidates to upgrade current optical networks and enable implementation of advanced multilevel modulation formats with densely spaced constellation points.

3.1 Noise in Optical Amplifiers

In optical amplification spontaneous emission emits undesirable photons with arbitrary frequencies and polarisation state which are amplified together with the signal (79, 80). This amplified spontaneous emission is considered as noise. The ASE's noise power spectral density (taking into account two orthogonal polarisation states) can be defined as (81):

$$\rho(\lambda) = 2n_{sp}\frac{hc}{\lambda}[G(\lambda) - 1], \tag{3.1}$$

where $G(\lambda)$ is the optical gain of the amplifier at the wavelength λ, c is the speed of light, h is Plank's constant and n_{sp} is the spontaneous emission factor of the quality of the population inversion of the optical amplifier

$$n_{sp} = \frac{\sigma_e N_2}{\sigma_e N_2 - \sigma_a N_1}, \tag{3.2}$$

where σ_e and σ_a indicates the emission and absorption cross-section of the fibre and N_1 and N_2 are carrier densities at the lower and upper energy levels. The noise power within the bandwidth B_0 can be approximated by integrating the Eq. 3.3

$$P_{ASE} \approx 2n_{sp}hf[G(f) - 1]B_0, \tag{3.3}$$

The fundamental definition of an amplifier's noise figure (NF) is defined as a ratio of the input signal to noise ration (SNR_{in}) and the output SNR_{out}:

$$NF = \frac{SNR_{in}}{SNR_{out}} \tag{3.4}$$

SNR_{in} and SNR_{out} is derived in (81) and simplifies to:

$$NF = 2n_{sp}\frac{G-1}{G} + \frac{1}{G}, \tag{3.5}$$

where G is an optical gain of the amplifier. We can notice that for a large optical gain the leading factor quantifying amplifiers noise is n_{sp}. The minimum value of n_{sp} is 1, which defines the 3 dB minimum NF of a phase-insensitive optical amplifier.

3.2 Erbium-Doped Fibre Amplifiers

Erbium-doped fibre amplifiers are attractive in optical communication systems because of the operational wavelength window which covers lowest attenuation region of single mode silica fibres. High pumping efficiency of 3.7 dB/mW (61) and 11 dB/mW reported in 1990s (82) is a big advantage over Raman amplifiers. The gain distribution in EDFA depends on several parameters. The amplifiers length, type of fibre, erbium concentration and pump configuration makes the design optimisation rather uneasy. Absorption spectrum of Er^{3+} doped fibre (Fig. 2 in Ref. (83)) offers great flexibility in pump source deployment.

Lumped EDFA consists of a source pump coupled with the Er^{3+} doped fibre in co-, counter- or bi-directional configuration. Forward pumping in an EDFA offers great noise performance at the output of the Er^{3+} doped fibre, however, the optical power of the signal is also low. Backward pumping provides higher gain with the expense of increased forward ASE. The wavelength of the pump and the length of the fibre is design related. In a simple single stage C-band EDFA, pump at 980 nm is typically coupled with less than 100 m of doped fibre. An L-band amplifier usually requires several times longer fibre lengths than C-band in order to keep population inversion level low. The schematic design of single stage bidirectional EDFA is in Fig. 3.1.

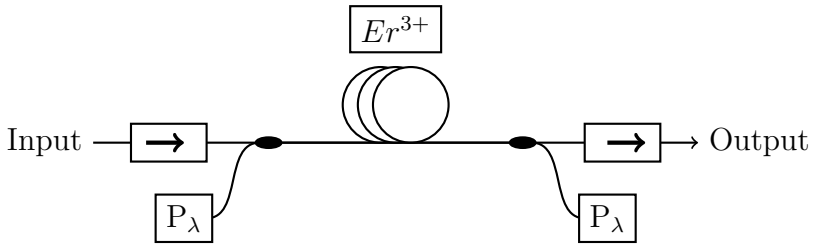

Figure 3.1: Schematic diagram of single stage bidirectional EDFA

In multichannel WDM applications the uniform gain across the band is important. Even a small gain variation becomes problematic in long-haul transmission with several in-line amplifiers where the gain difference between individual channels grows exponentially. Cascaded multi stage EDFAs design with two or more source pumps used in unidirectional or bidirectional configuration can optimise

more than one performance parameter, provide better gain flatness across the band and help to reduce noise level (84, 85, 86). Extended flat bandwidth can also be achieved by doping a tellurite fibre with Er^{3+} ions (87). The schematic design of multi-wavelength EDFA is in Fig. 3.2.

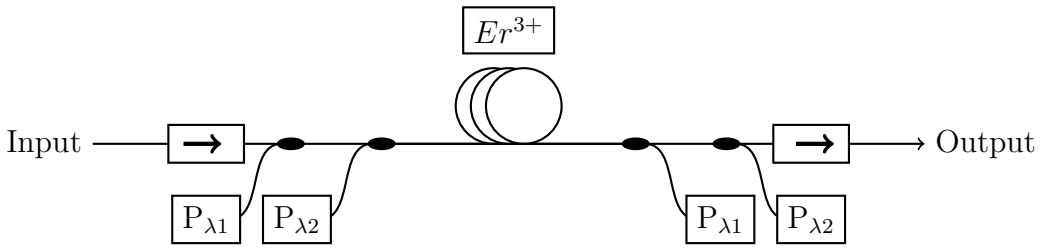

Figure 3.2: Schematic diagram of multi-pump EDFA

An example of schematic design of two stage EDFA where the first stage serves as a pre-amplifier and second stage, separated by the optical isolator, acts as a booster is in Fig. 3.3.

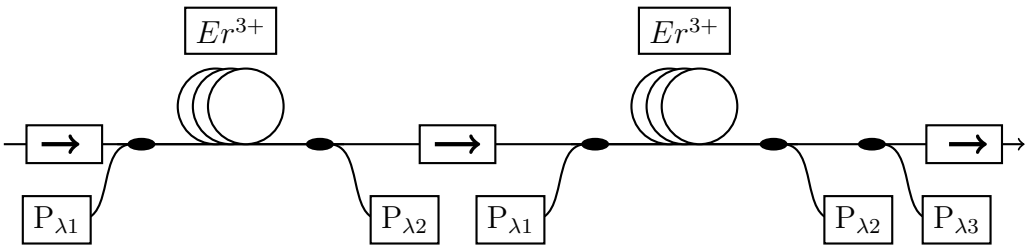

Figure 3.3: Schematic diagram of two stage multi-wavelength EDFA

Optical networks are affected by noise which ultimately limits the system performance. The level of ASE accumulated over the chain of EDFAs degrades optical SNR and may saturate the amplifiers. The excess noise figure due to spontaneous emission in EDFA depends on amplifier length and the pump power. Careful optimisation can realise NF close to the quantum limit of 3 dB even in high gain amplifiers (74, 88). Reduction of backward propagating ASE which depletes the pump power by implementing an optical isolator can enhance the gain while keeping NF low (75).

The models which enable performance study of noise and gain characteristics in EDFA using propagation and rate equation has been proposed in Ref. (89) and in (90). An analytic description of the gain and noise behaviour is presented in Ref. (91).

3.3 Raman Amplifiers

Amplification based on nonlinear stimulated Raman scattering process is an attractive alternative to commonly used EDFAs. In Raman amplifiers the energy from the pump source is transferred through inelastic scattering to the signal downshifted in frequency. Contrary to EDFA, amplification using SRS can be provided practically at any frequency by carefully choosing appropriate pump wavelength. In particularl ultra-wideband systems can benefit from Raman amplification as the gain bandwidth can be extended by coupling different pump wavelengths (92, 93). Flat-gain 100 nm bandwidth has been achieved with 12 wavelength-channel WDM laser diodes (94).

The superior noise performance in distributed Raman amplification (DRA) (95) where the transmission fibre is used as a gain medium, leads to higher optical signal to noise ratio (OSNR) and allows higher reach between the repeaters (96, 97) as well as long distances in unrepeatered transmissions (98)

In discrete amplifiers relatively short lengths of speciality highly nonlinear fibre with a high Raman gain coefficient can be used. These can be included as components at the end of transmission spans. An advantage of discrete Raman amplifiers is that the pump power requirement can be reduced whilst maintaining a high overall gain value and bandwidth (99).

3.3.1 Noise in Raman Amplifiers

The noise in Raman amplifiers predominantly originates from spontaneous Raman scattering, nonlinear Kerr effects caused by high pump power intensities and relative intensity noise (RIN) transfer.

3.3.1.1 Spontaneous Raman Scattering

The origin of amplified spontaneous emission (ASE) in Raman amplification is spontaneous Raman scattering which is an unavoidable process assisting SRS (100, 101). Shot noise, signal-spontaneous (signal-ASE) and spontaneous-spontaneous (ASE-ASE) beat noise are major components of ASE affecting the quality of the transmission. The ASE-ASE beat is relatively small and can be further reduced with the implementation of a narrowband optical filter therefore ignored while defining signal to noise ratio (SNR) in the electrical domain (102). The leading factor contributing to noise is the copolarised signal-ASE beat noise propagating with the same direction as signal producing the intensity fluctuations after photo-detection and the shot noise. Based on these two parameters the NF equation (Eq. 3.4) can be approximated by (71):

$$NF \approx \frac{2P_A^+(L)}{hvB_{ref}G_{net}} + \frac{1}{G_{net}}, \tag{3.6}$$

$$NF = \frac{P_s(0)}{hvB_{ref}OSNR_{out}} + \frac{1}{G_{net}}, \tag{3.7}$$

where $P_A^+(L)$ is the ASE power, hv is the photon energy, B_{ref} is a reference bandwidth, G_{net} is a net gain and $P_s(0)$ is the input power.

The mathematical derivation of ASE components is found in Ref. (103). The analytical model that enables the measurement of amplified spontaneous Raman scattering and gain in a fibre Raman amplifier is proposed in Ref. (104).

3.3.1.2 Double Rayleigh Backscattering

Rayleigh backscattering related loss is a phenomena which ultimately limits the performance of DRA and is inherent to all silica fibres. Double Rayleigh backscattering (DRB) originates from the phenomena that the light is being reflected twice. The limitations imposed by DRB will degrade the SNR by amplifying double scattered spontaneous emission. It may also cause multiple-path interference (MPI) where the signal will experience more than one optical path (105).

The effect of DRB depends on the polarisation state (106) therefore MPI induced noise will be dominant when the light is copolaraised with the signal. Single and double Rayleigh backscattering are enhanced in long spans with high Raman pump powers (105) and put ultimate limit on unrepeatered transmission distance that can be achieved. DRB induced MPI can be described by the set of ordinary differential equations (ODE) (107):

$$\frac{dP_s}{dz} = -\alpha_s P_s + \frac{g}{A_{eff}} P_p P_s \tag{3.8}$$

$$-\frac{dP_{SRB}}{dz} = -\alpha_s P_{SRB} + \frac{g}{A_{eff}} P_p P_{SRB} + k P_s \tag{3.9}$$

$$\frac{dP_{DRB}}{dz} = -\alpha_s P_{DRB} + \frac{g}{A_{eff}} P_p P_{DRB} + k P_{SRB} \tag{3.10}$$

where the P_{SRB} and P_{DRB} is the single- and double backscattered power, k is the coupling coefficient related Rayleigh scattering loss at the fibre composition. The boundary conditions in the Eqs. 3.8 - 3.10 are:

$$P_{SRB}(L) = P_s(L) \tag{3.11}$$

$$P_{DRB}(0) = P_{SRB}(0) \tag{3.12}$$

The total noise figure in Eq. 3.13 can be updated to include the contribution from the DRB (71):

$$NF \approx \frac{2P_A^+(L)}{h\nu B_{ref} G_{net}} + \frac{1}{G_{net}} + \frac{(\frac{5}{9})P_{DRB}}{h\nu\sqrt{\frac{B_e^2+B_s^2}{2}}G_{net}}, \tag{3.13}$$

where B_s and B_e is the signal bandwidth and electrical filter bandwidth respectively.

Optimum design of bidirectionally pumped DRA can minimise the beat noise between signal and DRB (108). Higher order DRA can further decrease the noise and improve overall system performance (109).

3.3.1.3 Relative Intensity Noise Transfer

Relative intensity noise (RIN) refers to semiconductor pump laser fluctuations of intensity, phase and frequency predominantly due to spontaneous emission (110). It is defined as noise power spectral density divided by the square of the average signal power in the electrical domain (81):

$$RIN(\omega) = F\left\{\frac{\left\langle (P_{opt} - P_{opt,ave})^2 \right\rangle}{P_{opt,ave}^2}\right\} \tag{3.14}$$

where $P_{opt,ave}$ is the average optical power and F indicates Fourier transformation. The Eq. 3.15 can be further simplified and expressed as the ratio of the electrical noise power spectral density $S_p(\omega)$ and the signal electrical power $\Re^2 P_{opt,ave}^2$

$$RIN = \frac{S_p(\omega)}{\Re^2 P_{opt,ave}^2} \tag{3.15}$$

In Raman amplifiers RIN of the pump can lead to time-dependent gain variation affecting the signal. The noise transfer from pump to the signal (RIN transfer) can be defined as the frequency-dependent transfer function:

$$H(\omega) = \frac{RIN_s(\omega)}{RIN_p(\omega)} \tag{3.16}$$

where subscripts s and p refers to signal and pump respectively. RIN transfer in distributed Raman amplifiers depends on pumping configuration and properties of the medium.

In DRA with the spans longer than 40 km fibre length parameter can be neglected and predominant factor defining the 3 dB corner frequency f_c in counterpumping configuration at which RIN transfer decreases by 20 dB per decade can be approximated by (111):

$$f_c = \frac{\alpha_p V_s}{4\pi} \tag{3.17}$$

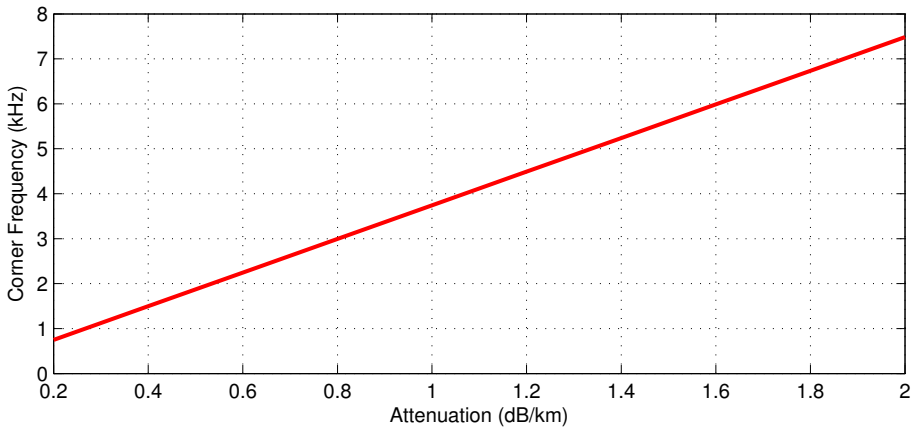

Figure 3.4: Simulation results: RIN corner frequency as a function of fibre attenuation in counterpumped distributed Raman amplifier

where V_s is the signal velocity and α_p is the fibre attenuation at the pump wavelength. The corner frequency as a function of fibre attenuation in counterpumped configuration is in Fig 3.4.

In copumping configuration the corner frequency is also dependent on relative dispersion between signal (λ_s) and pump (λ_p) wavelengths as well as dispersion slope (γ) and zero dispersion wavelength (λ_0) (111):

$$f_c = \frac{\alpha_p}{2\pi\gamma(\lambda_s - \lambda_p)|\frac{\lambda_s+\lambda_p}{2} - \lambda_0|} \tag{3.18}$$

The corner frequency is greatest when the zero dispersion wavelength is between pump and signal wavelength. The corner frequency dependance in the system with the fibre where $\lambda_0 = 1500$ nm for the pump and signal wavelengths as in Table 3.2 is plotted in Fig. 3.5

Detailed analytical model for pump to signal RIN transfer in copumped and counterpumped first order DRA is derived in Ref. (111).

The RIN transfer from pump to signal can be reduced by careful design of Raman amplifier. Fibre type have to be chosen with respect to the pumping configurations. The attenuation at the pump frequency and zero dispersion wavelength

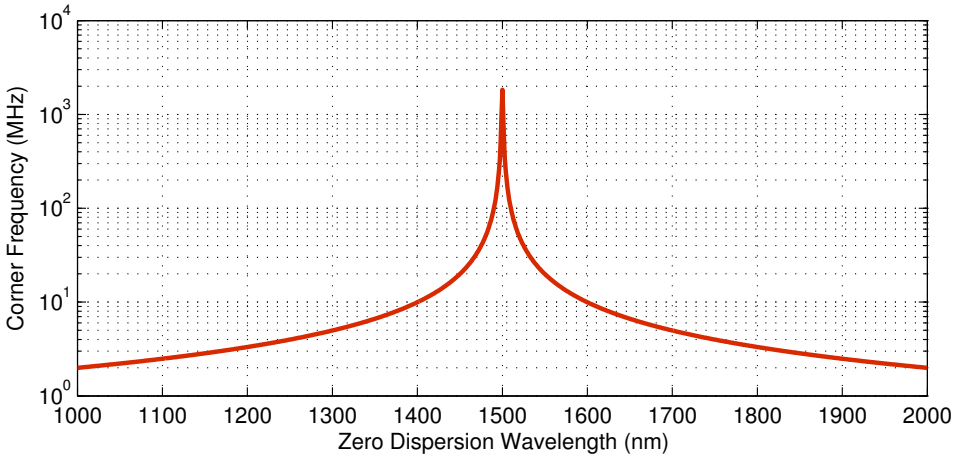

Figure 3.5: Simulation results: RIN corner frequency as a function of zero dispersion wavelength in copumped distributed Raman amplifier with source pump at 1450 nm.

will have great impact on system performance. Higher and dual order pumping can suppress the RIN by reducing the first order pump powers (112, 113), especially in forward direction where RIN transfer is most pronounced. In 2^{nd} order bidirectional ultra-long Raman fibre laser (URFL) based amplification the corner frequency can be reduced by using high reflectivity FBGs and increased span length. Appropriate pump power ratio will also benefit the system (114).

Table 3.2: Simulation Parameters: Corner Frequency in Copumped DRA Configuration

Parameter	Value	Unit
α_p	0.26	dB/km
γ	0.092	$ps/(nm^2 \cdot km)$
λ_s	1550	nm
λ_p	1450	nm
λ_0	1500	nm

3.3.2 Distributed Raman Amplifiers

Distributed amplification counterbalance fibre attenuation and prevents signal drop which reduces ASE accumulation. To illustrate the benefits of DRA we may use the total noise figure of the amplifier chain (115):

$$NF_{total} = NF_1 + \frac{NF_2 - 1}{G_1} + \frac{NF_3 - 1}{G_1 G_2} + ... \tag{3.19}$$

where subscripts indicate the n^{th} amplifier. In discrete post amplification the NF_{total} consist of the loss of the passive span ($NF_{1(span)}$) and the noise figure of the discrete amplifier (NF_2). The passive span attenuates the signal and worsen the output OSNR, increasing the total noise figure. Distributed amplification effectively combats fibre attenuation creating transparent span. Forward pumping can further reduce NF because the power of the signal and the amplifiers ASE noise on the beginning of the span will experience the attenuation over the fibre length. This explains the reason why in multistage discrete amplifiers the pre-amplifier is copumped. However, increased power on the front of the span will result in Kerr nonlinearities enhancement which will counterbalance the benefits of lower NF.

The first order DRA consists of a Raman pump at the wavelength that is Stokes shifted with reference to the signal frequency. The wave-division multiplexed (WDM) signal is amplified in forward (copumping) or backward (counterpumping) direction. In bidirectional configuration both pumps counter propagate against each other simultaneously resulting in more evenly distributed signal power along the transmission span. The schematic design of first order DRA is in Fig. 3.6. The pump and signal power distribution with ASE and Rayleigh backscattering noise in first order DRA configuration can be described by the set of coupled ODEs (116):

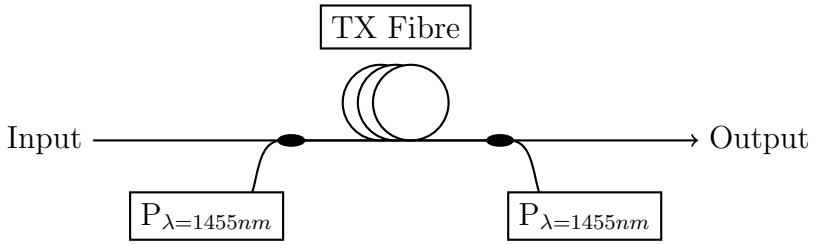

Figure 3.6: Schematic diagram of first order DRA

$$\frac{dP_p^{\pm}}{dz} = \mp\alpha_p P_p^{\pm} \mp \frac{v_p}{v_s}\frac{g}{A_{eff}}\left(P_s + n_s^+ + n_s^- + 4hv_s\Delta v_s\left(1 + \frac{1}{e^{\frac{h(v_p - v_s)}{kT}} - 1}\right)\right)P_p^{\pm} \tag{3.20}$$

$$\frac{dP_s}{dz} = -\alpha_s P_s + \frac{g}{A_{eff}}P_p^{\pm}P_s \tag{3.21}$$

$$\frac{dn_s^+}{dz} = -\alpha_s n_s^+ + \frac{g}{A_{eff}}P_p^{\pm}\left(n_s^+ + 2hv_s\Delta v_s\left(1 + \frac{1}{e^{\frac{h(v_p - v_s)}{kT}} - 1}\right)\right) + \epsilon n_s^- \tag{3.22}$$

$$\frac{dn_s^-}{dz} = -\alpha_s n_s^- - \frac{g}{A_{eff}}P_p^{\pm}\left(n_s^- + 2hv_s\Delta v_s\left(1 + \frac{1}{e^{\frac{h(v_p - v_s)}{kT}} - 1}\right)\right) - \epsilon(n_s^+ + P_s) \tag{3.23}$$

where (+) and (-) superscripts represent co- and counter propagation respectively, (p) and (s) subscripts refers to Pump and Signal, P is the optical power, α is the attenuation, n_s^+ and n_s^- are forward and backward-propagating noise at the signal frequency v_s, Δv_s is the signal bandwidth, v_p is the pump frequency, g is the Raman gain coefficient, h is Plank's constant, K_B is Boltzmann's constant, T is the absolute temperature and ϵ is the Rayleigh backscattering coefficient. The constant values, coefficients and variables used in numerical modelling simulations in this thesis are listed in Table 3.4 at the end of the chapter.

To solve ODEs describing first order bi-directional distributed Raman amplification (Eqs. 3.20 - 3.23) numerical simulations using the shooting method with 5^{th} order Runge-Kutta (117) formulas were used. The step size used in the simulations was 100 m and the offset accuracy of all components was set to 1e-8. The results for quasi-lossless 100 km span with a 0 dBm launch signal at 1555 nm and source pump at 1455 nm are in Fig. 3.7.

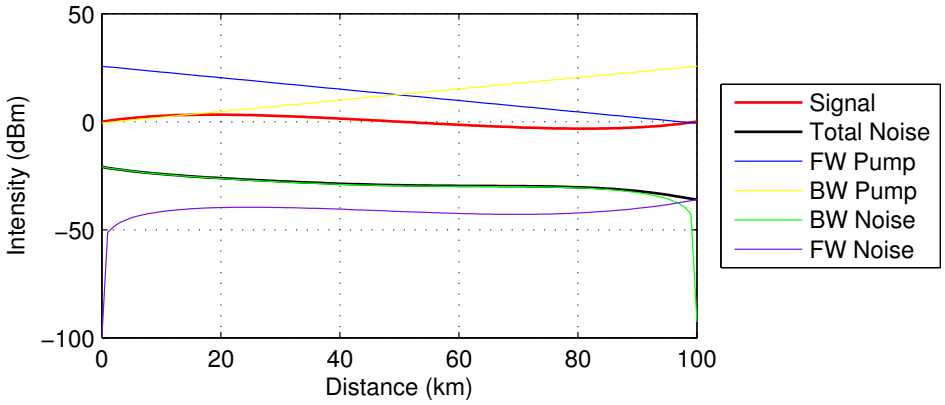

Figure 3.7: 1^{st} Order DRA: Simulation results for 100 km quasi-lossless link. FW: forward; BW: backward.

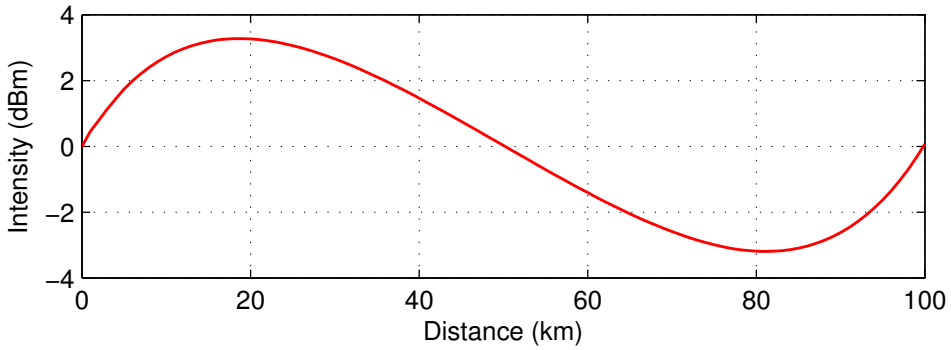

Figure 3.8: 1^{st} Order DRA: Simulation results of signal power distribution in 100 km quasi-lossless link.

The quasi-lossless signal power distribution was achieved with symmetric bidirectional pumping with 370 mW of an optical power per pump. Total signal power variation was 6.5 dB as shown in Fig. 3.8. The received OSNR as a function of gain in bidirectional symmetrically pumped 1^{st} order DRA is in Fig. 3.9.

The gain spectrum in Raman amplification can be adjusted by combining multiple pump wavelengths (94, 118, 119) as well as applying dual order configuration where first- and higher order pumps are combined (92, 120, 121). Both configurations can provide broadband gain bandwidth extending 100 nm. In the scenario where higher order pumps are deployed the system will benefit from improved noise figure.

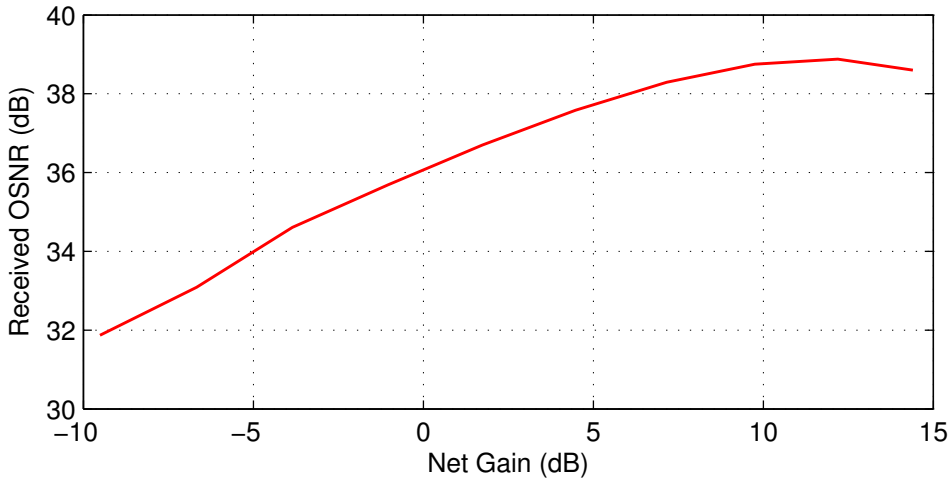

Figure 3.9: 1^{st} Order DRA: Simulation results of received OSNR as a function of gain.

The schematic diagram of multi wavelength, dual order or dual order multi wavelength Raman amplifier is in Fig. 3.10. The difference between both configurations is pumps wavelength spacing. In multi wavelength setup pumps are usually spaced by few *nm* whereas dual order configuration requires secondary pump wavelength to be at least one Stokes shifted from the primary one. Both configurations can be implemented in a single design.

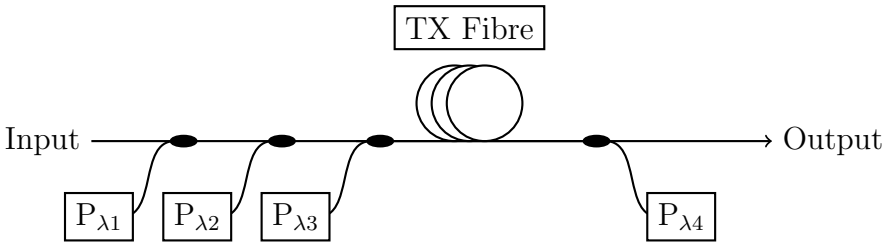

Figure 3.10: Schematic diagram of multi wavelength / dual order DRA.

3.3.3 Higher Order Distributed Raman Amplification

In higher order distributed Raman amplifiers the Raman pump is downshifted in wavelength by two (2^{nd} order), three (3^{rd} order) or more Stoke's shifts. The usual configuration consists of cascaded 1^{st} and 2^{nd} order pumps (dual order) where the gain from the second order pump assists the first one. The idea behind such design is to push the gain further into the span and reduce the intensity of the first order pump. Both pumps may be cascaded and launched from the same end of the fibre co- or counter propagating with the signal (unidirectional) or alternatively pumps may be installed to counter propagate against each other (bidirectional configuration). The number of possible configurations is large. The 4^{th} order pumping (122) and 6^{th} order cascaded pumping with FBGs has been reported (123). The overall benefit of higher order pumping is reduced Rayleigh backscattering (122), most notable in high on-off Raman gain, extended gain bandwidth (124), improved noise figure (95, 121, 122, 125) and receivers sensitivity (124).

The novel ultra-long Raman fibre laser based amplifier is an alternative method of distributed Raman amplification. This configuration takes advantage of a single wavelength pump downshifted by two Stokes from the signal. In 2^{nd} order URFL amplifier (5) the virtual primary pump is created by feeding back the Stokes shifted light using high reflectivity FBGs which act as mirrors. The cavity can be optimised by changing the wavelength and the bandwidth of FBGs (6).

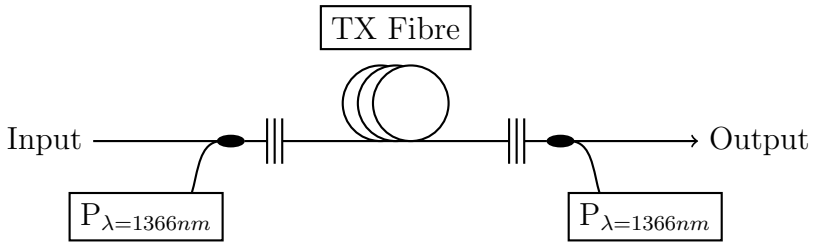

Figure 3.11: Schematic diagram of 2^{nd} order distributed URFL based amplifier with high reflectivity FBGs

Quasi lossless transmission over standard single mode fibre was a long term goal in telecommunication systems. The URFL based amplification can turn transmission fibre into virtually lossless optical medium (5, 126, 127, 128, 129)

by providing almost ideal signal power distribution. The schematic diagram of 2nd order URFL based amplifier is in Fig. 3.11.

The initial pump intensity at 1366 nm is shifted by approximately 13 THz towards the cavity created by the pair of FBGs. The lasing acts as a virtual primary pump at the wavelength determined by the FBGs and amplifies signal in desired C-band telecommunication region. The signal power evolution along the transmission fibre in this truly distributed amplification method is described by the set of ODEs (5):

$$\frac{dP_{P1}^{\pm}}{dz} = \mp\alpha_1 P_{P1}^{\pm} \mp \frac{g_1}{A_{eff}}\frac{v_1}{v_2}P_{P1}^{\pm}\left(P_{P2}^{+}+P_{P2}^{-}+4hv_2\Delta v_2\left(1+\frac{1}{e^{\frac{h(v_1-v_2)}{K_BT}}-1}\right)\right)\pm \epsilon_1 P_{P1}^{\mp} \tag{3.24}$$

$$\frac{dP_{P2}^{\pm}}{dz} = \mp\alpha_2 P_{P2}^{\pm} \mp \frac{g_1}{A_{eff}}\left(P_{P2}^{+}+2hv_2\Delta v_2\left(1+\frac{1}{e^{\frac{h(v_1-v_2)}{K_BT}}-1}\right)\right)(P_{P1}^{+}+P_{P1}^{-})\mp \frac{g_2}{A_{eff}}\frac{v_2}{v_s}P_{P2}^{\pm}\left(P_s+n_s^{+}+n_s^{-}+4hv_s\Delta v_s\left(1+\frac{1}{e^{\frac{h(v_2-v_s)}{K_BT}}-1}\right)\right)\pm \epsilon_2 P_{P2}^{\mp} \tag{3.25}$$

$$\frac{dP_s}{dz} = -\alpha_s P_s + \frac{g_2}{A_{eff}}P_s + (P_{P2}^{+}+P_{P2}^{-}) \tag{3.26}$$

$$\frac{dn_s^{+}}{dz} = -\alpha_s n_s^{+} + \frac{g_2}{A_{eff}}\left(n_s^{+}+2hv_s\Delta v_s\left(1+\frac{1}{e^{\frac{h(v_2-v_s)}{K_BT}}-1}\right)\right)(P_{P2}^{+}+P_{P2}^{-})+ \epsilon_s + n_s^{-} \tag{3.27}$$

$$\frac{dn_s^{-}}{dz} = \alpha_s n_s^{-} - \frac{g_2}{A_{eff}}\left(n_s^{-}+2hv_s\Delta v_s\left(1+\frac{1}{e^{\frac{h(v_2-v_s)}{K_BT}}-1}\right)\right)(P_{P2}^{+}+P_{P2}^{-})- \epsilon_s + (P_s+n_s^{+}) \tag{3.28}$$

where subscripts 1, 2 and s refers to 1st order pump, 2nd order pump and signal respectively. The boundary conditions in the Eqs. 3.24 - 3.28 are:

$$P_{P1}^{+}(0) = P_{P1}^{-}(L) = P_0; \tag{3.29}$$
$$P_{P2}^{+}(0) = R_1 P_{P2}^{-}(0); \tag{3.30}$$
$$P_{P2}^{-}(L) = R_2 P_{P2}^{+}(L); \tag{3.31}$$
$$N_s^{+}(0) = N_0; \tag{3.32}$$
$$N_s^{-}(L) = 0; \tag{3.33}$$
$$P_s(0) = P_{IN}; \tag{3.34}$$

where R_1 and R_2 is the strength of the fibre Bragg gratings and L is the total length of the span.

The simulation results for the 2nd order bi-directional URFL based amplifier in 100 km link is in Fig. 3.12. The parameters used are in Table 3.4. The reflectivity of the FBGs with a bandwidth of 200 GHz was 98%. The step size was set to 100 m.

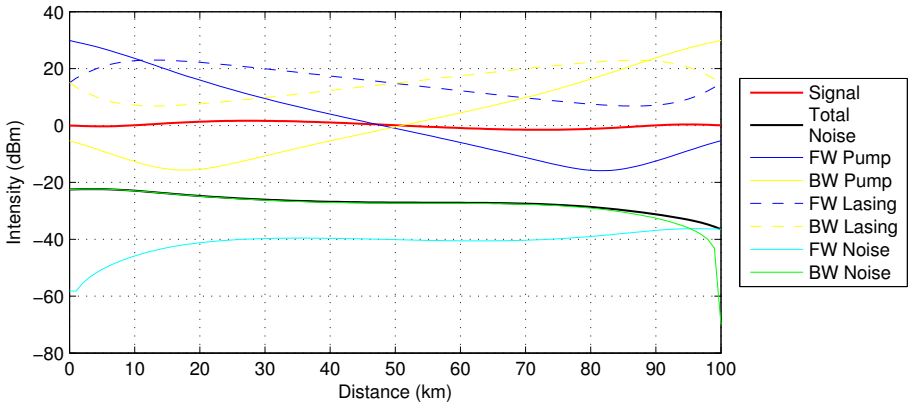

Figure 3.12: URFL: Simulation results for 100 km quasi-lossless link

Total peak to peak signal power variation in 100 km was 3.1 dB. That's over a 50% improvement in power distribution comparing with 1st order DRA as shown in Fig. 3.14. The disadvantage of the URFL configuration is that of higher pump powers required to achieve quasi-lossless transmission. Total pump power in URFL amplifier was 1.94 W whereas only 0.74 W was needed for the

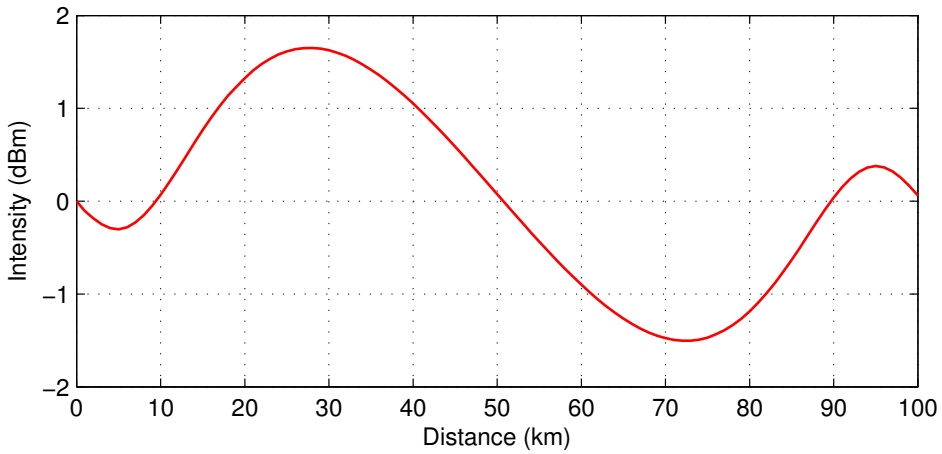

Figure 3.13: URFL: Simulation of signal power distribution in 100 km quasi-lossless link

1st order DRA. The comparison of pump efficiencies in 100 km SMF-28 link for 1st order DRA and URFL based amplifier is in Fig. 3.15. In both configurations symmetric pump power ratio was applied.

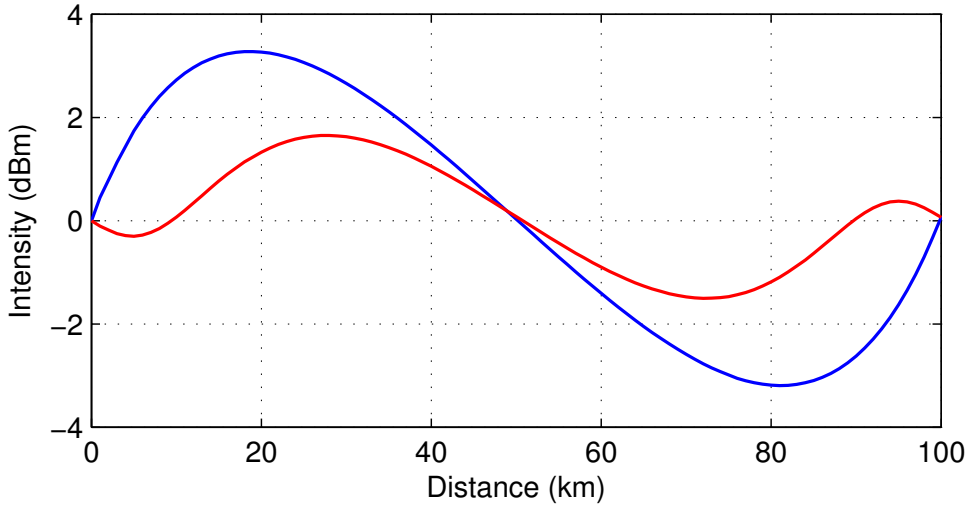

Figure 3.14: Simulation results of signal power distribution: comparison of 2nd order URFL (red) and 1st order DRA (blue) in 100 km quasi-lossless link

Power variation of the signal increases with distance. Fig. 3.16 and Fig. 3.17 shows simulated signal distribution across quasi-lossless 60 km, 80 km, 100 km

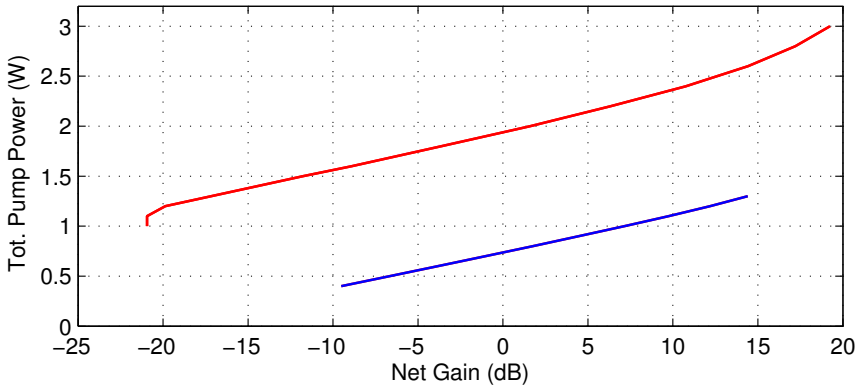

Figure 3.15: Simulation results of pump efficiency in 100 km SMF-28 link for 1st order DRA (blue) and URFL (red) based amplifiers.

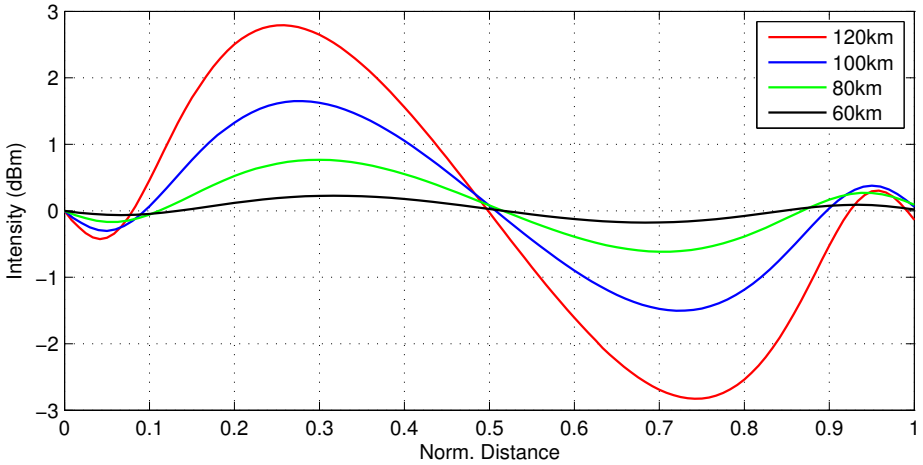

Figure 3.16: URFL: Simulation results of signal power distribution at different span lengths in normalised distance scale

and 120 km span. All simulations were performed with symmetric pump power distributions in forward and backward direction. The pump powers and signal variations across the spans are listed in Table. 3.3.

The RIN transfer in 2nd order URFL based amplification can be described by additional set of ODEs (114):

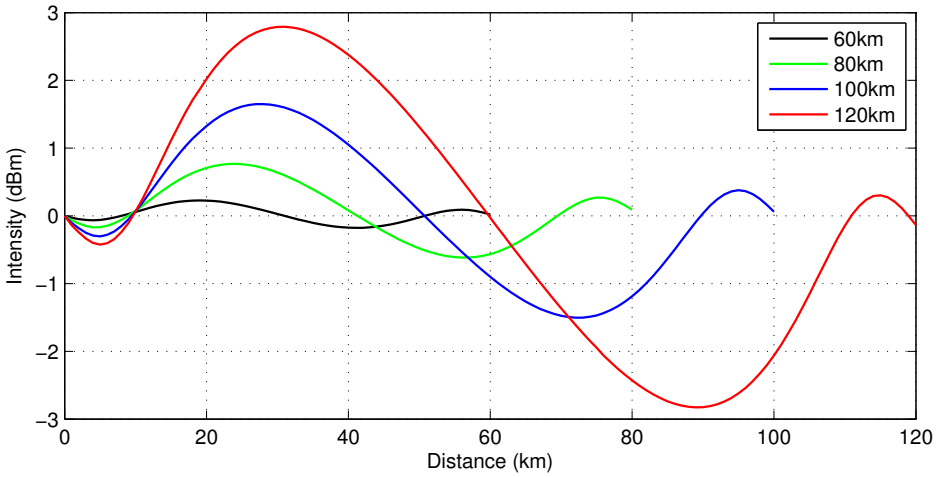

Figure 3.17: URFL: Simulation results of signal power distribution at different distances.

Table 3.3: 2nd Order URFL: Simulation Pump Powers and Signal Variation.

Distance (km)	Tot. Pump Power (W)	Signal Variation (dB)
60	1.17	0.4
80	1.56	1.38
100	1.94	3.15
120	2.3	5.62

$$\frac{dn_1^{\pm}}{dz} + id_1^{\pm}\omega n_1^{\pm} = \mp\alpha_1 n_1^{\pm} \mp g_1\frac{v_1}{v_2}P_1^{\pm}(n_2^{+} + n_2^{-}) \mp g_1\frac{v_1}{v_2}(P_2^{+} + P_2^{-})n_1^{\pm} \pm \epsilon_1 n_1^{\mp} \tag{3.35}$$

$$\frac{dn_2^{\pm}}{dz} + id_2^{\pm}\omega n_2^{\pm} = \mp\alpha_1 n_1^{\pm} \mp g_1 P_2^{\pm}(n_1^{+} + n_1^{-}) \pm g_1 n_2^{\pm}(P_1^{+} + P_1^{-}) \mp g_2\frac{v_2}{v_s}P_2^{\pm}n_s \mp g_2\frac{v_2}{v_s}P_s n_2^{\pm} \pm \epsilon_2 n_2^{\mp} \tag{3.36}$$

$$\frac{dn_s}{dz} = -\alpha_s n_s + g_2 P_s(n_2^{+} + n_2^{-})g_2 n_s(P_2^{+} + P_2^{-}) + \epsilon_s n_s^{-} \tag{3.37}$$

where $d_i^{\pm} = 1/v_s \pm 1/v_i$ is the relative propagation speed of different spectral components. The boundary conditions for the Eqs. 3.35 - 3.37 are:

$$n_1^+(0) = n_{10} \tag{3.38}$$
$$n_1^-(0) = n_{20} \tag{3.39}$$
$$n_2^+(0) = R_1 n_2^-(0) \tag{3.40}$$
$$n_2^-(L) = R_2 n_2^+(L) \tag{3.41}$$
$$n_s(0) = 0 \tag{3.42}$$

Table 3.4: Simulation Parameters

Parameter	Notation	Value	Unit
Signal Frequency	v_s	1550	nm
Signal Bandwidth	Δv_s	0.5	THz
Raman Gain Coefficient at 1366 nm	g_1	0.51	$W^{-1}km^{-1}$
Raman Gain Coefficient at 1450 nm	g_2	0.36	$W^{-1}km^{-1}$
Rayleigh coefficient at 1366	ϵ_1	1.0×10^{-4}	km^{-1}
Rayleigh coefficient at 1450	ϵ_2	6.0×10^{-5}	km^{-1}
Rayleigh coefficient at 1550	ϵ_s	4.3×10^{-5}	km^{-1}
Signal Attenuation at 1550 nm	α_s	0.2	dB/km
Pump Attenuation at 1366 nm	α_1	0.33	dB/km
Pump Attenuation at 1455 nm	α_2	0.26	dB/km
Plank's Constant	h	6.626e-34	Js
Boltzmann's constant	K_B	1.381e-23	J/K
Absolute Temperature	T	298	K

Chapter 4

Ultra-long Raman Fibre Laser Based Amplifier

In long-haul and unrepeatered links, distributed Raman amplification offers good noise performance and can be used to optimise the signal power evolution within the transmission span. It counterbalance fibre attenuation and prevents signal drop as in lumped amplifiers. Constant gain along the span in quasi-lossless transmission suppresses ASE noise accumulation and leads to lower NF. The schematic comparison of signal variation along the span with distributed Raman (red) and EDFA (blue) amplifier is in Fig 4.1.

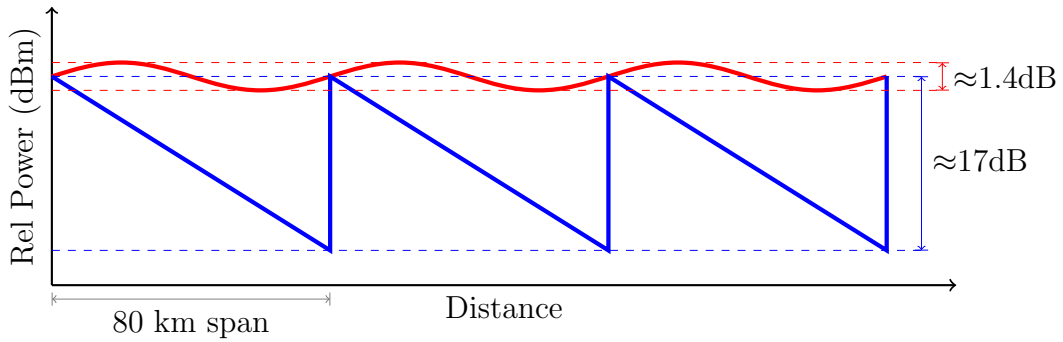

Figure 4.1: Relative signal power distribution in lumped EDFA (blue) and distributed Raman (red) amplification. The power variation was experimentally verified

There is only 1.4 dB power variation along the 80 km span using distributed Raman amplification scheme. Higher-order pumping can reduce the variations of the effective gain-loss coefficient even further, however, it usually requires Raman pumps at different wavelengths which higher the overall cost of the system.

A novel amplification scheme that uses fibre Bragg grating reflectors to form an ultra-long Raman fibre laser along the fibre span to achieve second-order pumping of the signal can be implemented in already existing links with standard SMF-28 silica fibre using single wavelength pump only. This can be used to realise a quasi-lossless span up to certain distance, approximating the optimal case for transmission performance (7).

The optical spectrum of the URFL amplification process is shown in Fig. 4.2. Secondary pump at 1366 nm transfers energy to the cavity created by FBGs in 1450 nm region. The lasing creates virtual primary pump which shifts energy to C-band telecommunication window. Bidirectional 2^{nd} order URFL configuration can extend the transmission distance in unrepeatered systems considerably (130) without employing speciality fibres or remote optical pre-amplifiers (ROPA).

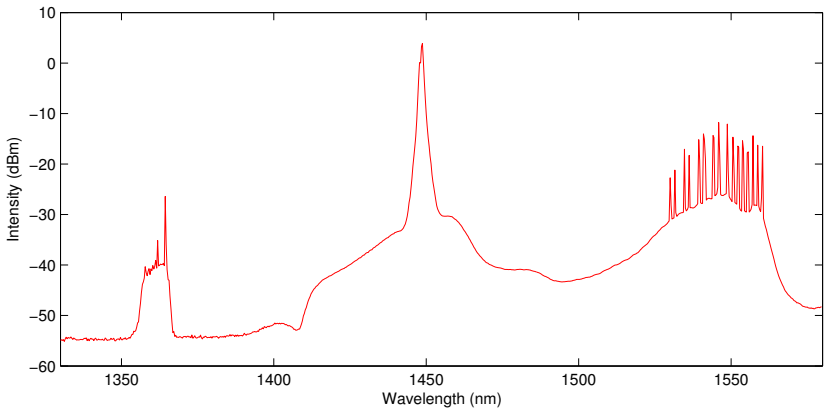

Figure 4.2: Optical spectrum of the 2^{nd} order URFL based amplification

This chapter is focused on optimisation of URFL based amplifier in order to maximise the data transmission performance. The choice of fibre is justified theoretically and confirmed experimentally. Different pairs of FBGs are tested and selected to provide best performance for unrepeatered transmission. Performance of the amplifier is characterised for each individual span length. Experimental

results of on-off gain, optical signal to noise ratio (OSNR) and signal power distribution measurements are confirmed with simulations and referenced. The final section of the chapter presents the benefits of URFL based amplifier and compares it with lumped EDFA.

4.1 Experimental Set-up

The schematic diagram of an experimental setup for optimisation and characterisation of the 2nd order bidirectional URFL based amplifier is shown in Fig. 4.3. Components investigated in the experiments are marked in red.

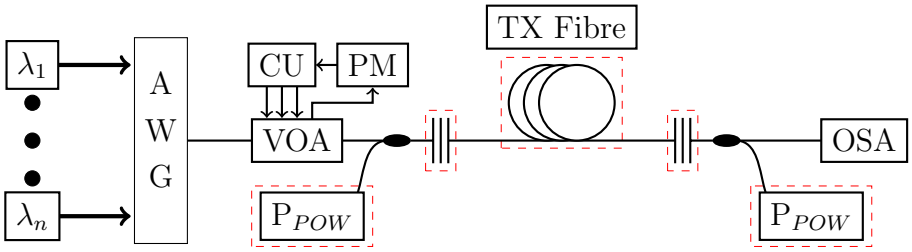

Figure 4.3: Experimental setup for optimisation and characterisation of 2^{nd} order distributed URFL based amplifier with high reflectivity FBGs. Total input power into the span is digitally controlled by VOA connected to control unit (CU) and calibrated power meter (PM). Optimised elements are marked by dashed red line.

Continuous wave distributed feedback (CW-DFB) laser diodes (LDs) are multiplexed using passive athermal arrayed wave-guide grating (AWG) multiplexer to form 16 even channels spread across C-band. In order to keep DFBs noise figure (NF) fixed, LDs power was fixed and total launch power into the span was adjusted by variable optical attenuator (VOA). Output signal is multiplexed by 1366/1550 nm coupler with high power Raman pump at 1366 nm. High reflectivity FBGs with a bandwidth of 0.5 nm and 0.7 dB loss were spliced at each end of the transmission span to reflect the Stokes shifted light generated by the secondary pump. Optical spectrum analyser (OSA) with sensitivity of -70 dBm and 0.1 nm resolution bandwidth was calibrated to a peak power of a single channel after the WDM Mux measured on the power meter.

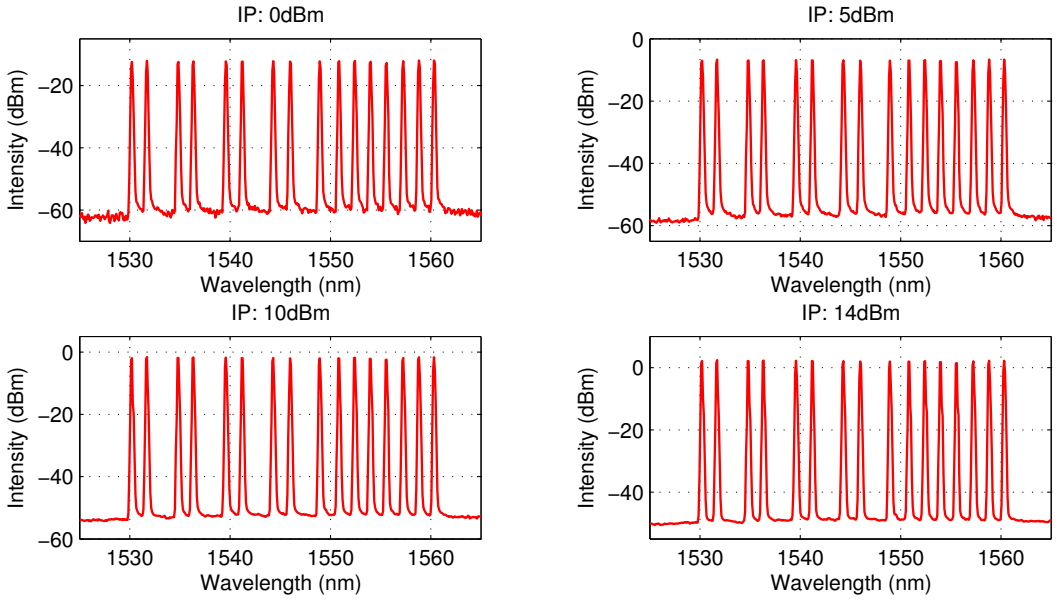

Figure 4.4: Spectra of the 16 channel grids used in the experiment for total input power (IP) of 0, 5, 10 and 14 dBm, measured after VOA.

The 16 channel WDM grid used in OSNR and on-off gain measurements is shown in Fig. 4.4. A 30 nm bandwidth (1530 nm - 1561 nm) of C-band telecommunication window was fully covered. The spectra at different launch powers of 0 dBm, 5 dBm, 10 dBm and 14 dBm with the initial peak power ripples of 0.78 dB, 0.81 dB, 0.87 dB and 1 dB respectively were measured after VOA.

4.2 Optimisation

Design of URFL amplifier requires the choice of appropriate parameters such as pump wavelength, fibre type, fibre length and fibre Bragg gratings. Careful co- and counter propagating pump power ratio adjustment can optimise the gain profile in the span, reduce nonlinear noise and pump to signal RIN transfer.

4.2.1 Type of Fibre

The choice of fibre type in DRA design is related to fibre attenuation, CD, PMD, zero dispersion wavelength and the size of the fibre core. Low loss large effective area fibres (LEAF) allow for higher launch powers with no significant nonlinear penalties, hence are suitable for high capacity and unrepeatered transmissions (131, 132). Non-zero dispersion shifted fibres (NZ-DSF) are optimum for WDM transmission with no inline dispersion compensation modules (133, 134). Measured dispersion slop for different fibers is in Fig. 4.5 (135).

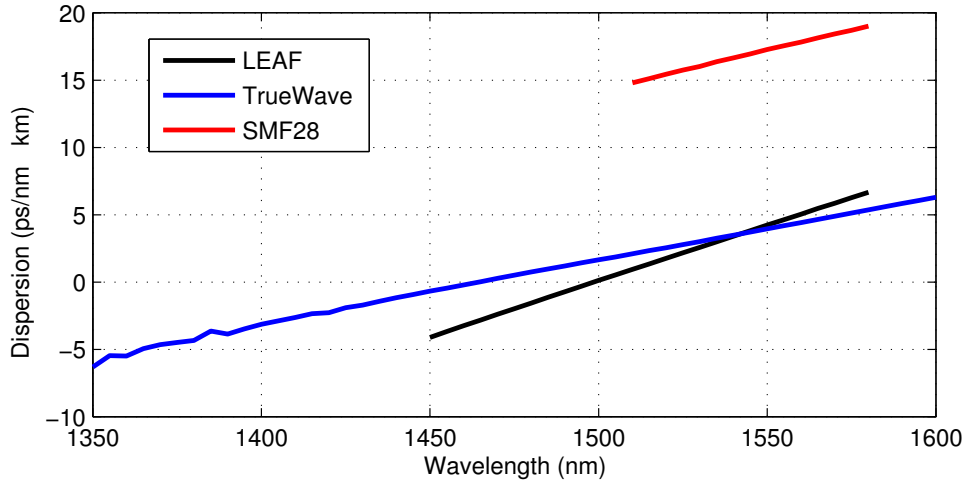

Figure 4.5: Measured dispersion slope in SMF-28, LEAF and TrueWave fibres

Table 4.1: Raman pump powers and fibre parameters

	SMF28	DCF	TrueWave	LEAF
Power per Pump (W)	1.1	0.6	1.0	0.9
Zero Dispersion Wavelength (nm)	1310		1460	1500

Dispersion properties of NZ-DSF fibre can also have destructive impact on DRA due to FWM (54, 136, 137). In higher order broadband DRA zero dispersion wavelength λ_0 should not be located between pump wavelengths to avoid strong pump-pump FWM effect (138, 139). In DRA configuration with forward pumping

pump-signal FWM is most effective for λ_0 located between the pump and the signal bands (140, 141, 142) therefore should be avoided.

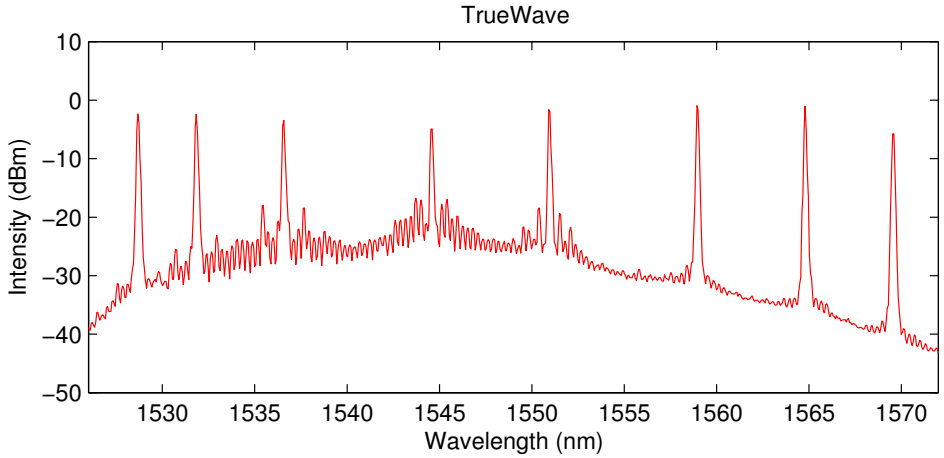

Figure 4.6: The performance of TrueWave fibre in 2nd order URFL based amplifier

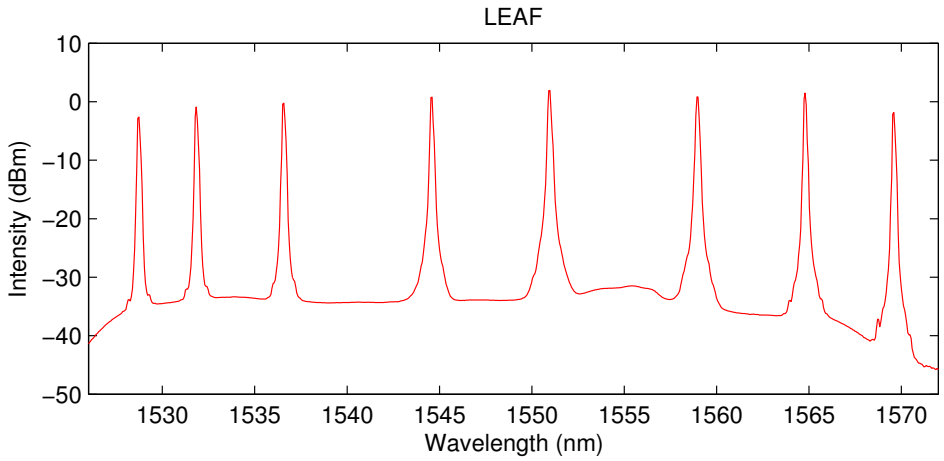

Figure 4.7: The performance of LEAF in 2nd order URFL based amplifier

Dispersion compensating fibre (DCF), TrueWave, LEAF and standard SMF-28 with it's dispersion slopes measured and plotted in Fig. 4.5 has been tested in 2nd order bidirectional URFL based amplifier (schematic design in Fig. 4.3) with symmetric launch pump power ratios listed in Table 4.1. The 8 channel grid with total bandwidth over 40 nm and 0 dBm of input power per channel was spread across C-band. The span length in each experiment was 60 km with the same

pair of FBGs centred at 1455 nm. Secondary pump wavelength was at 1366 nm. The difference in total pump power in each span comes from different effective area A_{eft} which is directly related to Raman gain coefficient. In each experiment the pump powers were set to allow quasi-lossless transmission.

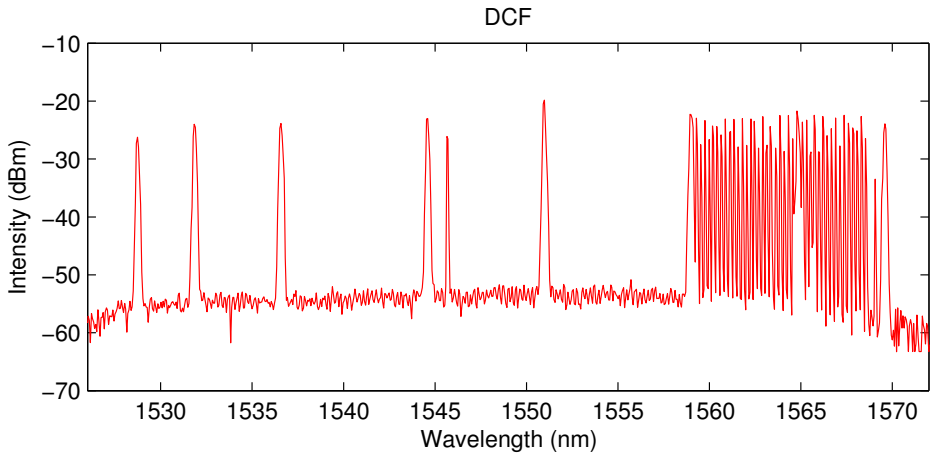

Figure 4.8: The performance of DCF in 2nd order URFL based amplifier

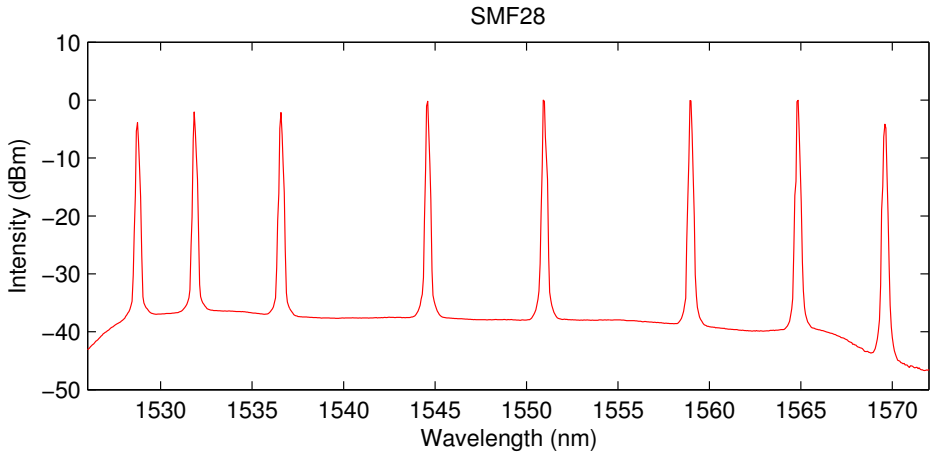

Figure 4.9: The performance of SMF-28 in 2nd order URFL based amplifier

Both NZ-DSF (Fig. 4.6 and Fig. 4.7) are unsuitable for the URFL based amplification due to zero dispersion wavelengths located between the initial secondary pump wavelength, Stokes and the signal which leads to strong pump-pump and pump-signal FWM effect.

Dispersion compensating fibres (Fig. 4.8) have a high attenuation at the signal wavelength therefore are unsuitable for the transmission medium on it's own. The sparks at the higher wavelengths in Fig. 4.8 are the result of high Raman gain in DCF fibre where the 3rd Stoke begins to create. The aim of the experiment was to check if it's possible to use DCF as a medium for discreet URFL Raman amplifier and to compensate for the dispersion in long unrepeatered direct detection transmission.

It was not possible to compensate the loss of 60 km DCF fibre using 2nd order bidirectional URFL based amplification which makes it unsuitable to be used as a medium in URFL amplifier.

Standard SMF-28 (Fig. 4.9) was the most suitable fibre for the URFL amplifier therefore has been chosen for further experiments to investigated FBGs and optimisation process of the rest of the components.

4.2.2 Fibre Bragg Gratings

The gain profile in novel URFL based amplifier can be optimised by selecting appropriate FBGs with respect to the source pump wavelength. The choice of FBGs will have an impact on on-off gain as well as gain flatness and gain bandwidth. With a fixed pump at 1366 nm the wavelength of FBGs should be chosen by taking into account the transmission distance and total bandwidth of WDM grid used in the experiment.

To optimise the gain profile for unrepeatered (up to 360 km) OSNR and on-off gain measurements, two sets of FBGs (Fig. 4.10) centred at 1448 nm (black) and 1458 nm (red) has been tested in 320 km SMF-28 span using configuration as in Fig. 4.3. The first peak at 1366 nm in Fig. 4.10 is a source pump. The broadband gain of distributed Raman amplification with peak downshifted by approximately 13 THz is visible in 1450 nm region. The peak in 1450 nm region is the Stokes shifted light reflected by the cavity created by the pair of gratings at 1448 nm (black) and 1458 nm (red) respectively. The reflected light acts as a virtual primary pump and amplifies the signal in 1550 nm region (Fig. 4.11).

The 360 km span loss was 72 dB, therefore primary target of the optimisation was evenly distributed high gain across C-band rather than gain bandwidth

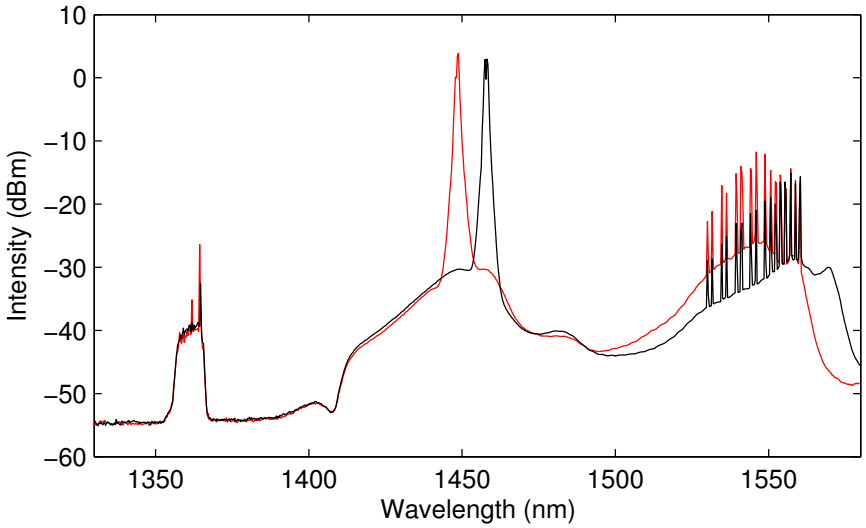

Figure 4.10: Comparison of FBGs at 1448nm (red) and 1458nm (black)

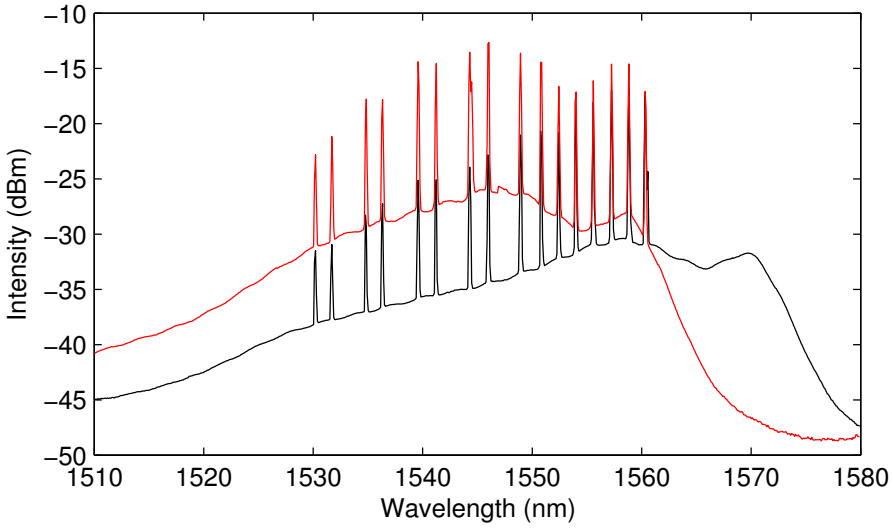

Figure 4.11: Comparison of FBGs at 1448nm (red) and 1458nm (black)

extension. The results in Fig. 4.10 and Fig. 4.11 shows that lower wavelength set of FBGs at 1448 nm (red) provides higher on-off gain and better gain flatness across the WDM grid used in the experiment therefore have been chosen. The FBGs centred at 1458 nm are more suitable for shorter span lengths due to improved gain flatness with lower pump powers and extended gain bandwidth

towards L-band by approximately 11 nm.

4.2.3 Forward and Backward Pump Power Distribution

The Raman pump power distribution in bidirectional pumping is related to span length. In short links with relatively small pump powers required for quasi-lossless transmission, symmetric pumping will give the best gain distribution across the span with a small power variation (5, 126, 129). The accumulated ASE can be further reduced by pushing the gain into beginning of the span which will prevent signal decay. Increased forward pumping will result in improved noise figure, however, care must be taken to balance off the benefits of higher OSNR and possible disadvantage imposed by Rayleigh scattering and nonlinear effects (7).

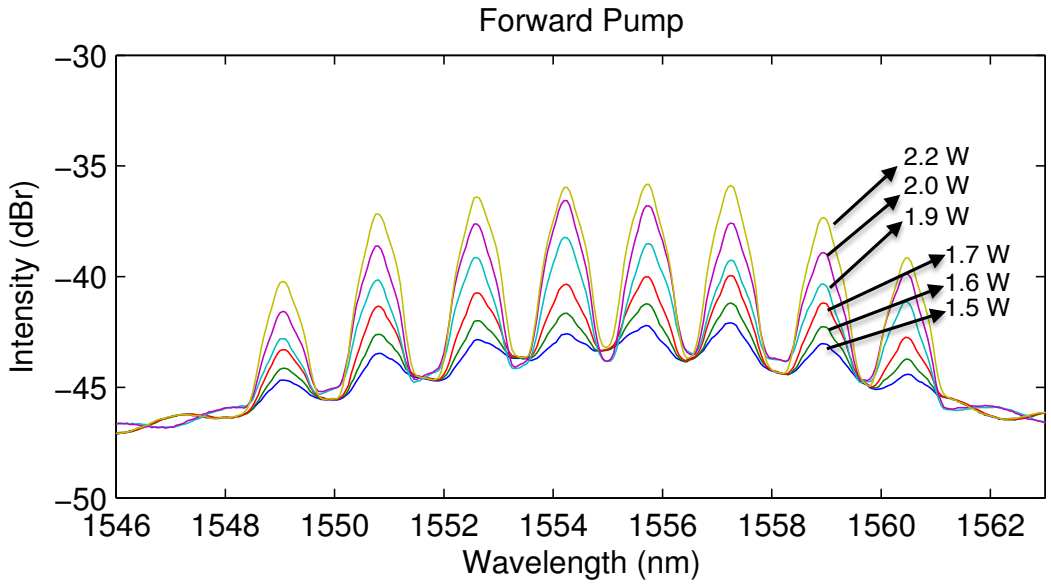

Figure 4.12: Experimental results of forward pump power optimisation in 320 km SMF-28 link.

The experimental results of forward and backward pump influence on received OSNR and on-off gain measured in 320 km span are shown in Fig. 4.12 and 4.13. We can notice OSNR improvement with increased forward pump power.

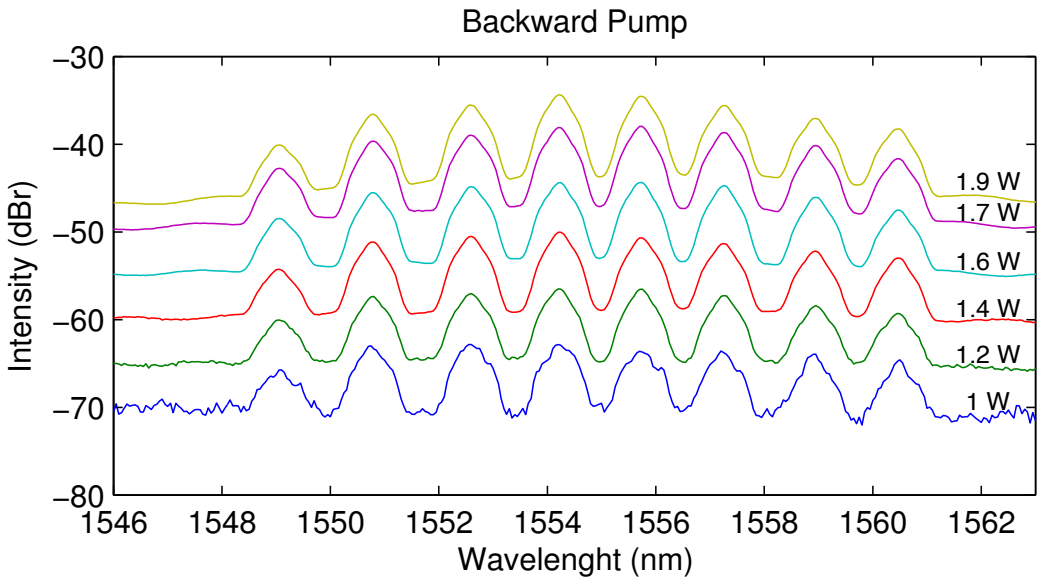

Figure 4.13: Experimental results of backward pump power optimisation in 320 km SMF-28 link.

Improved received OSNR with forward pumping configuration can benefit repeatered systems by extending the reach between the repeaters (97) as well as higher the distance in unrepeatered transmission (130).

Backward pumping in DRA can benefit the system by pushing the gain further into the span at the received end. In Fig. 4.13 we can notice the gain dependance with increased backward pump power.

The optimal pump power ratio between co- and counterpropagating pumps is system specific and depends on fibre type which will decide on best trade off between both. Large effective area fibres allows for higher launch powers, therefore nonlinearities from forward pumping will be reduced.

Experimental forward and backward pump power optimisation in 320 km SMF-28 link as a function of bit error rate (BER) in 8 × 42.7 Gb/s DPSK transmission with direct detection, measured for the best performing channel is in Fig. 4.14. For the best BER the possible forward pump power adjustment is restricted to 100 mW of an optical power. The flexibility of backward pump power is much higher and can be varied by 450 mW. The best performance in terms of BER was the split ration of 55% and 45% for forward and backward pump

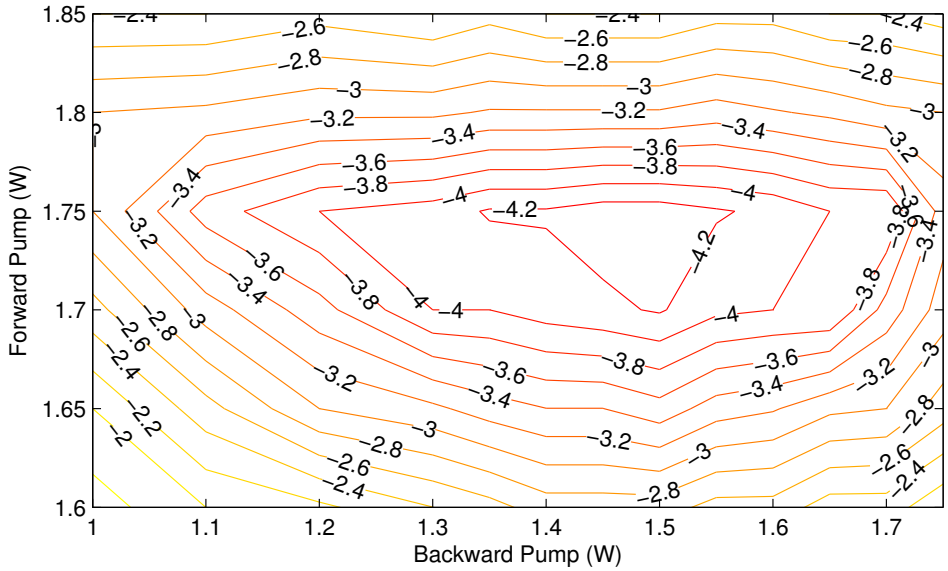

Figure 4.14: Experimental results of forward and backward pump power optimisation in 320 km link as a function of BER of the best performing channel in 8 × 42.7 Gb/s DPSK transmission with direct detection

respectively. However, this ratio might be misleading as the backward pump would have to be pumped harder if there was no post EDFA amplification in the system design due to 100% post dispersion compensation. The optimisation of bidirectionally pumped DRA are proposed in Ref. (108, 143) where both authors agree that best performance is achieved with lower forward pump powers in range of 30-50%.

4.2.3.1 Gain Profile

The gain profile in URFL based amplifier depends to a great degree on the properties of FBGs with respect to the initial secondary pump wavelength. With a pump wavelength at 1366 nm and FBGs with a bandwidth of 0.5 nm centred at 1455 nm gain profile will be determined by the on-off Raman gain which will increase with distance.

Fig. 4.15 shows the gain profile measured in 82 km SMF-28 span. In this symmetric bidirectional configuration the power per pump was varied from 0.5 W

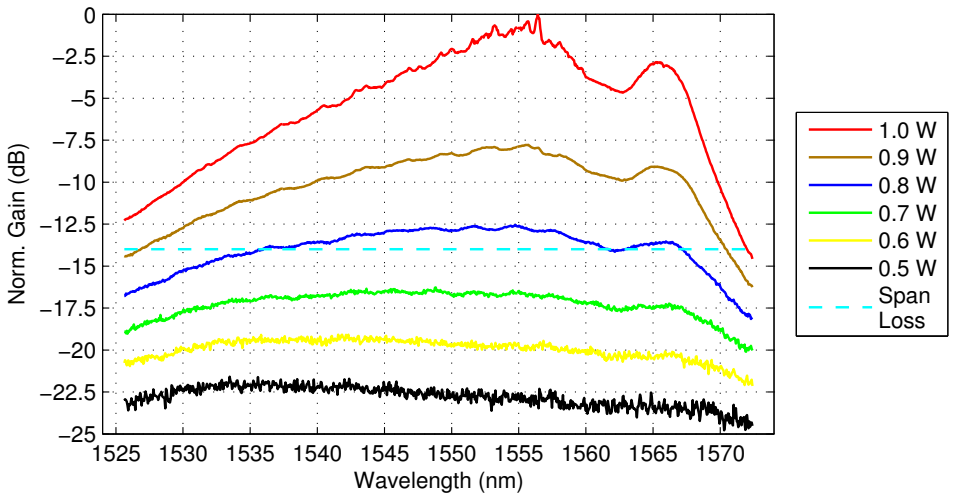

Figure 4.15: Experimental results of Raman gain profile in 82 km URFL based amplifier with symmetrical pump power distribution.

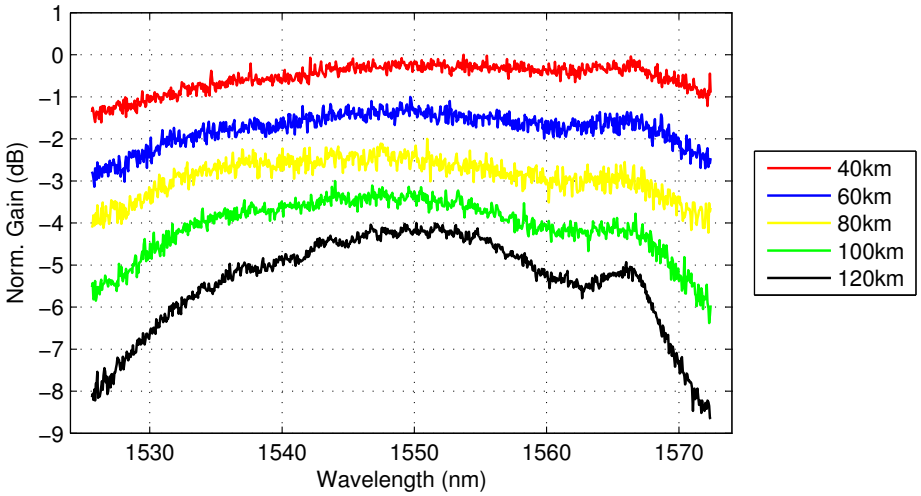

Figure 4.16: Measured URFL gain profile with different span lengths. The pump power ratio was split symmetrically for the best gain distribution in quasi-lossless transmission. For clarity the plot for each distance was shifted not to overlap.

to 1 W. The 16 dB span loss (dashed light blue) was fully compensated with 0.8 W (blue) per pump providing 40 nm broadband gain bandwidth with less than 2.5 dB gain ripple. This figure has been achieved without any gain flattening filter, with raw Raman pumps only as in schematic design in Fig. 4.1. The gain flatness

degradation is most prominent at the longer wavelength region and decreases sharply with increased on-off gain.

The gain bandwidth can be slightly extended towards L-band by employing higher wavelength FBGs with the expense of overall on-off gain as shown in Fig. 4.11.

Gain profile spectra in different span lengths ranging from 40 km to 120 km is in Fig. 4.16. In this experiment span loss for each length was fully compensated with symmetric bidirectional pumping to permit transparent link, however, to improve clarity of the graph, the spectra for each span were intensionally shifted by 1 dB with respect to each other. The Raman gain spectrum is more pronounced in longer spans due to increased on-off gain required to counterbalance the attenuation.

4.2.3.2 Gain Distribution

The signal power variation across the span length decreases with higher order pumping. In relatively short length URFL based amplifier, truly distributed gain can be realised with symmetric bidirectional pumping (5, 144). This configuration may turn the transmission span into a virtually lossless medium by reducing the effective gain loss. The main advantage of the quasi-lossless transmission over lumped amplification is improved noise figure by a factor of 3 dB (145).

Table 4.2: Pump Powers in Quasi-lossless configuration

Distance (km)	Forward Pump (dBm)	Backward Pump (dBm)
80	26.4	30.9
100	29.7	31.3
120	30.7	31.8

The power distribution along transmission fibre has been measured for a single channel in the middle of C-band at 1550 nm with a modified optical time-domain reflectometer (OTDR). The signal distribution for 80 km, 100 km and 120 km in quasi-lossless transmission is shown in Fig. 4.17 and Fig. 4.18. The smooth solid

line in each spectra is a simulation fit to the experimental data. There is only 1.4 dB power variation for 80 km span, 2.5 dB and 4.4 dB for 100 km and 120 km respectively. Pump powers used in experiment are in Table 4.2.

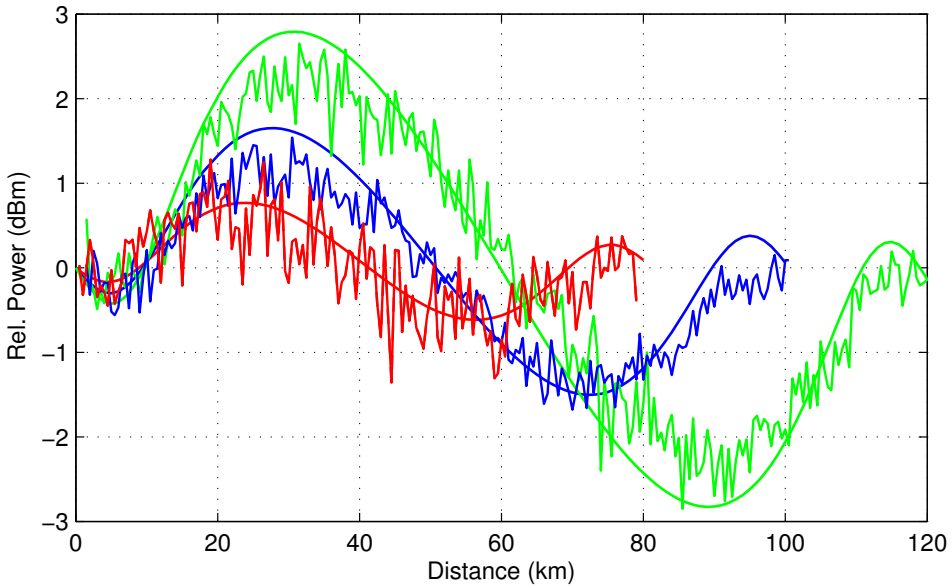

Figure 4.17: Experimental (rough) and simulation (smooth) results of signal power distribution in quasi-lossless transmission measured with modified OTDR for the span length of 80 km (red), 100 km (blue) and 120 km (green).

The symmetric sinusoidal power distribution detritus with increased span length as the loss cannot be fully compensated. The numerical simulations (5, 146) in Fig. 4.19 - 4.22 shows uneven signal power distribution in 280 km, 320 km, 340 km and 360 km links due to fibre loss and double Rayleigh backscattering. The signal power variation along these spans increases to 37 dB , 46 dB, 49 dB and 53 dB for 280 km, 320 km, 340 km and 360 km respectively.

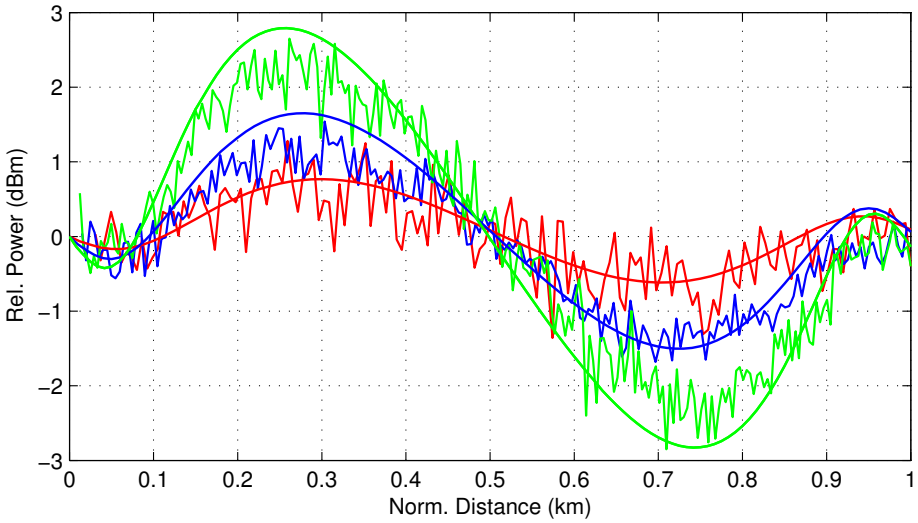

Figure 4.18: Experimental (rough) and simulation (smooth) results of signal power distribution in quasi-lossless transmission measured with modified OTDR for the span length of 80 km (red), 100 km (blue) and 120 km (green). The distance was normalised.

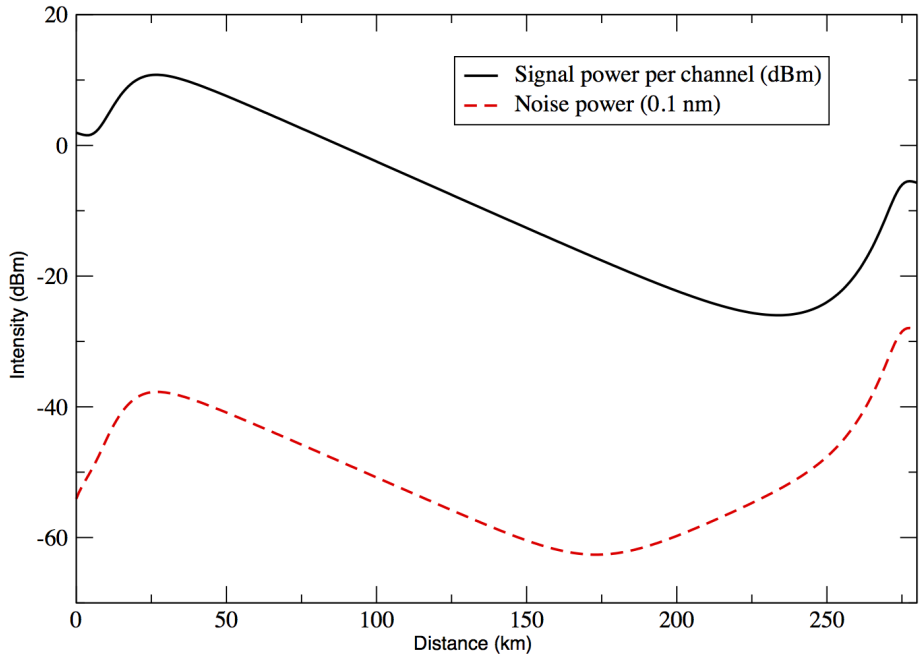

Figure 4.19: Simulation results of signal distribution in 280 km link

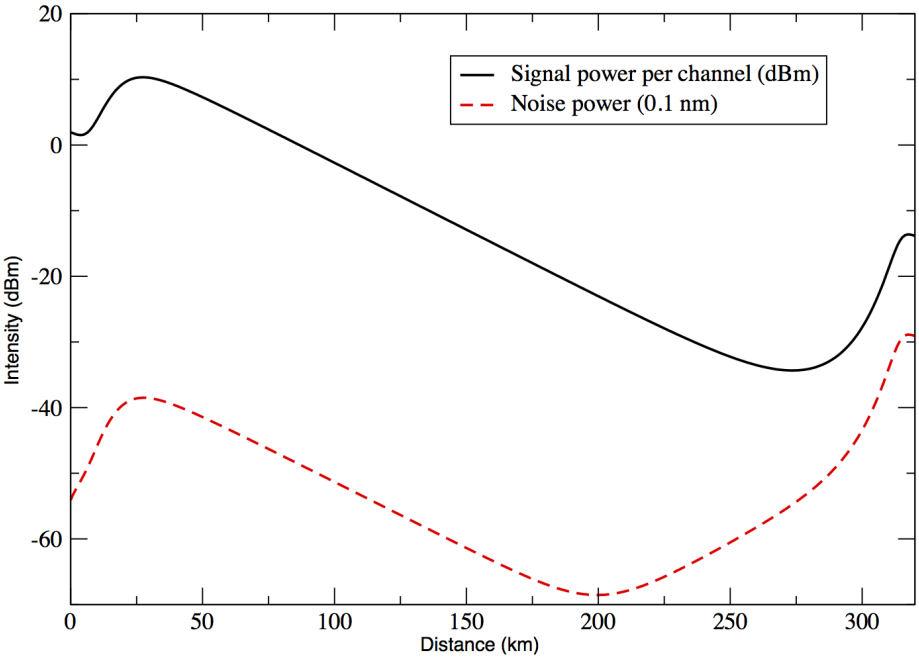

Figure 4.20: Simulation results of signal distribution in 320 km link

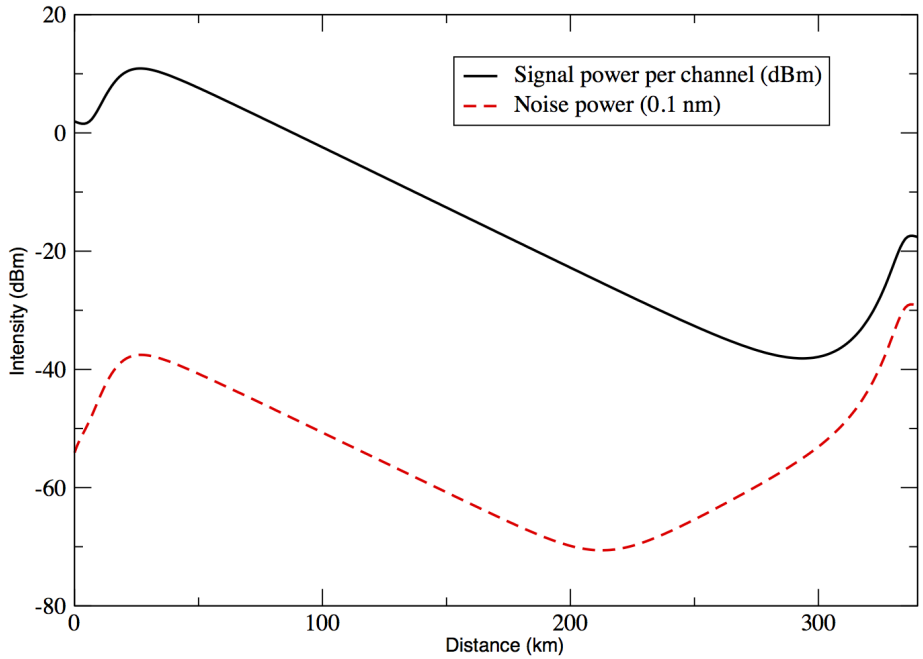

Figure 4.21: Simulation results of signal distribution in 340 km link

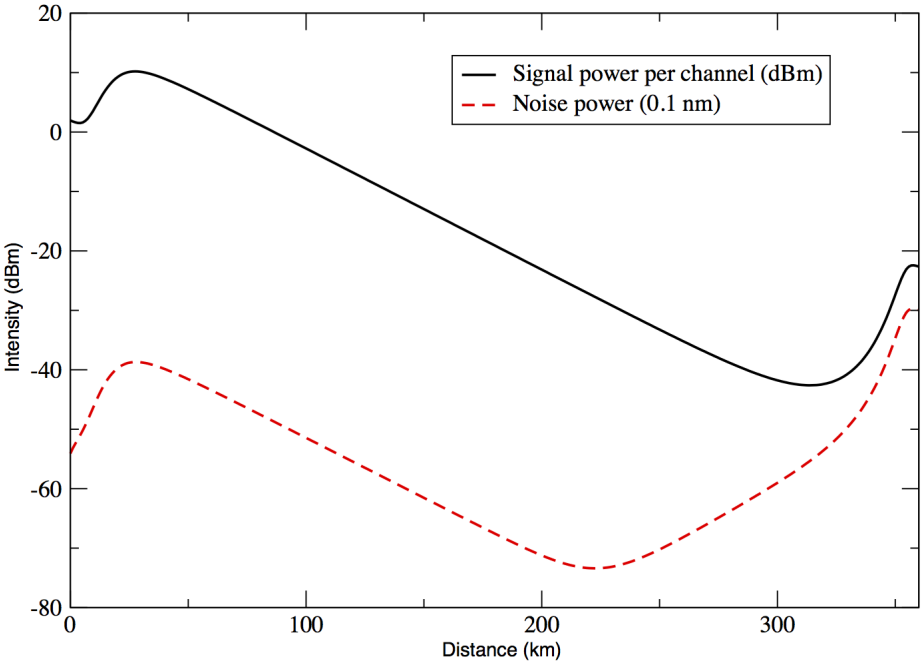

Figure 4.22: Simulation results of signal distribution in 360 km link

4.3 On-Off Gain

Improved noise figure (147), extended gain bandwidth (92, 94, 119) and improved gain flatness (119) which can be accomplished by combining several pump wavelengths are the major benefits of Raman amplifiers. Distributed amplification allows for signal to be amplified at the distance from the fibre end where the pump is launched which improves received OSNR. Higher order DRA can push the gain further into the medium. This attribute allows for high distance unrepeatered submarine systems which makes use of ROPA and low loss speciality fibres. High on-off gain in Raman fibre laser amplifiers can extend the system reach with standard fibres and single pump wavelength.

The on-off gain in URFL based amplifier has been measured for span lengths up to 360 km. Total launch powers used in the experiments were 0 dBm, 5 dBm, 10 dBm and 14 dBm (Fig. 4.4). Pump powers used in the experiment which were optimised for best gain profile across C-band are listed in Table 4.3 at the end of the chapter.

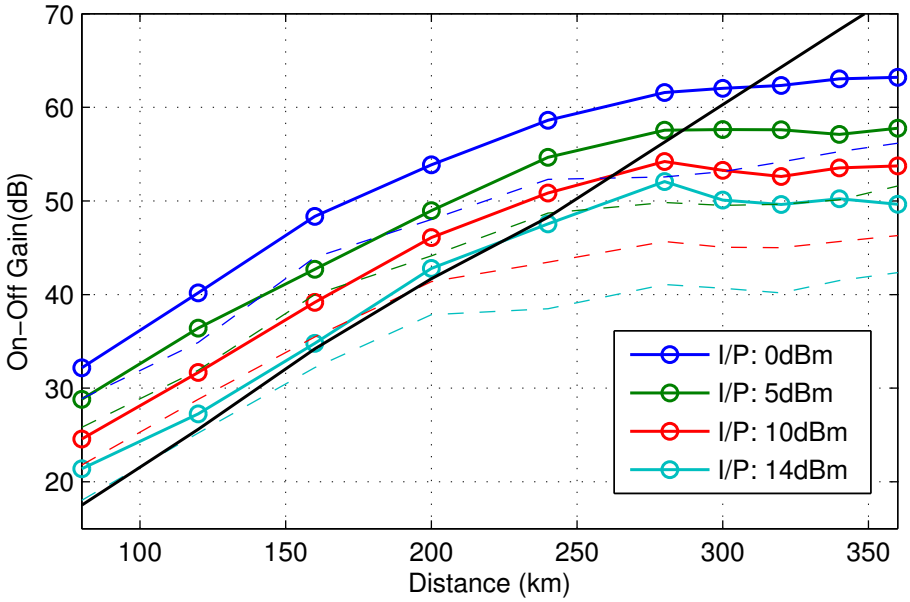

Figure 4.23: Experimental results of on-off gain measurement as a function of distance. All 16 channels were measured. For the transparency only the best (solid) and the worst (dashed) channels are plotted

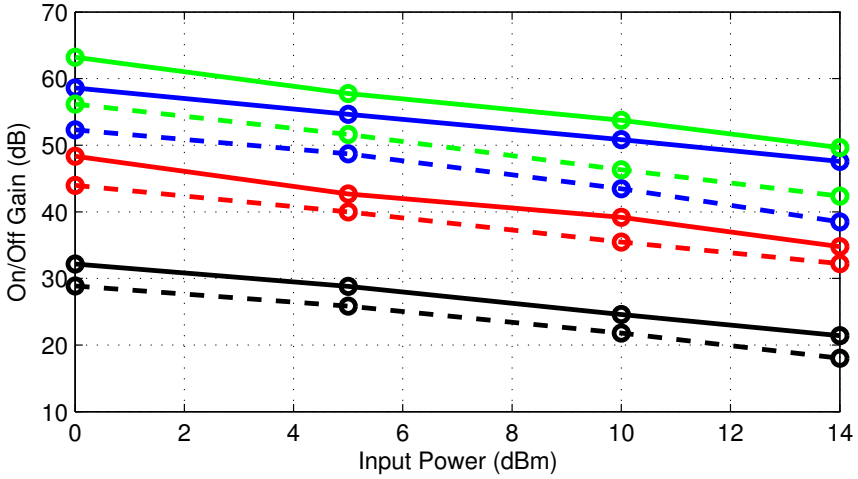

Figure 4.24: Experimental results of on-off gain measurement as a function of I/P for 80 km (black), 160 km (red), 240 km (blue) and 360 km (green). All 16 channels were measured. Only the best (solid) and the worst (dashed) channels are plotted.

The results (Fig. 4.23) show the best (solid line) and the worst (dashed line) performing channel. The black line is a measured fibre loss for each span length. The maximum on-off Raman gain achieved for the best performing channel was 64 dB. We can notice that for low launch power, span loss up to 280 km can be fully compensated. With increased input to 14 dBm the fibre loss could be compensated only up to 200 km. The gain dependance of a launch power for 80 km (black), 160 km (red), 240 km (blue) and 360 km (green) is plotted in Fig. 4.24. In all scenarios the highest gain was achieved for the lowest launch powers. The increased difference between best and worst performing channels in higher distances is due to residual channels.

4.4 OSNR

OSNR is typically defined as the ratio of the average optical signal and ASE power within nonzero bandwidth:

$$OSNR = \frac{P_{out}}{P_{ASE}}, \tag{4.1}$$

where P_{out} is the received signal power and P_{ASE} is the power of the amplified spontaneous emission within bandwidth B_m approximated by

$$P_{ASE} \approx 2n_{sp}hv(G-1)B_m, \tag{4.2}$$

where v is the optical frequency of the noise, G is the gain and n_{sp} is the spontaneous emission factor. In Raman amplifier n_{sp} is defined as (148)

$$n_{sp} = \frac{1}{1-e^{-hv_s/kT}} \tag{4.3}$$

where v_s is the frequency difference between pump and the signal. Substituting Eq. 4.2 into Eq. 4.1 where $P_{out} = P_{in}G$ we get

$$OSNR = \frac{GP_{in}}{2n_{sp}hv(G-1)B_m} \tag{4.4}$$

$$\approx \frac{P_{in}}{2n_{sp}hvB_m} \tag{4.5}$$

This definition, however, does not include nonlinear noise and pump-signal RIN transfer which are important factors in noise generation in high power Raman amplifiers. Measured OSNR in this section is defined as the ratio of the peak power of the signal and the noise power measured on OSA within 0.1 nm resolution bandwidth and sensitivity of -70 dB.

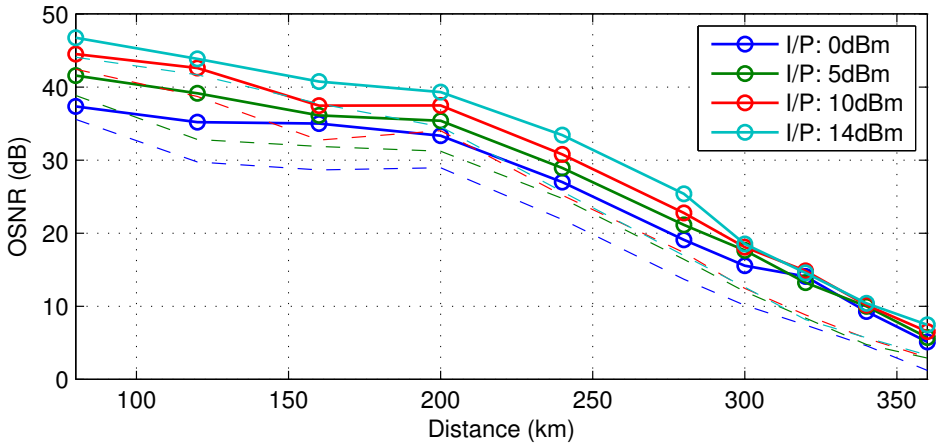

Figure 4.25: Experimental results of the OSNR measurements. All 16 channels were measured. For clarity only the best (solid) and the worst (dashed) channels are plotted.

The OSNR was measured for every channel in WDM grid as in Fig. 4.4. The best (solid line) and the worst (dashed line) performing channels are plotted as a function of distance in Fig. 4.25. The launch powers in the experiment were 0 dBm, 5 dBm, 10 dBm and 14 dBm. Simulation results (146) for a single channel in the middle of the C-band of 14 dBm grid at 1550 nm are plotted together with the experimental results for best and worst performing channels in Fig 4.26. There is a great agreement between simulation and experimental results.

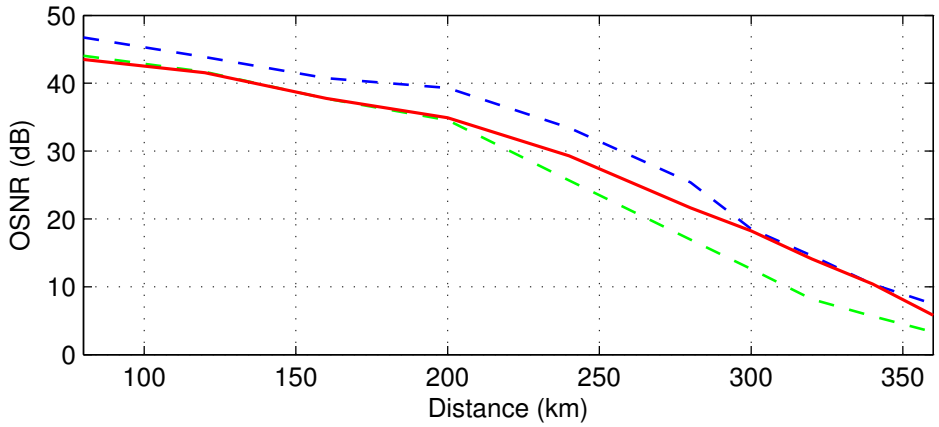

Figure 4.26: Simulation results (red) of OSNR measured for a single channel in the middle of the 14 dBm grid. Dashed lines are experimental results for the best (blue) and worst (green) performing channel.

The signal degradation for the span lengths up to 200 km is relatively small, however, there is a sharp decline in OSNR for higher distances, reaching value of less than 7 dB for 360 km which is critical even for low level modulation formats. In URFL based amplification technique the distance of 360 km using standard SMF-28 fibre appears to be a limit for unrepeatered data transmission.

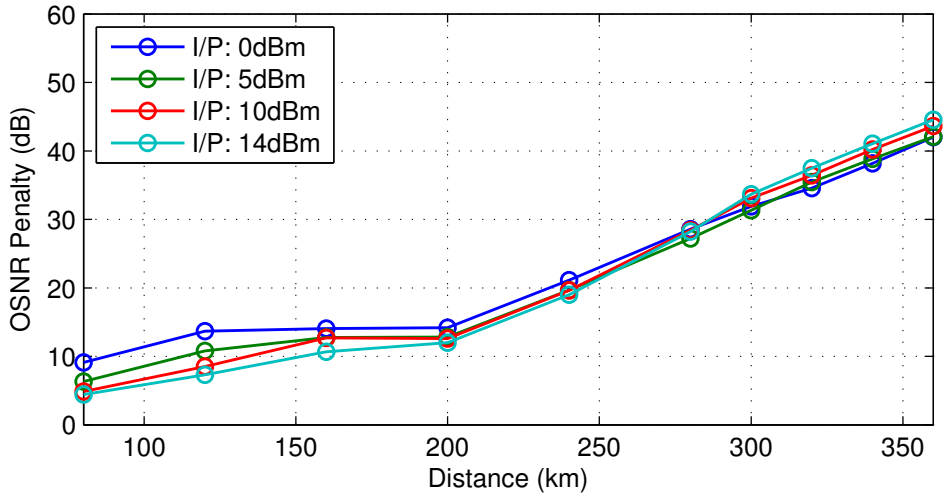

Figure 4.27: OSNR penalty as a function of distance. All 16 channels were measured. For clarity only the best performing channels are plotted.

OSNR penalty defined as the difference between transmitted and received OSNR at the end of the span is plotted in Fig. 4.27. In Fig. 4.28 we can observe OSNR penalty as a function of an average on-off gain based on 16 channel count. For each launch power measured the penalty increases sharply with the span length longer than 200 km.

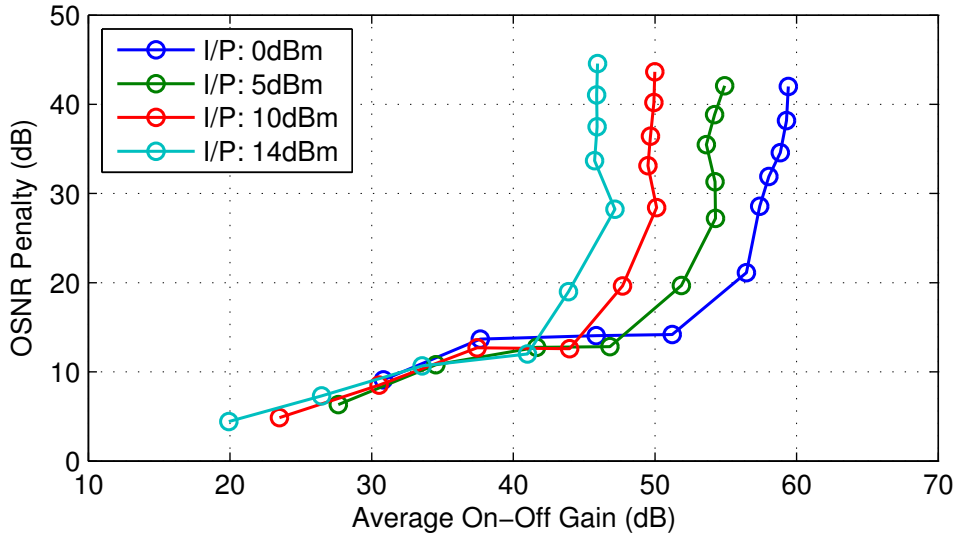

Figure 4.28: OSNR penalty as a function of distance (top) and on-off gain (bottom) for launch powers of 0 dBm (blue), 5 dBm (green), 10 dBm (red) and 14 dBm (cyan). All 16 channels were measured. For clarity only the best performing channels are plotted.

The benefit of improved noise figure in distributed Raman amplifiers where gain is distributed along the fibre (147) and hybrid Raman/EDFA (148) allows for higher reach between the repeaters as well as record distances in unrepeatered systems (130, 149).

4.5 Comparison of EDFA and URFL based amplification

The choice of amplifier in optical network design depends on the application. High pump efficiency (82) makes EDFA an attractive amplifier for urban deployment. Long distance single hop transmission requires distributed amplification which are not suitable for EDFA configuration due to required low loss speciality erbium doped fibre (150). Raman amplification has number of advantages over EDFA in terms of physical performance, however, the implementation costs makes it hard to be commercialised.

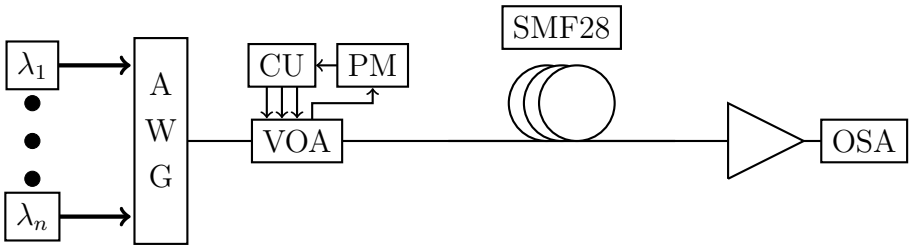

Figure 4.29: Schematic diagram for EDFA configuration. The FBGs in the scenario are passive. Total input power into the span is digitally controlled by VOA connected to control unit (CU) and calibrated power meter (PM).

Important advantage of Raman based amplifiers is improved OSNR. If we refer to the approximated OSNR equation (Eq. 4.5) we can see that the only parameter which will change for the same system setup is spontaneous emission factor n_{sp}. Using Eq. 4.3 with the parameters $v_s = 13.2$ THz and temperature $T = 300$ K the n_{sp} factor for Raman amplifier is ≈ 1.14. In EDFA n_{sp} depends on the pumps wavelength and pumping rate and may vary from 1.4 - 4 with a typical value of ≈ 2 (151). Substituting n_{sp} for EDFA and Raman amplifier in Eq. 4.5 we can verify that received OSNR is approximately 3 dB better in Raman.

URFL based amplification is experimentally compared with EDFA in 82 km span. Bidirectional URFL (Fig. 4.3) configuration was symmetrically pumped whereas EDFA (Fig. 4.29) was optimised for the best gain flatness performance for transparent transmission of an unmodulated 16 channel grid. In Fig. 4.30

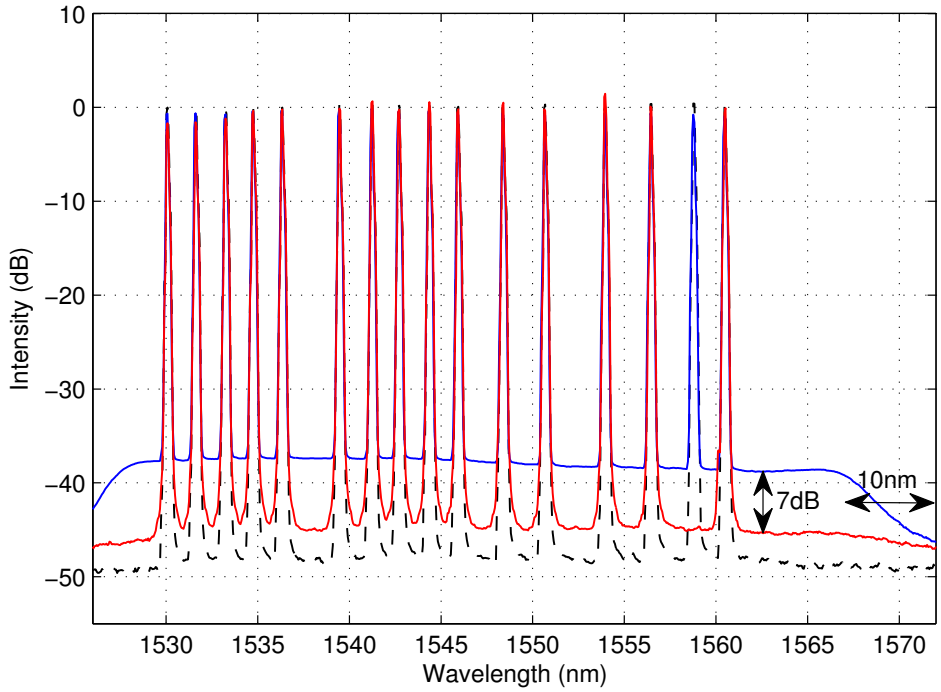

Figure 4.30: Received optical spectra after 82 km SMF span using EDFA (blue) and URFL (red) based amplifier with the input (dashed black) of 0 dBm per channel. The resolution bandwidth in OSA was 0.1 nm

we can see received optical spectra after 82 km SMF-28 span using EDFA (blue) and URFL based amplifier (red) with the initial input (dashed black) of 0 dBm per channel. The fibre loss was fully compensated in both amplification methods across the whole band used with the total peak to peak gain flatness variation of 3 dB in URFL and 1 dB in EDFA case. No gain equalisation filters were used in URFL based amplifier. There is over 10 nm of bandwidth extension and 7 dB OSNR improvement in URFL based amplifier. The noise floor spectra for different launch powers for both amplifiers are plotted in Figs. 4.32 - 4.35

In Fig. 4.31 received OSNR at the end of the span for the best (solid) and the worst (dashed) performing channels is compared with EDFA and URFL based amplifier as a function of input power per channel with 1 dBm step. There is over 10 dB OSNR improvement with URFL for most of the input powers measured. The figure decreases slightly with higher input powers. Unsymmetrical pumping

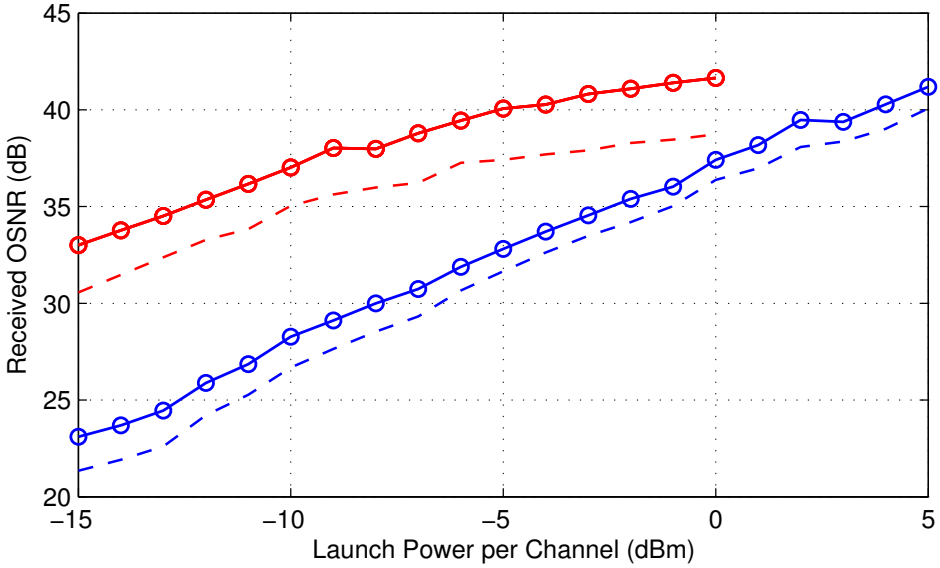

Figure 4.31: Received OSNR in 82 km span using EDFA (blue) and URFL (red) based amplifier as a function of the input power per channel. The resolution bandwidth in OSA was 0.1 nm

with emphasised forward pump can further increase received OSNR with the expense of higher nonlinear effects.

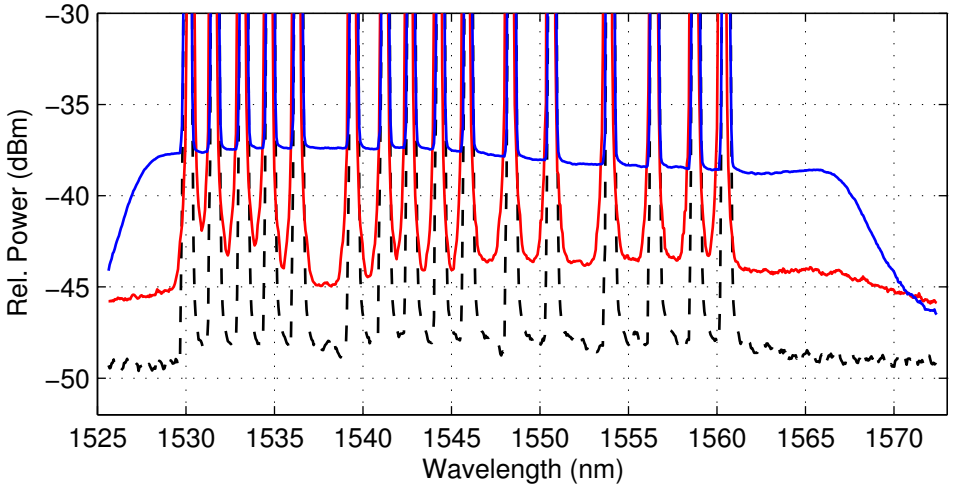

Figure 4.32: Noise floor comparison for I/P of 0 dBm per channel in 82 km link. Blue: EDFA; red: URFL; dashed black: 0 dBm input

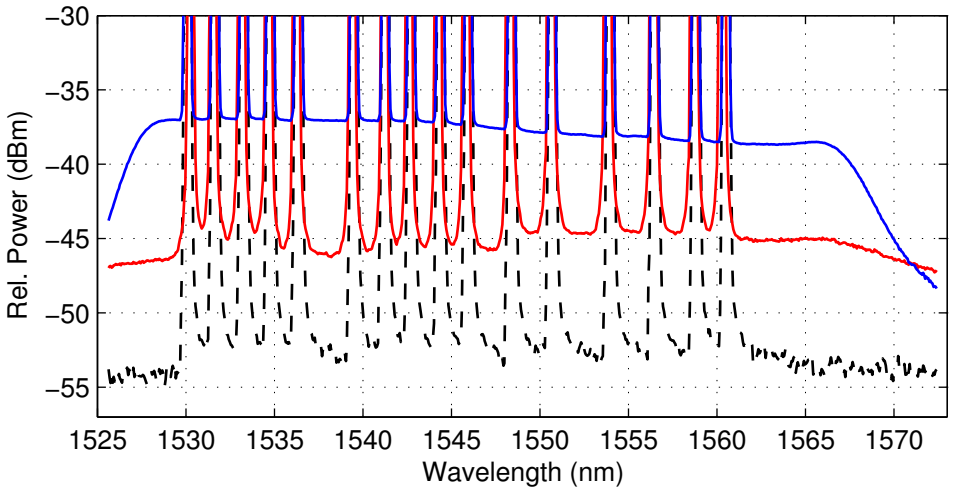

Figure 4.33: Noise floor comparison for I/P of -5 dBm per channel in 82 km link. Blue: EDFA; red: URFL; dashed black: -5 dBm input

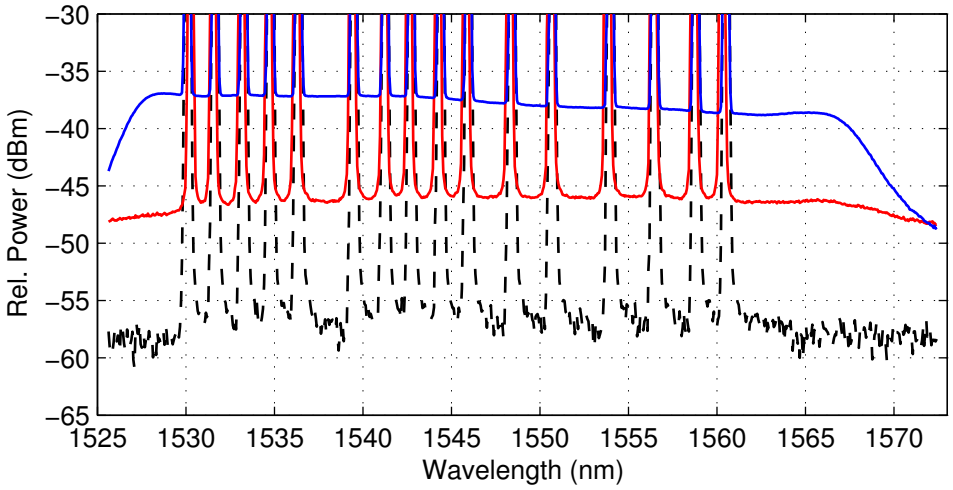

Figure 4.34: Noise floor comparison for I/P of -10 dBm per channel in 82 km link. Blue: EDFA; red: URFL; dashed black: -10 dBm input

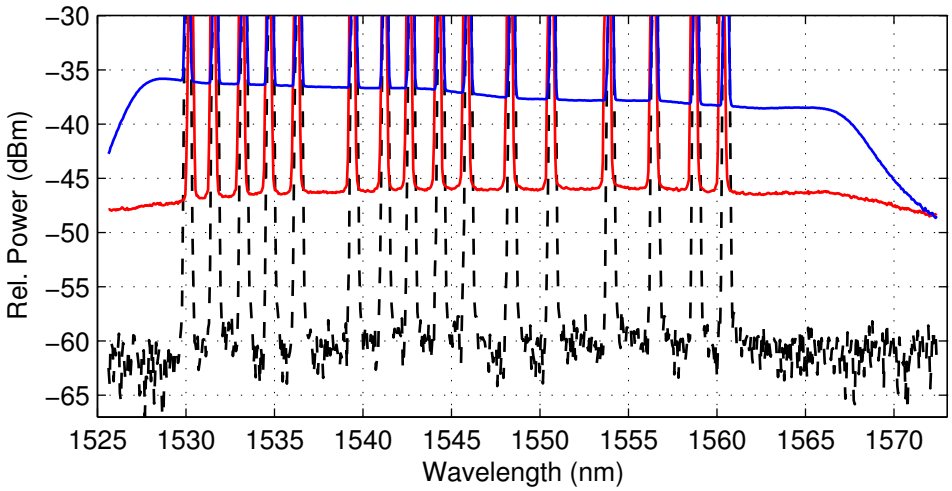

Figure 4.35: Noise floor comparison for I/P of -15 dBm per channel in 82 km link. Blue: EDFA; red: URFL; dashed black: -15 dBm input

Raman and hybrid Raman/EDFA amplification can improve transmission performance of WDM systems (152, 153). In ROPA higher order backward Raman pump amplifies the signal by delivering optical power to piece of erbium doped fibre located about 100 km (depending on the pump order and the fibre type) from the front or end of the span (or both). This configuration combined with ultra low loss fibres led to record distances in unrepeatered transmissions up to 601 km 1 × 10 Gb/s RZ-DPSK (154), 500 km 1 × 100 Gb/s PDM-QPSK (155) and 401 km 26 × 100 Gb/s PDM-QPSK (156). In hybrid Raman/EDFA design 365 km transmission of 40 × 112 Gb/s was achieved (157).

Table 4.3: Forward and Backward Raman Pump Powers

	I/P: 0 dBm		I/P: 5dBm		I/P: 10 dBm		I/P: 14 dBm	
D	P_F	P_B	P_F	P_B	P_F	P_B	P_F	P_B
(km)	(dBm)							
80	26.4	30.9	26.4	31.1	26.9	31.4	27.2	31.5
120	29.7	31.3	29.8	31.6	29.9	31.9	30.2	32.0
160	30.7	31.8	30.9	32.1	31.1	32.2	31.3	32.3
200	31.8	31.9	31.8	31.9	31.8	31.9	32.0	32.2
240	32.1	32.1	31.9	32.2	31.9	32.4	32.1	32.5
280	32.1	32.4	31.9	32.5	31.9	32.5	32.0	32.5
300	32.1	32.4	31.8	32.5	32.1	32.5	32.2	32.5
320	32.1	32.4	31.9	32.4	32.1	32.4	32.4	32.4
340	32.1	32.4	31.9	32.4	32.0	32.4	32.4	32.4
360	31.0	32.4	31.9	32.4	32.0	32.4	32.2	32.4

Chapter 5

Data Transmission

The information in fibre optic communication systems can be transmitted by modulating data onto a carrier using intensity modulation where the optical signal is switched on and off using a simple binary code. The data throughput using this method can be extended by increasing the rate at which symbols are being modulated onto a single optical carrier. This approach, however, is limited by the speed of optoelectronics currently deployed as well as physical properties of the signals modulated with very high rate.

Directly modulated lasers (DML) (158, 159), Electro-absorption (EAM) (160, 161) and most commonly used (162) Mach-Zehnder modulators (MZM) (163, 164) are examples of modulator technologies supporting binary data rates up to 80 Gb/s (160) and 112 Gb/s demonstrated in 40 km field transmission (165). The schematic diagram of dual-drive MZM modulator is in Fig. 5.1.

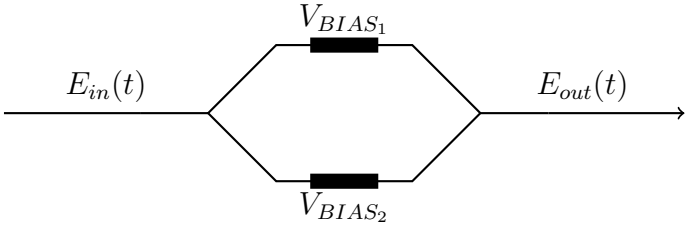

Figure 5.1: Dual-drive Mach-Zehnder modulator

The optical output $E_{out}(t)$ of an ideal dual-drive Mach-Zehnder modulator (Fig. 5.1) is given by (166):

$$E_{out}(t) = \frac{E_{in}(t)}{2}\left[exp\left(j\frac{\pi}{V_\pi}(v_1(t) + V_{BIAS_1})\right) + \left(j\frac{\pi}{V_\pi}(v_2(t) + V_{BIAS_2})\right)\right] \quad (5.1)$$

where V_π is the intensity switching voltage, $v_1(t)$ and $v_1(t)$ are the drive voltages whereas V_{BIAS_1} and V_{BIAS_2} are the bias voltages.

The amplitude in OOK modulation format is changed by impressing a voltage on one side of the MZM to change the optical path length to a half cycle. At the output of the MZM, where the waveforms from both sides are recombined, the optical power is hight for binary *1* or low for binary *0*.

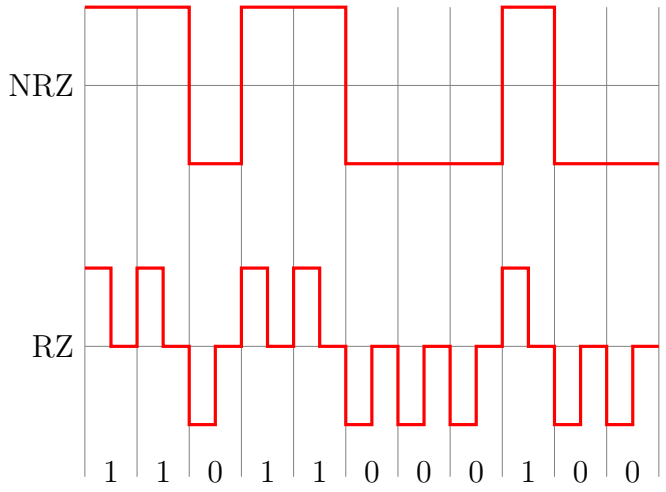

Figure 5.2: NRZ (top) and CSRZ (bottom) coding techniques

The optical pulses can *return-to-zero* (RZ) within each bit slot or *not-return-to-zero* (NRZ) carrying the intensity over several bit slots. Although less bandwidth efficient and more complex in design, RZ singling is more robust to fibre nonlinearities (167). To generate RZ pulses an additional modulator is required for data rates of 40 Gb/s and above. MZM based pulse carver can drive the signal at the data rate between it's minimum and maximum (50% duty cycle) or

at half the data rate at it's maximum (33% duty cycle) or minimum (67% duty cycle) transmission (Fig. 5.3). In carrier-suppressed return-to-zero (CSRZ) (168) format the sign of the optical field is reversed at each bit transition resulting in zero-mean optical field envelope. The phase of a signal can be modulated by implementing additional phase modulator which would generate chirped (CRZ or C-NRZ) modulated signal. The advantage of CRZ is that of increased resistance to nonlinearities which makes it most suitable for high capacity optical links (169).

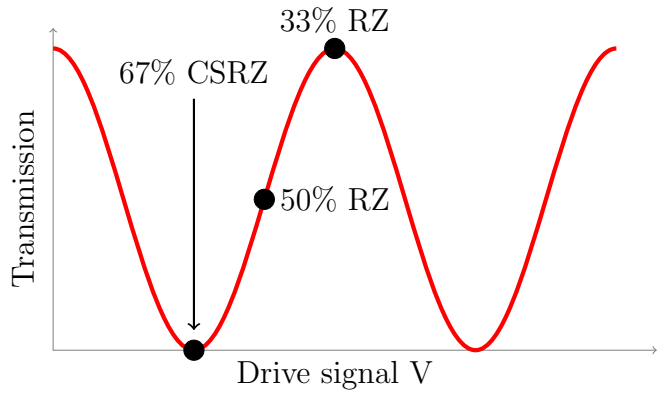

Figure 5.3: MZM bias points for 33%, 50% and 67% RZ duty cycles

5.1 Modulation Formats

In telecommunication systems the information is modulated onto the carrier prior to the transmission. The electric field of carriers electromagnetic wave can be described as

$$E(t) = pAcos(\omega t + \varphi) \tag{5.2}$$

where p is the polarisation, A is the amplitude, ω is the frequency and φ is the phase of the carrier.

In optical communication the information data can be encoded in amplitude, phase, frequency and polarisation of the carrier. These might be combined together to create high level modulation techniques with multilevel signaling. Advanced optical modulation formats allows for $log_2(M)$ data bits being encoded on M symbols by utilising several attributes of optical field combined together or on they own. Multilevel signaling allows for higher data rates at a fixed symbol rate which results in improved spectral efficiency (SE). Improved SE may be realised by multiplexing two signals at the same wavelength using two orthogonal polarisations or wave-division multiplex several wavelengths in one single mode fibre. WDM combined with multilevel polarisation-division multiplexed (PDM) signals will result in further data rate enhancement.

5.1.1 Amplitude Shift Keying

Amplitude Shift Keying (ASK) is a modulation format that encodes the information in the amplitude of the carrier where each amplitude encodes an equal number of bits. Binary ASK signal, sometimes referred as an on-off keying, transmits logical *1* when intensity of the pulse is high and logical *0* when it's low. Multilevel ASK (M-ASK) encodes the data on different amplitude levels enhancing the SE.

5.1.2 Phase Shift Keying

Phase shift keying (PSK) is a modulation format where the information is encoded in phase of the optical signal. Instead of transferring data by switching the optical signal *on* and *off*, the signal is always on and the information is carried on the shifting signal phase which reduces nonlinearity caused by the changes in optical power. The PSK signal, however, cannot be detected using direct detection due to the absence of the phase reference and requires a local oscillator (LO) for the demodulation at the receiver which makes the system implementation harder.

Binary differential PSK (DPSK) encodes the information on the phase change or phase difference rather than phase itself. The phase reference in DPSK is provided by preceding bit which allows for a simpler demodulation by implementing delay line interferometer (DLI). In DLI (Fig. 5.4) the signal is split by the coupler

where one path is delayed by the duration of one bit slot T and then coherently recombined to let two paths interfere with each other. The interference converts differentially precoded phase modulated signal into intensity modulation with high intensity for no phase difference and low whenever the difference is detected (170). The optical fields at the output of the DLI are:

$$E_1(t) = E(t-T) - E(t) \tag{5.3}$$

$$E_2(t) = jE(t-T) + jE(t) \tag{5.4}$$

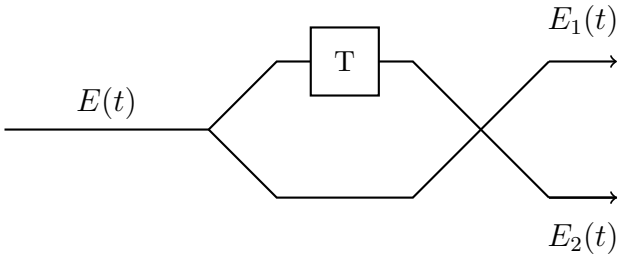

Figure 5.4: Delay line interferometer with delay period T

The main advantage of DPSK modulation over OOK is ∼3 dB lower OSNR requirement for a given bit-error rate (BER) if balanced detection scheme at the receiver is used (171, 172, 173) as well as higher robustness to fibre nonlinearities (174, 175) due to reduced peak power than OOK for the same average power. The advantage of this property has been successfully demonstrated in 10 Gb/s (176, 177, 178, 179, 180), 40 Gb/s (130, 181, 182, 183, 184) and 166 Gb/s (185) DPSK transmission experiments.

The schematic design of balanced DPSK receiver is in Fig. 5.5.

$E_1(t)$ and $E_2(t)$ are derived from Eqs. 5.3 and 5.4. The received photocurrent I_{bal} is obtained by:

$$I_{bal} = |E_1(t)|^2 - |E_2(t)|^2 \tag{5.5}$$

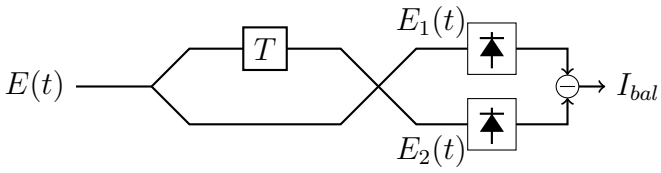

Figure 5.5: Schematic diagram of differentially coherent balanced DPSK phase detection

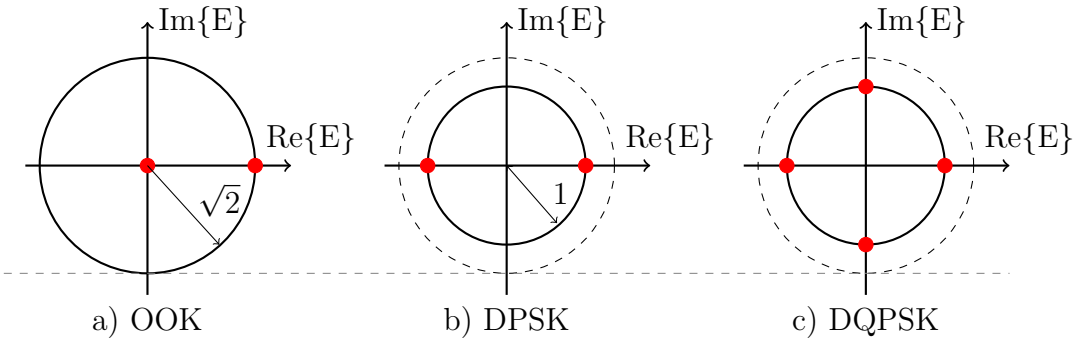

Figure 5.6: Constellation diagrams in OOK (a), DPSK (b) and DQPSK (c) modulation formats.

Spectral efficiency in PSK modulation can be increased by applying multilevel signaling. Differential quadrature phase shift keying (DQPSK) encodes information on four phases where each symbol represents two bits. The symbol rate for a given data rate is reduced by a factor of two comparing with binary DPSK modulation. The schematic design of DQPSK receiver is in 5.7.

The differential phase in QPSK is set to $\pi/4$ and $-\pi/4$ for I and Q arms respectively. The optical fields in each arm are:

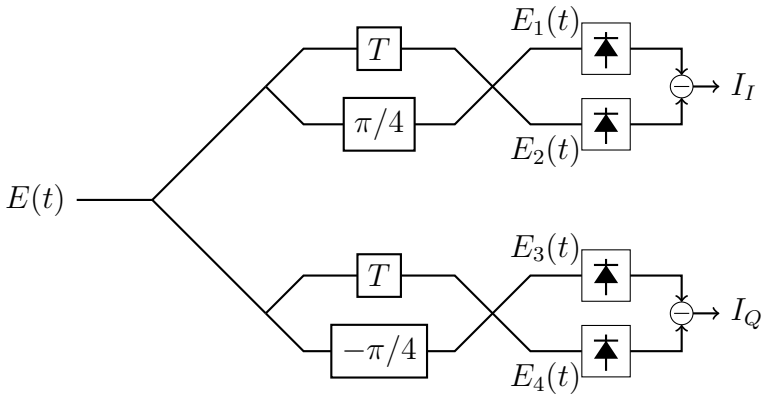

Figure 5.7: Schematic diagram of differentially coherent balanced DQPSK phase detection

$$I:$$

$$E_1(t) = E(t-T) - E(t)e^{j\frac{\pi}{4}} \tag{5.6}$$

$$E_2(t) = jE(t-T) + jE(t)e^{j\frac{\pi}{4}} \tag{5.7}$$

$$Q:$$

$$E_3(t) = E(t-T) - E(t)e^{-j\frac{\pi}{4}} \tag{5.8}$$

$$E_4(t) = jE(t-T) + jE(t)e^{-j\frac{\pi}{4}}. \tag{5.9}$$

Received photocurrent in I_I and I_Q arms is then defined as:

$$I_I = |E_1(t)|^2 - |E_2(t)|^2 \tag{5.10}$$

$$I_Q = |E_3(t)|^2 - |E_4(t)|^2 \tag{5.11}$$

DQPSK modulation format offers great OSNR performance, increased SE as well as improved PMD and CD tolerance (186, 187, 188). The penalty for increased SE in DQPSK with respect to DPSK is reduced robustness to frequency offset tolerance between the laser and DI by a factor of six (189) and increased OSNR

requirement for a given BER by 1-2 dB (190). DQPSK has been proven to be an attractive format in long-haul 100 Gb/s optical transmission systems (191, 192) and is suitable for an upgrade of existing optical links. Real field trials at 40 Gb/s have been demonstrated in (193, 194) and 112 Gb/s in (195).

5.1.3 Coherent Detection

Coherent detection is the most advanced optical signal detection method. It allows for the full electric field recovery which includes the information of amplitude and phase. Information encoded in all four degrees of freedom maximises spectral efficiency allowing to go beyond the limits imposed by noncoherent or differentially coherent formats which cannot exceed 1 b/s/Hz per polarisation (172). Digital signal processing (DSP) can overcome linear time-varying impairments by applying adaptive algorithms on received Nyquist rate sampled digitalised waveform (196, 197). Nonlinear compensation using digital back-propagation has been proposed in (198, 199) and confirmed experimentally (200, 201).

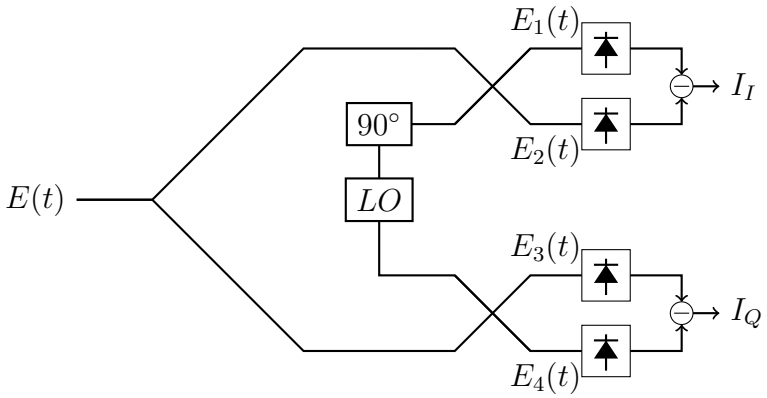

Figure 5.8: Schematic diagram of single polarisation homodyne downconverter.

Demodulation of received signal in coherent receiver requires the local oscillator (LO) in polarisation downconverter which provides phase reference. Optical to electrical downconversion can be implemented with LO frequency tuned to transmission channel $\omega_s = \omega_{LO}$ (homodyne) or detuned by an intermediate frequency

(IF) $\omega_{IF} = \omega_s - \omega_{LO}$ where further downconversion is performed by electrical LO (heterodyne).

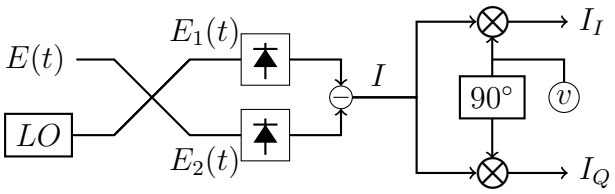

Figure 5.9: Schematic diagram of single polarisation heterodyne downconverter.

In ASE limited systems, heterodyne (Fig. 5.9) and homodyne (Fig. 5.8) implementations, have the same performance (202). The main difference between both is that heterodyne downconversion requires only one balanced photodetector whereas homodyne two. The disadvantage of heterodyne downconverter is required photodetectors bandwidth which is twice as large as in homodyne scheme. The spectra of homodyne and heterodyne after photodetectors is in Fig. 5.10 and Fig. 5.11 respectively.

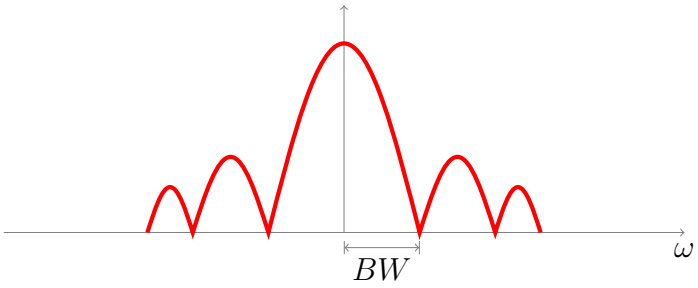

Figure 5.10: Spectrum of a homodyne downconverter after balanced photodetector.

The schematic implementation of coherent receiver is in Fig. 5.12.

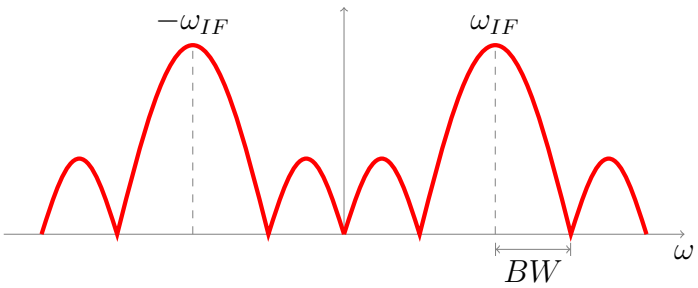

Figure 5.11: Spectrum of a heterodyne downconverter after balanced photodetector where intermediate frequency $\omega_{IF} \approx BW$.

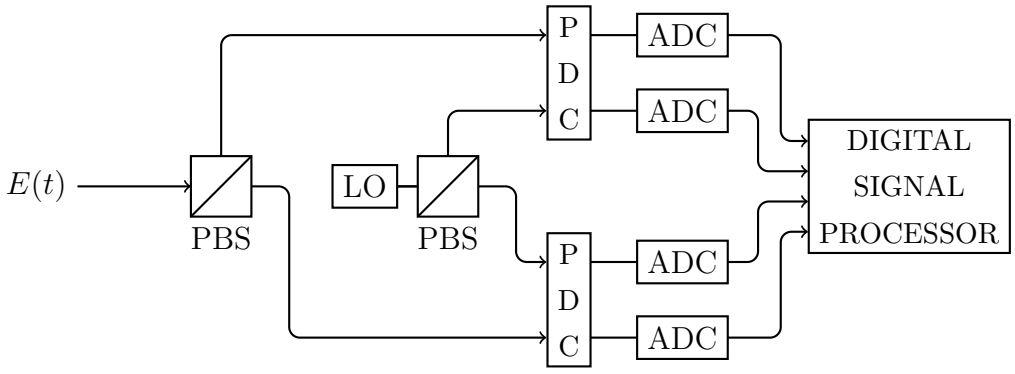

Figure 5.12: Schematic design of a digital coherent receiver. PBS: polarisation beam splitter; PDC: single polarisation downconverter; ADC: analog to digital converter

5.1.4 Spectrum Efficiency Improvement with Nyquist WDM and CO-OFDM

High spectral efficiency can be achieved by combining multilevel modulation formats with polarisation multiplexing (203, 204). Advanced coherent detection permits the recovery of full electric field which gives flexibility for encoding the information in amplitude and phase. Digital signal processing enabled full chromatic dispersion compensation without inline DCM and significant OSNR penalty (197). Two promising techniques to boost SE are coherent orthogonal frequency-division multiplexing (CO-OFDM) (205) and Nyquist wavelength-division multiplexing (N-WDM) (206, 207, 208).

In CO-OFDM data is transmitted through multiple orthogonal subcarriers spaced at symbol rate in the frequency domain (209). This technique has shown great resistance to chromatic dispersion and enabled transmissions of more than 1 Tb/s per channel (206, 210, 211).

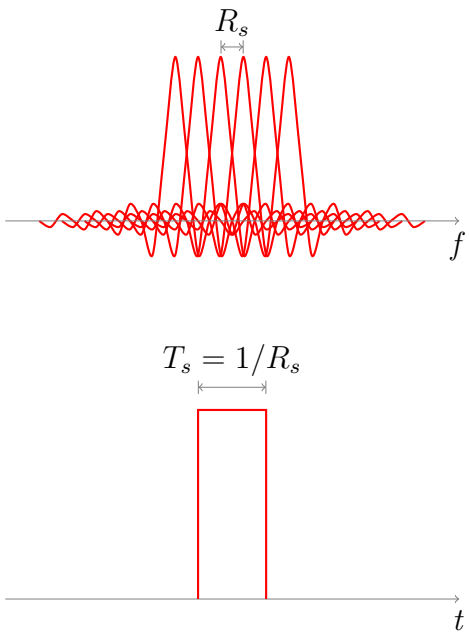

Figure 5.13: Ideal WDM spectrum (top) and time pulse (bottom) in CO-OFDM. R_s is the baud-rate and T_s is the time duration of the pulse equal to a symbol time $T_s = 1/R_s$.

N-WDM maximises spectral efficiency through the use of optimal, almost rectangular pulse shaping, allowing inter-symbol interference (ISI) free transmission with WDM channel spacing at, or close to, the baud rate (212, 213). The performance of N-WDM is comparable to CO-OFDM and can achieve high SE of 4 bit/s/Hz with PDM-QPSK (214, 215) and 7.47 bit/s/Hz with PDM 16-QAM (216), however, N-WDM is much more robust to optical filtering and ISI (217) as well as practical implementation at the receiver (212). Furthermore, it has been shown that standard SMF-28 fibre allows for higher reach than NZ-DSF due to higher CD and lower nonlinear coefficient (213) which enables N-WDM implementation in already existing links. Long-haul transmission with in-line

EDFA was demonstrated in (218) where Nyquist-WDM signals up to 1 Tb/s per channel were transmitted in a field experiment with a link consisting of 8 nodes and 950 km of standard SMF-28 fibre.

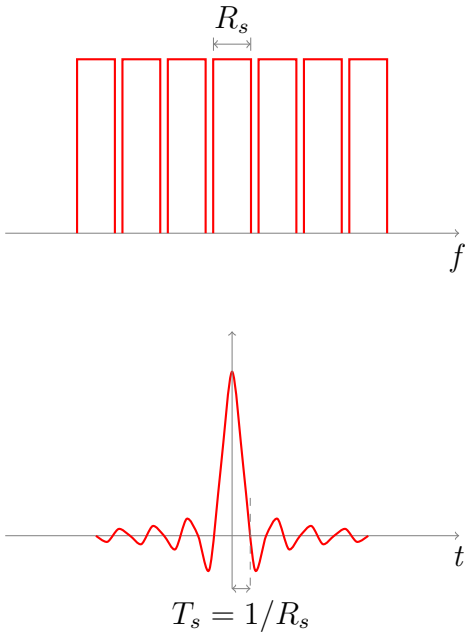

Figure 5.14: Ideal WDM spectrum (top) and time pulse (bottom) in N-WDM. R_s is the baud-rate and T_s is the time duration of the pulse equal to a symbol time $T_s = 1/R_s$.

5.2 Transmission Experiments with Direct Detection

Signal to noise requirement at the receiver ultimately limits the reach of optical transmission systems. Demonstrations of unrepeatered transmission have made use of ROPAs to improve the OSNR at the receiver (219). New fibre designs with low loss have also been used to allow the fibre span length to be increased for a given power budget (220) and large effective area fibres reduce nonlinear penalties and allow higher launch power (221). URFL based amplifier can extend

the transmission reach without speciality fibres using single pump wavelength and direct detection.

This section presents experimental results of unrepeatered direct detection RZ-ASK and RZ-DPSK transmission performance in standard SMF-28 fibre using URFL based amplification method.

5.2.1 Experimental Setup

The experimental set-up for BER measurements of RZ-ASK and RZ-DPSK modulated signal is shown in Fig. 5.15. Data is modulated on 16 channel grid (DPSK) and 8 channel grid (ASK) with 42.7 Gb/s $2^{31} - 1$ pseudorandom bit sequences (PRBS) data pattern by the lithium niobate MZM. To generate RZ signal, modulated data is fed into second MZM driven by frequency that is half of the data rate. To compensate for the transmitter loss, modulated signal was amplified by EDFA and transmitted over the span using bidirectional URFL based amplification method with pair of FBGs at 1448 nm for RZ-DPSK and 1455 nm for RZ-ASK. Total launch power was varied by VOA connected to power meter and controlled digitally for better accuracy. The type of fibre used in both experiments was standard SMF-28. Chromatic dispersion was post-compensated with dispersion compensating module followed by EDFA at the receive path in DPSK experiment and split 2:1 between pre and post compensation in ASK. Tuneable filter with 0.4 nm bandwidth was used to demultiplex WDM channels. To compensate for residual dispersion, temperature tuned dispersion compensation module (TDCM) was deployed after the filter. Received signal was split for clock recovery (CR) and demodulator with 90/10 coupler. Direct detection was used to demodulated RZ-ASK signal whereas balanced detection was used to demodulate RZ-DPSK signal using 40 G DLI with a differential delay equal to one bit period and two photodetectors.

The system has been optimised for an unrepeatered transmission. Pump power ratio was set to transmit largest number of channels with BER below forward error correction (FEC) threshold. The bandwidth of tuneable filter was set for the best BER performance and kept fixed for all channels. TX lasers were not tuned to ITU grid therefore software written in LabView was used to sweep

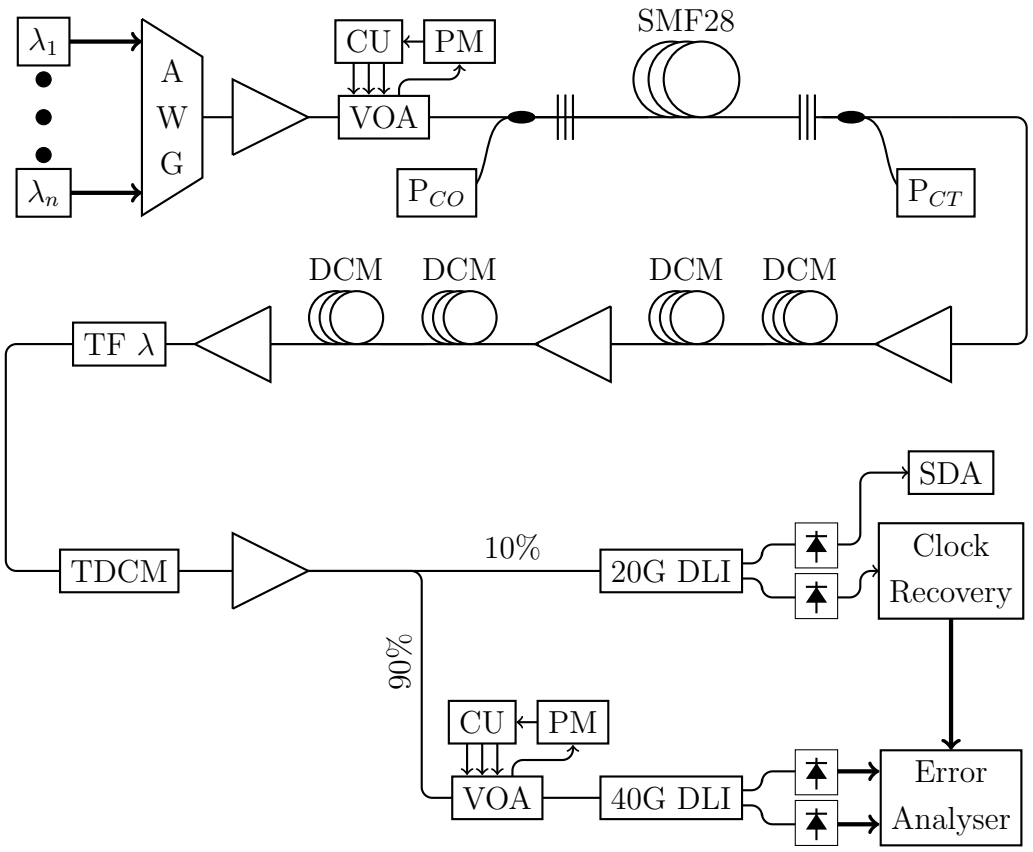

Figure 5.15: Experimental setup for 42.7 Gb/s RZ-DPSK and RZ-ASK transmission using 2^{nd} order distributed URFL based amplifier. AWG: Arrayed waveguide grating; CU: control unit; PM: power meter; P: (CO) co- and (CT) counter-propagating pump; DCM: dispersion compensation module; TF: tuneable filter; TDCM: tuneable dispersion compensating module; DLI: delay line interferometer; SDA: serial data analyser

TDCM for frequency offset with 0.2 GHz step (Fig. 5.16) and dispersion with 1 ps step (Fig. 5.17) for each individual channel.

Delay in Optoplex's Optical DPSK Demodulator (222) was controlled digitally and swept with 1 ps step. Data bias and delay in SHF Error Analyser (223) was swept with external software for better accuracy. Total launch power and pump powers used in experiments are in the Table 5.1.

Table 5.1: Unrepeatered 42.7 Gb/s RZ-DPSK and RZ-ASK Transmission Parameters

Distance (km)	Modulation Format	TX Channels	Launch Power (dBm)	Fw. Pump (dBm)	Bw. Pump (dBm)
240	ASK	8	7	31.4	30.9
280	DPSK	16	13	31.6	32.2
320	DPSK	12	5	32.7	32.1
340	DPSK	6	17	32.2	32
360	DPSK	1	13.1	31.5	32

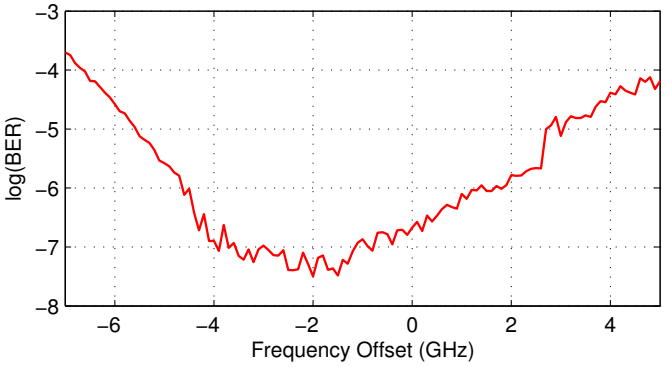

Figure 5.16: The measurement of TDCM frequency offset versus BER.

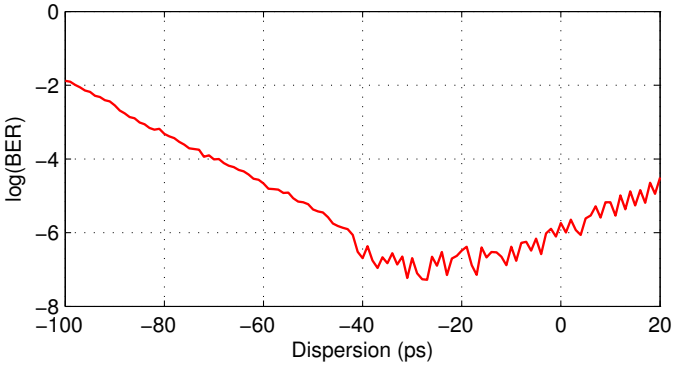

Figure 5.17: The measurement of TDCM dispersion offset versus BER.

5.2.2 Unrepeatered 42.7 Gb/s RZ-ASK Transmission

The 8 channel grid was spread across the C-band from 1532 nm to 1561 nm. Spectrum of WDM input used in RZ-ASK transmission is shown in Fig. 5.18. There was no pre-emphasis of channel power and gain flattening filter used in the experiment.

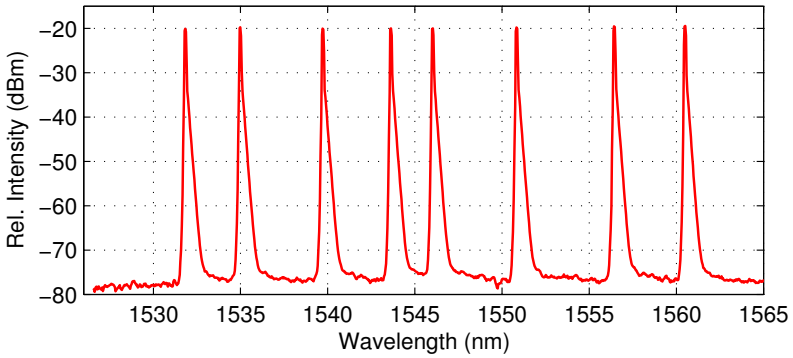

Figure 5.18: Spectrum of the 8 channel WDM input

The optimal launch power into 240 km fibre based on the BER measurement of a single channel in the middle of the C-band at 1446 nm was found to be 7-8 dB. The launch power sweep is plotted in Fig. 5.19. The transmission performance of 8 × 42.7 Gb/s ASK modulated signal was measured for all 8 WDM channels and plotted in Fig. 5.20.

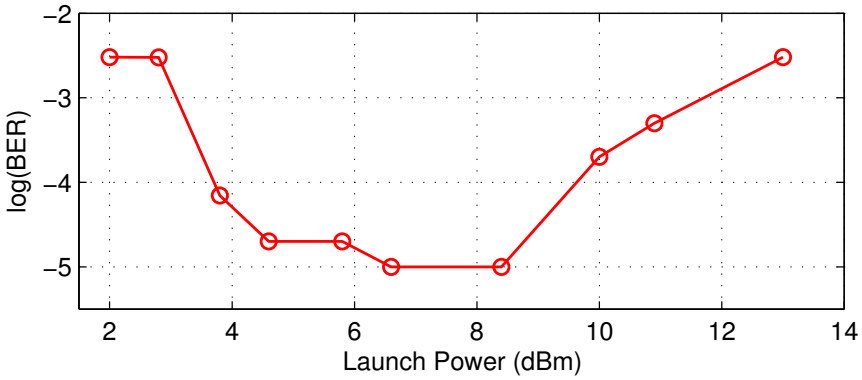

Figure 5.19: Optimal launch power measurement at 240 km based on the BER of the channel in the middle of the C-band

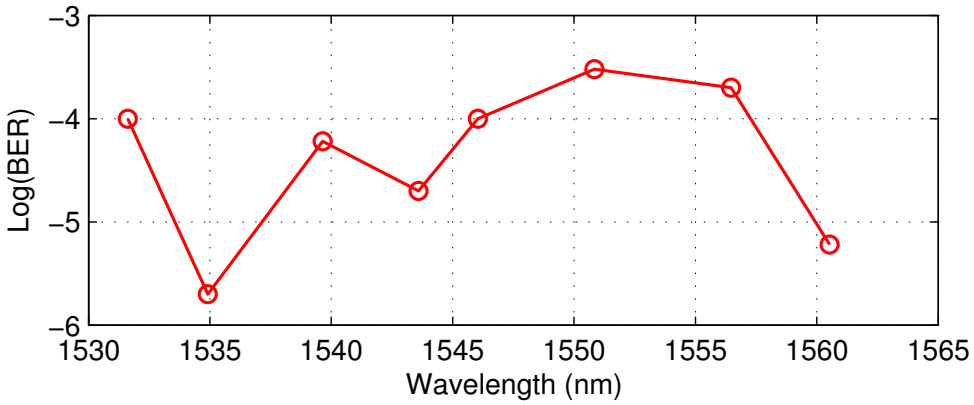

Figure 5.20: BER measurement at 240 km using RZ-ASK modulation format

BER below the FEC limit using hard decision 7% overhead could be achieved for all 8 channels spread across C-band window. This is the record distance achieved in 40 Gb/s ASK transmission in standard SMF-28 fibre up to date (130). The distance of 250 km with pre-distorted ASK transmission at 10 Gb/s has been reported in (224). No FEC was used in this experiment.

5.2.3 Unrepeatered 42.7 Gb/s RZ-DPSK Transmission

Differential Phase-shift keying is an attractive modulation format which can improve receiver's sensitivity by 3 dB compared to OOK if balanced detection is used (172). Return-to-zero (RZ) signaling format can further increase the performance of the receiver as well as higher the nonlinear threshold and noise tolerance.

Transmitted and received optical spectra of WDM channels in 280 km, 320 km, 340 km and 360 km unrepeatered links are shown in Fig. 5.21 - 5.24. There was no gain flattening filter and no pre-emphasis of channel power used in the experiment. The variation of gain is a result of the single wavelength pump Raman gain curve in silica-core SMF-28 fibre. Gain degradation in 1555 nm region can be shifted by changing the wavelength of FBGs (Fig. 4.10).

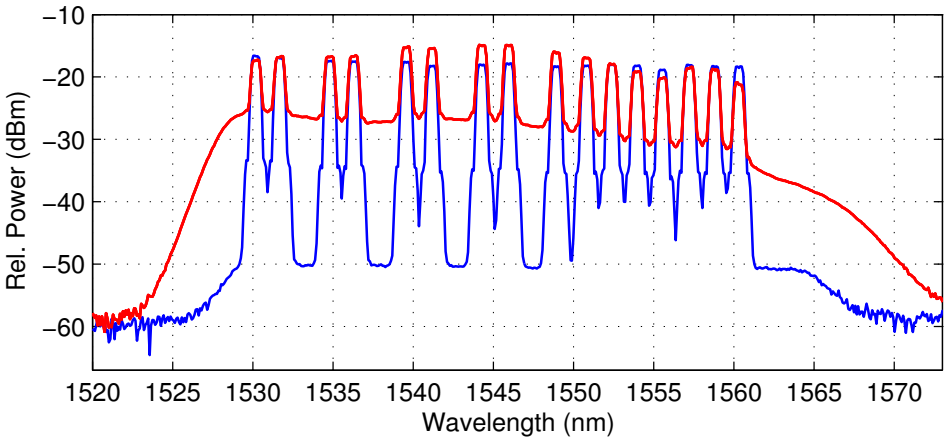

Figure 5.21: Transmitted (blue) and received (red) spectra of 16 channel grid in 280 km 42.7 Gb/s DPSK transmission

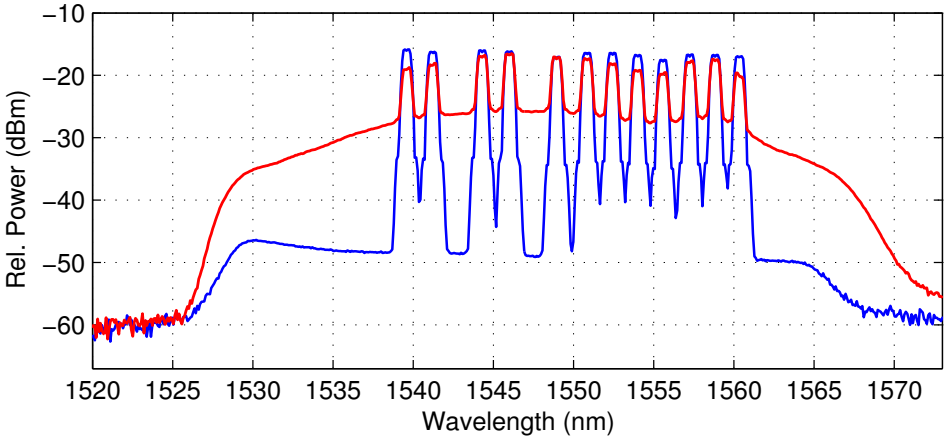

Figure 5.22: Transmitted (blue) and received (red) spectra of 12 channel grid in 320 km 42.7 Gb/s DPSK transmission

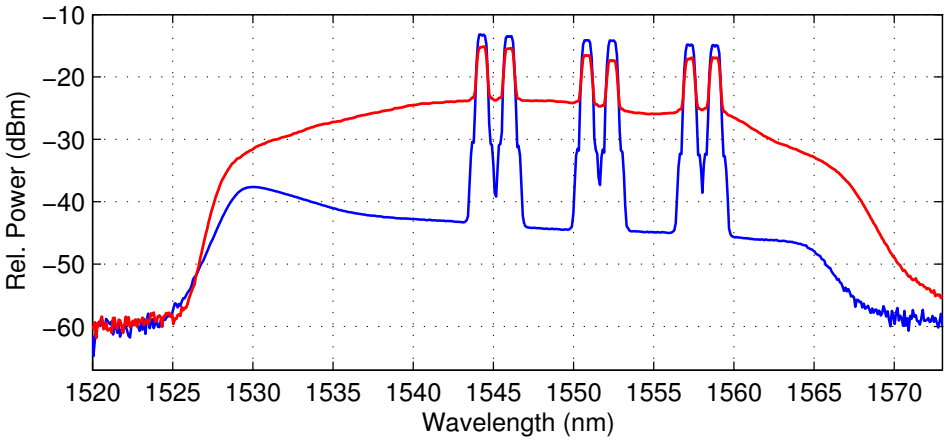

Figure 5.23: Transmitted (blue) and received (red) spectra of 6 channel grid in 340 km 42.7 Gb/s DPSK transmission

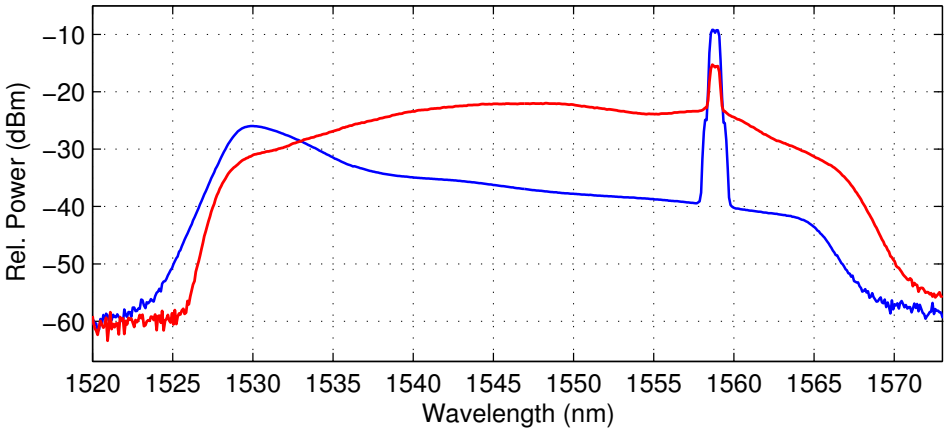

Figure 5.24: Transmitted (blue) and received (red) spectra of 1 channel grid in 360 km 42.7 Gb/s DPSK transmission

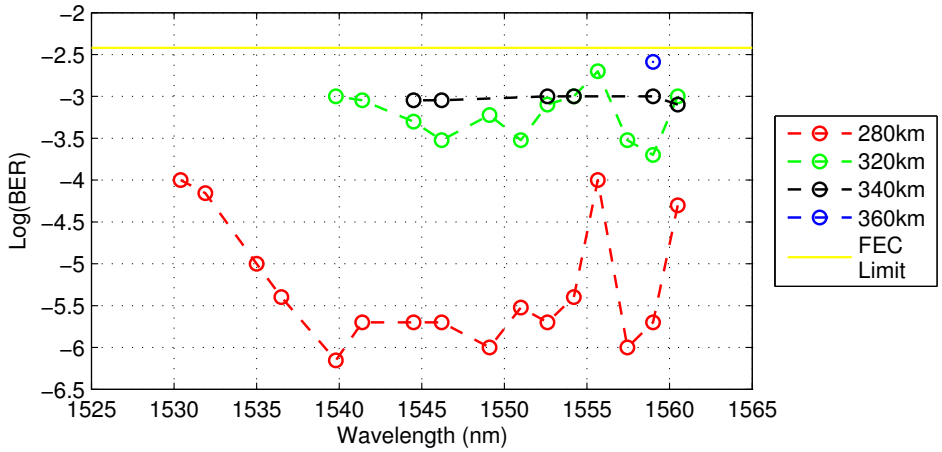

Figure 5.25: Experimental results of DPSK transmission with BER measured for each individual channel. Transmission distances measured were 280 km, 320 km, 340 km and 360 km

BER below FEC limit could be achieved for all transmission distances (Fig. 5.25). Error free transmission across the full C-band was achieved for 280 km. Transmission at higher distances was limited due to received OSNR and gain bandwidth. The operational bandwidth at 320 km link was 19.2 nm whereas only 6 channels could be transmitted at 340 km and a single channel at 360 km.

5.3 Transmission Experiments with Coherent Detection

Coherent detection offers better receivers sensitivity comparing to direct detection. It allows for multilevel modulation formats being used with comparable required OSNR per bit as in noncoherent OOK or DPSK formats (225) which in turn quadruples spectral efficiency. One of the key challenges in practical implementation of coherent transmission lines is high-speed analog-to-digital conversion and DSP. However, technological advancements makes coherent detection systems a promising candidate for an upgrade of currently installed links.

This section shows that URFL based amplification is compatible with unrepeatered coherent links as well as long-haul transmission using advanced Nyquist-

WDM channel spacing.

5.3.1 Unrepeatered PDM-QPSK Transmission

Dual polarisation QPSK transmission with coherent detection is a leading modulation format for 100 Gb/s optical networks (226). Long-haul WDM transmission experiments with 50 GHz spacing at 100 Gb/s has been investigated in (227, 228) and a single channel at 226 Gb/s in (229, 230). PM-QPSK transmission has been successfully demonstrated in real field experiments in (231). Ultra-long-haul 112 Gb/s PDM-QPSK transmission reaching 13,288 km with Raman amplification only has been demonstrated in (232).

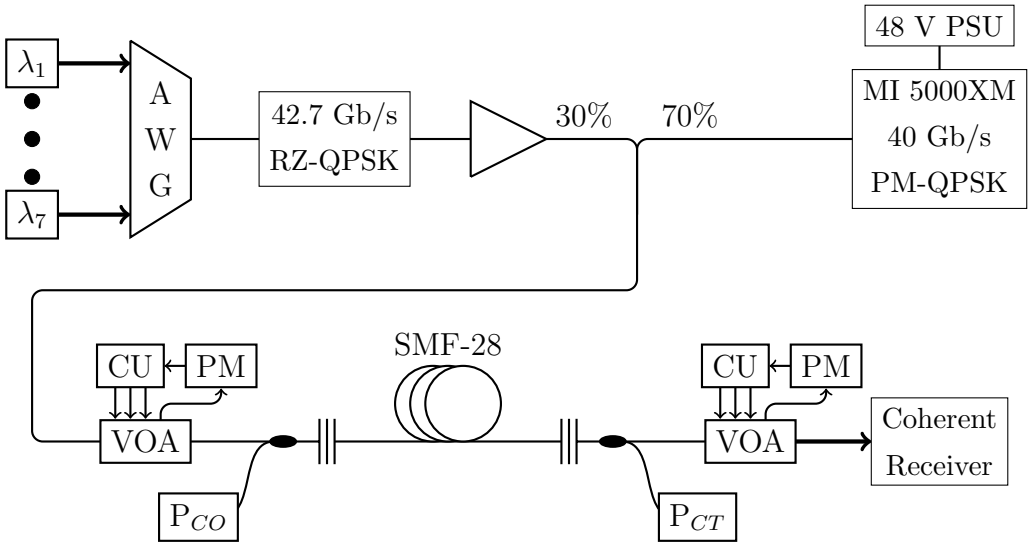

Figure 5.26: Experimental setup for 42.7 Gb/s RZ-DQPSK transmission using 2^{nd} order distributed URFL based amplifier. AWG: Arrayed waveguide grating;

In this experiment a single coherent 40 Gb/s PDM-QPSK channel is multiplexed with 7 × 42.7 Gb/s RZ-DQPSK channels with 50 GHz spacing and transmitted over unrepeatered links up to 320 km.

The experimental set-up for BER measurements of RZ-QPSK modulated signal transmission is shown in Fig. 5.26. 7 CW-DFB sources were modulated with 42.7 Gb/s RZ-DQPSK modulator and multiplexed by 70/30 coupler with a single coherent 40 Gb/s PDM-QPSK channel (1556.7 nm) from the MI 5000XM

300-Pin MSA Coherent PM-QPSK Transceiver (233) and transmitted over unrepeatered links using URFL based amplification. The spectrum of modulated WDM channels with 50 GHz spacing is shown in Fig. 5.27.

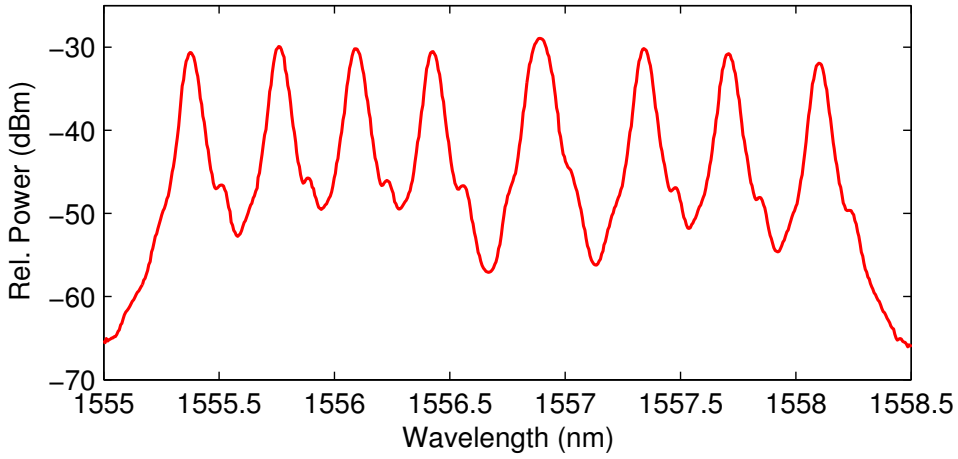

Figure 5.27: WDM spectrum of DQPSK and DPSK

The optimum launch power for all transmission distances was between 0-3 dBm. The sweep of the launch power as a function of BER of the coherent channel in 320 km link is shown in Fig. 5.28.

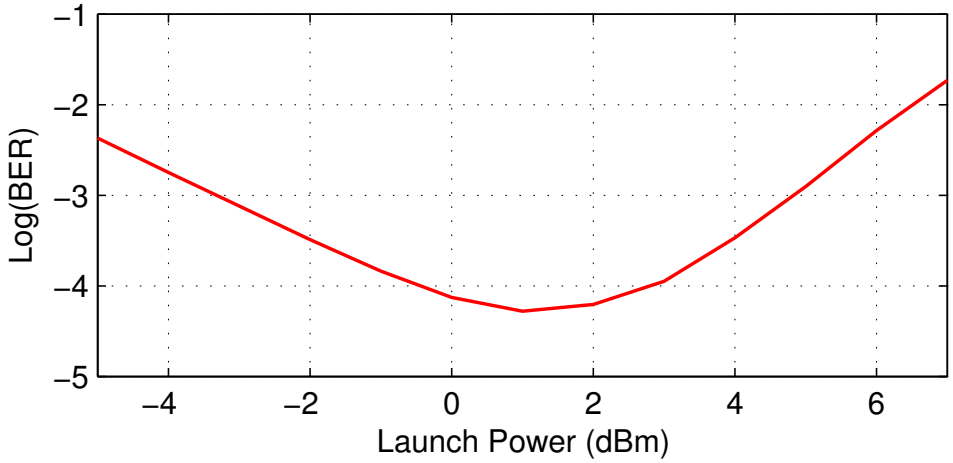

Figure 5.28: Optimal launch power measurement at 320 km based on the BER of the coherent channel at 1556.8 nm

BER was measured only for a single coherent channel. The pump powers as well as launch power and received OSNR for each span length are listed in Table. 5.2. The received spectrum after 320 km transmission is in Fig. 5.29.

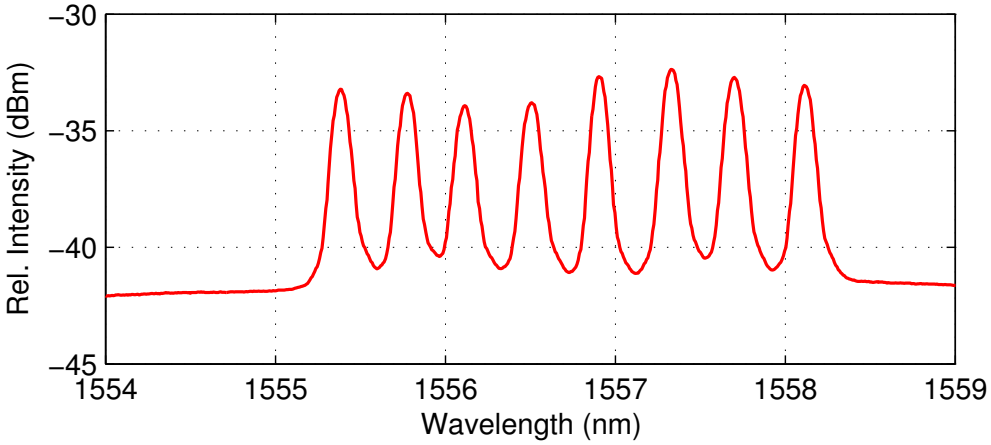

Figure 5.29: Received WDM spectrum after 320 km

Linear impairments such as CD and differential group delay was fully compensated in DSP of the coherent MI 5000XM transponder. The transmission performance of coherent channel at 1556.9 nm is shown in Fig. 5.30. The longest transmission distance with BER below FEC limit was 320m km.

Table 5.2: Transmission parameters for unrepeatered 40 Gb/s PM-QPSK links

Distance (km)	Launch Power (dBm)	RX OSNR (dBm)	Forward Pump (dBm)	Backward Pump (dBm)
160	3.2	35.5	29.5	32.1
200	3.2	23.6	29.5	31.8
280	3.2	23.4	31.4	32.2
320	1	14.6	31.8	32.1

5.3.2 Nyquist PDM-QPSK Transmission

In this experiment the Nyquist WDM signaling and 2^{nd} order distributed URFL based amplification is investigated. Experimental assessment of the transmis-

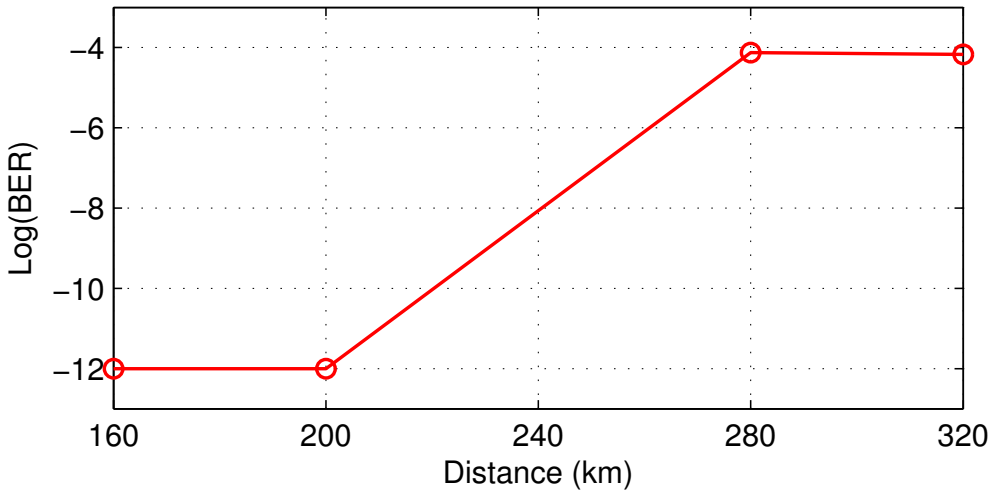

Figure 5.30: Transmission performance of the coherent channel at 1556.9 nm in unrepeatered transmission

sion performance of 9 x 10 Gbaud/s channels Ny-WDM PDM-QPSK with SE of 3.73 b/s/Hz over 6157 km of standard SMF-28 fibre in a recirculating loop and 320 km in an unrepeatered span without employing ROPA, large effective or ultra-low loss fibre is demonstrated.

5.3.2.1 Ny-PDM-QPSK Transmitter

The experimental set-up of the 10 GBaud Nyquist-WDM PDM-QPSK transmitter is shown in Fig. 5.31.

An external cavity laser (ECL) with a linewidth of 10 kHz is used at the input to an optical comb generator (OCG) (234). The OCG uses two cascaded phase modulators (one driven at 21.4 GHz) and an intensity modulator to generate 9 channels with a spacing of 10.7 GHz as shown in 5.32.

The nine lines from the comb generator are separated using cascaded interleavers to allow odd and even channels to be modulated separately. Modulator drive waveforms were generated offline with Matlab, quantised to 6 bits and uploaded to memories of two Xilinx Virtex 5 FPGAs. Nyquist pulse shaping (root raised cosine (RRC) filters with a roll-off factor of 0.01), and a pre-emphasis filter to compensate for the frequency response of the digital to analog convertors

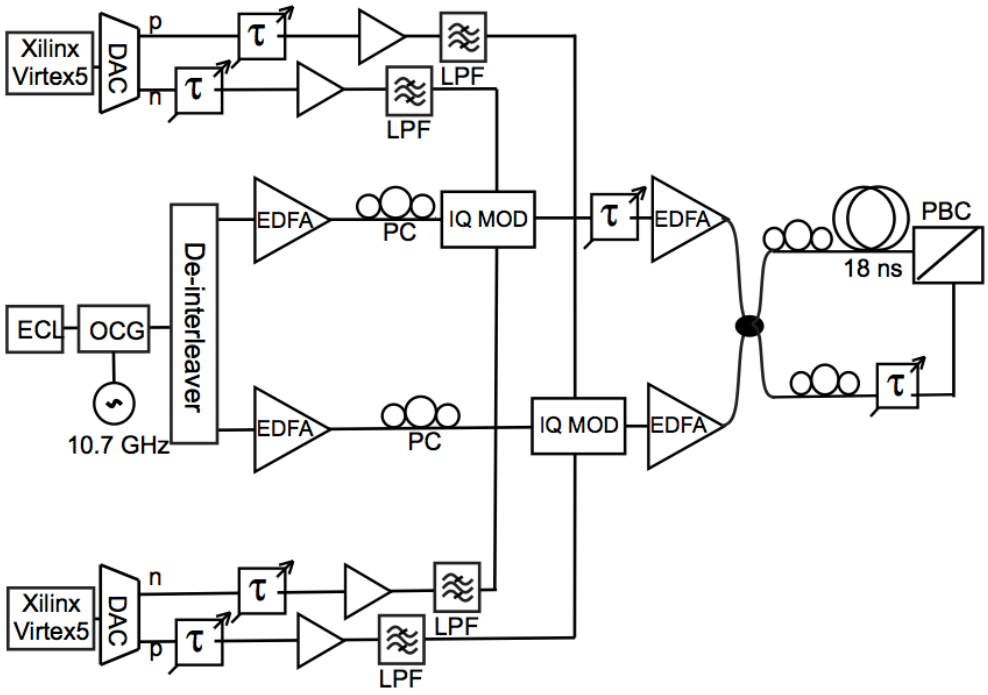

Figure 5.31: Experimental set-up of Nyquist-WDM PDM-QPSK transmitter (OCG optical comb generator, PBC polarisation beam combiner)

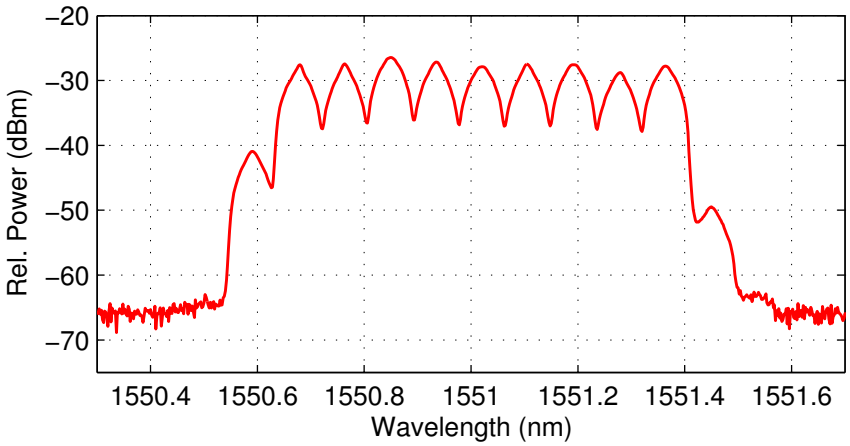

Figure 5.32: Optical spectrum of 9 x 10 GBaud Nyquist-WDM PDM-QPSK

(DAC), anti-imaging filters and RF-amplifiers were applied to four 215 de Bruijn sequences de-correlated by 0.25 of the pattern length in the DSP. The signals were passed to two Micram VEGA DACII digital-to-analog converters, the com-

plementary outputs which were used to drive two optical IQ modulators. After odd and even channels were separately modulated by the IQ-MZMs, the two sets of channels were amplified and combined with a 3 dB optical coupler to form the 9-channel 10 GBaud Nyquist QPSK signal with 10.7 GHz channel spacing. The signals were polarisation-division multiplexed by passing the signal through a polarisation multiplexing stage. In this stage, one of the arms is delayed by 18 ns using additional fibre and the other one with a variable optical delay line.

In both experiments coherent detection was used with a phase and polarisation-diverse digital coherent receiver. An ECL with a linewidth of 100 kHz was employed as the local oscillator at the receiver side. A real-time digital sampling oscilloscope (Tektronix DPO 72004) with a sampling rate of 50 GSa/s and a 16 GHz hardware bandwidth captured the waveforms which were processed off-line using DSP as follows: the signal was de-skewed, normalised and resampled to 2 samples per symbol. This was followed by digital CD compensation (235). A matched filter (RRC with a roll-off factor 0.01) was used to reduce the computational complexity at the adaptive equaliser stage. An 11-tap butterfly structure FIR filter using constant modulus algorithm (CMA) was used to compensate for PMD. For phase recovery, carrier phase estimation was performed using a 4th power Viterbi and Viterbi estimator (236). Finally, the signal was decoded using hard decision on symbols.

5.3.2.2 Unrepeatered Ny-PDM-QPSK Transmission

The experimental setup to investigate SMF-28 unrepeatered transmission is in Fig. 5.33. Total launch power of the modulated 9 $\times$ Ny-PDM-QPSK signal was varied by VOA and multiplexed with copropagating Raman pump with 1366/1550 coupler. The transmission performance was measured in single-span lengths of 240 km, 280 km and 320 km with losses of 48 dB, 56 dB and 64 dB respectively.

The experiment was performed with distributed 2^{nd} order bi-directional URFL based amplification. FBGs with a reflectivity of 95 %, bandwidth of 0.5 nm centred at 1457 nm were included at each end of the transmission span to reflect the Stokes shifted signal generated by the primary 1366 nm pump. The insertion loss of 1366/1550 nm coupler and FBGs measured at 1550 nm wavelength were

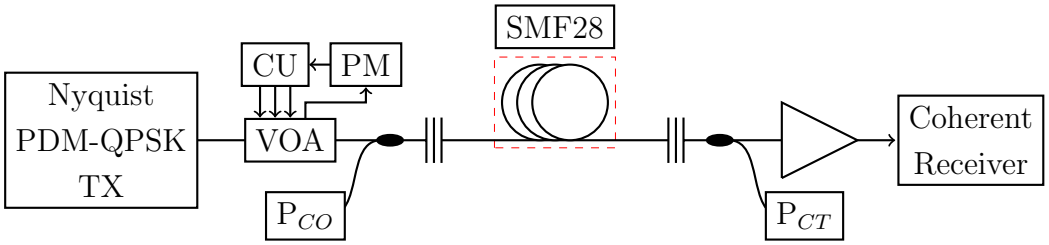

Figure 5.33: Schematic diagram for Ny-PDM-QPSK unrepeatered transmission

0.6 dB for forward and 0.8 dB for backward directions. It was not possible to fully compensate for the the span loss therefore EDFA was included on the receive path to provide extra gain to the coherent receiver. There was no pre- or post inline CD compensation in the system. Time varying impairments were fully compensated in DSP (235).

The pump powers used in the unrepeatered experiment were optimised to give the best BER performance and are listed in Table 5.3

Table 5.3: Unrepeatered 43 Gb/s Ny-PM-QPSK Transmission Parameters

Distance (km)	Forward Pump (dBm)	Backward Pump (dBm)
240	28.5	30.9
280	28.7	32.3
320	31.5	32.1

Fig. 5.34 shows numerical simulations of the signal power evolution for the longest, 320 km unrepeatered transmission experiment delivering a peak-to-peak signal power excursion of 40 dB (compared to a span loss of 64 dB) and an OSNR of $\sim$ 9 dB for a launch power of -10 dBm per channel.

The performance of the unrepeatered transmission with a standard SMF-28 fibre are shown in Fig. 5.35.

Unrepeatered 9 $\times$ 40 Gb/s Ny-PDM-QPSK transmission over 320 km was possible with no inline CD compensation giving an average BER, based on 10 measurements, below the FEC limit of 3.8×10^{-3}.

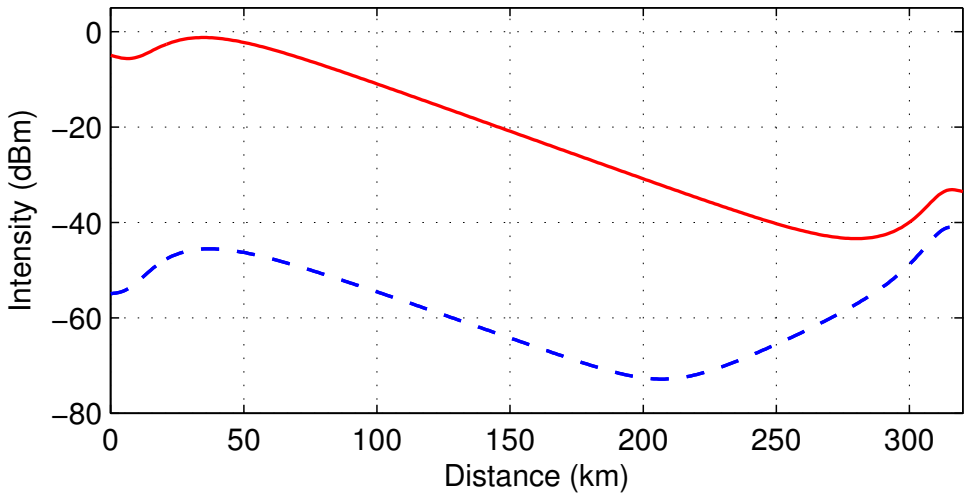

Figure 5.34: Simulation results of signal power (red) and noise (dashed blue) variation in a 320 km transmission link

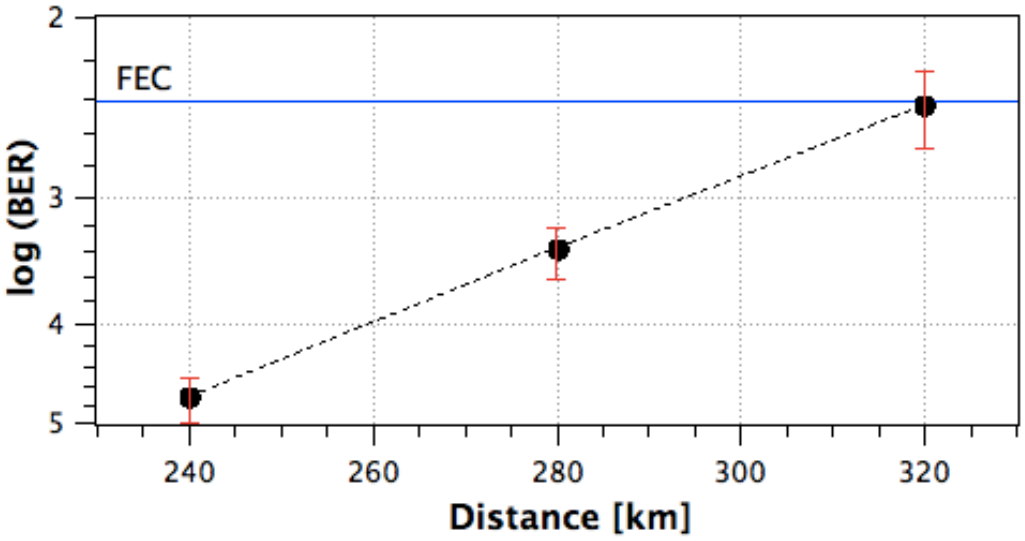

Figure 5.35: Unrepeatered Ny-PDM-QPSK transmission results

5.3.2.3 Long-haul Ny-PDM-QPSK Transmission with Recirculation Loop

To investigate transmission performance over long-haul distances a recirculating loop with a single 82.1 km of SMF-28 fibre span with 17 dB loss was used as shown schematically in 5.36.

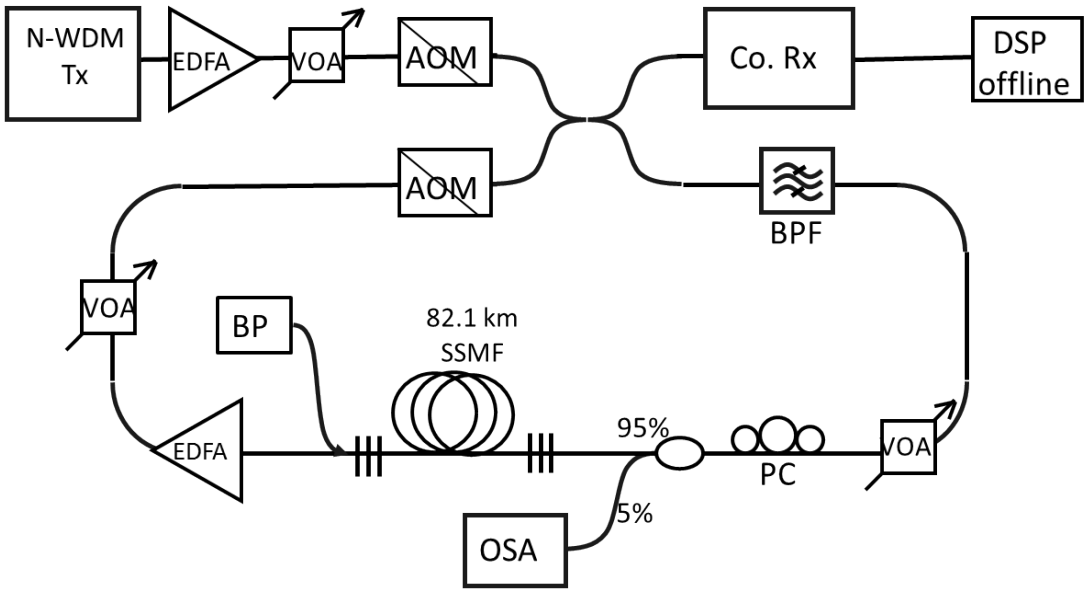

Figure 5.36: Recirculating loop transmission set-up

Modulated 9 × 40 Gb/s N-PDM-QPSK signal was amplified and injected into recirculation loop to simulate long-haul transmission. Recirculation loop consisted of 5 cascaded asymmetric MZM filters to reject out of band ASE as well as flatten the gain profile. The launch power into backward pumped 2^{nd} order URFL based amplifier (with the same setup and loss parameters as in unrepeatered transmission in previous section) was controlled with VOA and polarisation controller. To compensate for the insertion loss of the AOM, cascaded MZM filter and FBGs with the total loss of 13 dB an additional EDFA was implemented in the recirculation loop.

The backward pump power was optimised at 30.4 dBm for 75 recirculations (6157 km) and maintained at this level for all measurements.

The signal power distribution along the 82.1 km span was measured with a modified OTDR. In Fig. 5.37 we can see almost symmetrical power distribution with total power variation of only 4 dB over the entire length of the fibre span.

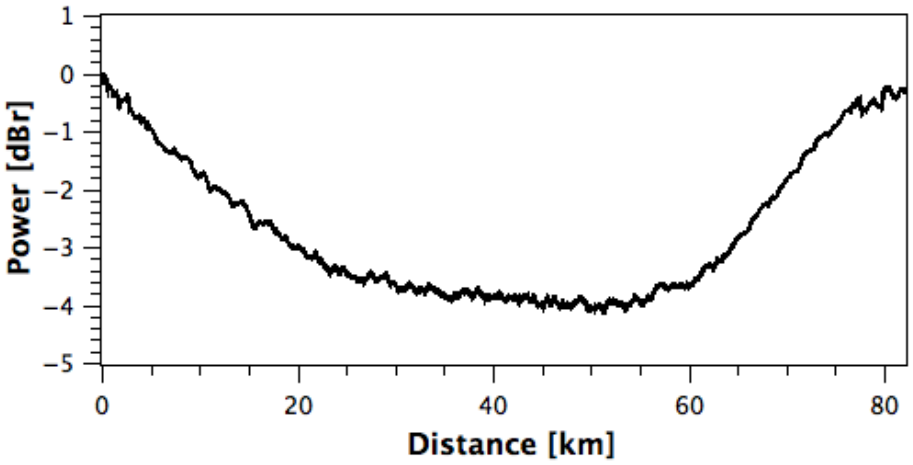

Figure 5.37: Signal power distribution in backward pumped 82.1km Raman span

The received digital spectrum of Nyquist channels after coherent detection is shown in Fig. 5.38

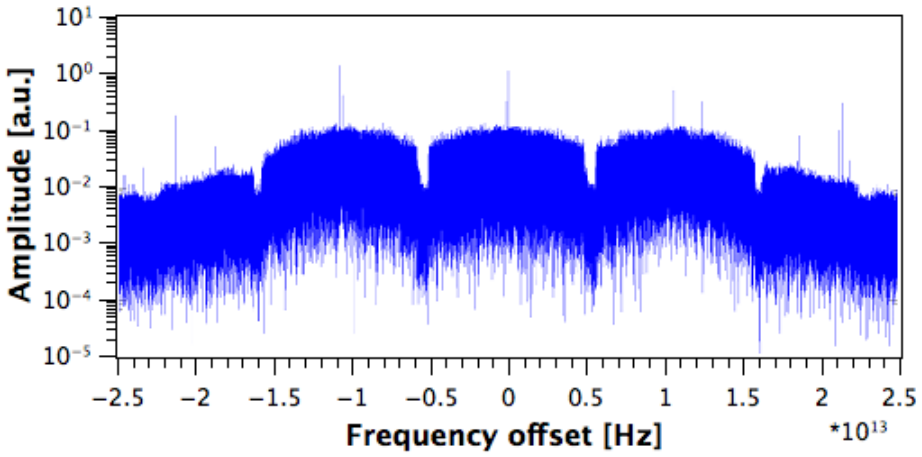

Figure 5.38: Measured BER versus distance for the central channel in 9 WDM channel Nyquist-WDM PDM-QPSK transmission

The transmission performance, as a function of distance, is shown in Fig. 5.39, at a launch power of -10 dBm per channel (measured at the input to the FBG). The error bars indicate the range of BER values measured over 10 consecutive measurements.

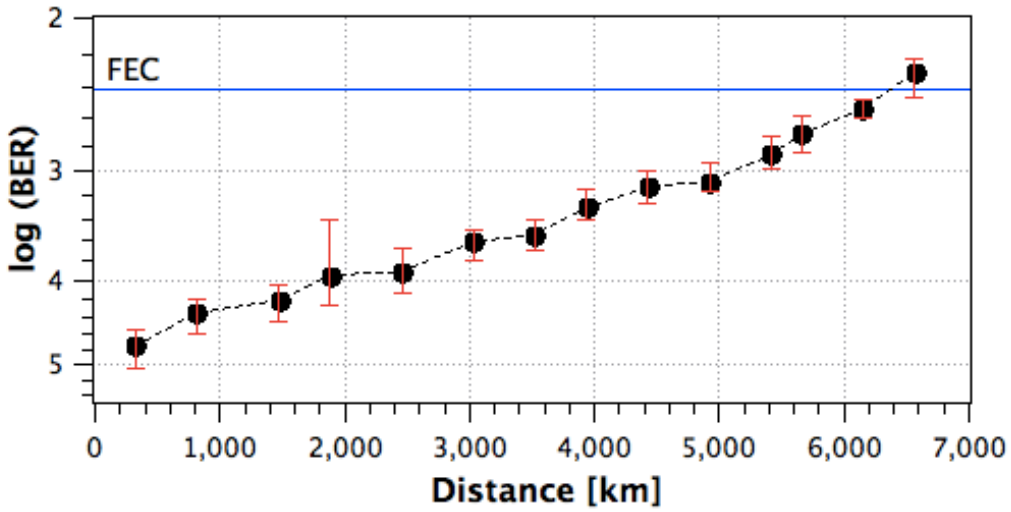

Figure 5.39: Measured BER versus distance for the central channel in 9 WDM channel Nyquist-WDM PDM-QPSK transmission

A transmission distance of 6157 km without inline CD compensation was achieved with BER below the FEC limit assuming 7% overhead. Note that the loop configuration restricted the launch power to -10 dBm, and we expect enhanced performance at the optimum fibre launch power level of -8.5 dBm.

Chapter 6

Conclusions

A novel ultra-long Raman fibre laser amplification method has been explored and characterised. Experimental results of power distribution, on-off gain and OSNR measurements in unrepeatered links are confirmed with numerical simulations. Data transmission with direct, differentially coherent and coherent detection was experimentally verified in long unrepeatered as well as long-haul trans-atlantic links using second order bi-directional URFL based amplification with standard SMF-28 fibre only.

The URFL based amplification offers the best signal power distribution over standard telecommunication fibre allowing for a quasi-lossless transmission with a single wavelength pump only. To achieve similar performance with a conventional Raman amplification, higher-order pumping have to be implemented which lowers the flexibility of the system as the wavelength and the bandwidth of the source pumps are fixed. In contrary, URFLs gain profile can be modified to achieve optimal performance for particular approach by selecting appropriate FBGs. Superior noise performance in higher-order distributed Raman amplification can extend the distance between repeaters and reduce the total number of amplifiers in trans-atlantic optical links. Improved noise figure allows for advanced multi-level modulation formats with high density constellations that leads to higher spectral efficiency. Multi-wavelength pump configuration can extend and utilise the available bandwidth in silica fibres.

The transmission results presents flexibility of URFL based amplification with bi-directional configuration in unrepeatered and backward pumped only long-haul

repeatered links. It was shown that standard SMF-28 was the most suitable fibre for URFL amplifier due to it's zero dispersion wavelength located outside the band between primary pump and signal frequency. This feature can be used to upgrade already existing links with standard fibre.

6.1 Further Work Recommendation

Further investigation should be performed in experimental analysis of pump-signal RIN transfer in URFL based amplifier in repeatered links as it was found that ideally distributed power along the fibre in bi-directional configuration does not allow for long-haul trans-atlantic transmission due to accumulation of RIN noise caused by forward pumping.

The data transmission with URFL based amplifier should be experimentally compared with conventional second order distributed Raman amplification with dual order pumping scheme to prove the advantage.

Increased span length may reduce the number of amplifiers in long-haul transmission, however the experimental research on optimal spacing needs more attention. The same distance covered with long span distributed Raman amplification in repeatered system should be directly compared with EDFA.

Bibliography

[1] Robert G. Gallager. **Claude E. Shannon: A Retrospective on His Life, Work, and Impact**. *IEEE*, **47**(7), 2001. 18

[2] C. E. Shannon. **A Mathematical Theory of Communication**. *The Bell System Technical Journal*, **27**:379–423, 623–656, 1948. 18

[3] Partha P. Mitra and Jason B. Stark. **Nonlinear limits to the information capacity of optical fibre communications**. *Nature*, **411**(28), 2001. 18

[4] K. S. Turitsyn and S. K. Turitsyn. **Nonlinear communication channels with capacity above the linear Shannon limit**. *Optics Letters*, **37**(17), 2012. 18

[5] J. D. Ania-Castañón. **Quasi-lossless transmission using second-order Raman amplification and fibre Bragg gratings**. *Optics Express*, **12**(19), 2004. 19, 50, 51, 66, 70, 71

[6] M. Alcon-Camas, A.E. El-Taher, J. D. Ania-Castañón, and P. Harper. **Gain Bandwidth Optimisation and Enhancement in Ultra-long Raman Fibre Laser based Amplifiers**. *in Proc. ECOC'10*, **P1.17**:1–3, 2010. 19, 50

[7] V. E. Perlin and H. G. Winful. **On trade-off between noise and nonlinearity in WDM systems with distributed Raman amplification**. *in Proc. OFC'02*, **WB**(WB1):178–180, 2002. 19, 58, 66

[8] John Zyskind and Atul Srivastava. *Optically Amplified WDM Networks*, **Ch. 10**. Academic Press, 2010. 19, 36

[9] W. Forysiak. **In private e-mail**. *Royal Society Industrial Fellow*, 2013. 19, 36

[10] R. Maurer, P. Schultz, and D. Keck. **Fused Silica Optical Waveguide**. *Patent 3,659,915*, 1972. 21, 33

[11] H. Wu, J. A. Tierno, P. Pepeljugoski, J. Schaub, S. Gowda, J. A. Kash, and A. Hajimiri. **Integrated transversal equalizers in high-speed fiber-optic systems**. *IEEE J. Solid-State Circuts*, **38**(12), 2003. 21

[12] S. Makino, K. Kogo, D. Kawamura, Y. Matsuoka, T. Sugawara, and S. Tanaka. **A 40-Gbit/s MMF Transmission with 1.3-m Lens-integrated EA/DFB Lasers for Optical Interconnect**. *in Proc. OFC'12*, **OTh3F.2**, 2012. 21

[13] G. P. Agraval. *Nonlinear Fiber Optics*, **Ch. 1**. Academic Press, 4th edition, 2007. 21, 22, 23, 24, 25, 26, 27

[14] Croning Inc. **http://www.croning.com**. *Products and Services*, 2013. 22

[15] OFS. **http://www.ofsoptics.com/fiber**. *Optical Fiber*, 2013. 22

[16] Cisco Systems Inc. **Fiber Types in Gigabit Optical Communications**. *White Paper*, 2008. 22

[17] G. P. Agraval. *Nonlinear Fiber Optics*, **Ch. 1, 3**. Academic Press, 4th edition, 2007. 22

[18] I N Sisakyan and A B Shvartsburg. **Nonlinear dynamics of picosecond pulses in fiber-optic waveguides (review)**. *Sov. J. Quantum Electron*, **14**(1146):1146–1157, 1984. 24

[19] I. P. Kaminov. **Polarization in Optical Fibers**. *IEEE J. Quantum Electron*, **QE-17**(15):15 – 22, 1981. 26

[20] G. P. Agraval. *Lightwave Technology: Telecommunication Systems*. Wiley, Hoboken, NJ, 2005. 26

[21] D. Marcuse. *Light Transmission Optics*, **Ch. 8**. Van Nostrand Reinhold, 1982. 27

[22] G. P. Agraval. *Nonlinear Fiber Optics*, **Ch. 2**. Academic Press, 4th edition, 2007. 27, 29, 30

[23] Fujio Shimizu. **Frequency Broadening In Liquids By A Short Light Pulse**. *Physical Review Letters*, **19**(19):1097 – 1099, 1967. 28

[24] R. H. Stolen and Chinlon Lin. **Self-phase-modulation in silica optical fibers**. *Physical Review A*, **17**(4):1448–1453, 1978. 28

[25] O. Boyraz, T. Indukuri, and B. Jalali. **Self-phase-modulation induced spectral broadening in silicon waveguides**. *Optics Express*, **12**(CThJ2):829–834, 2004. 28

[26] B. R. Washburn, J. A. Buck, and S. E. Ralph. **Transform-Limited Spectral Compression Due To Self-phase Modulation In Fibers**. *Optics Letters*, **25**(7):445–447, 2000. 28

[27] M. T. Myaing, J. Urayama, A. Braun, and T. Norris. **Nonlinear propagation of negatively chirped pulses: Maximizing the peak intensity at the output of a fiber probe**. *Optics Express*, **7**(5):210–214, 2000. 28

[28] G. P. Agraval. *Nonlinear Fiber Optics*, **Ch. 4**. Academic Press, 4th edition, 2007. 28, 29

[29] W. J. Tomlinson, R. H. Stolen, and A. M. Johnson. **Optical wave breaking of pulses in nonlinear optical fibers**. *Optics Letters*, **10**(9):457–459, 1985. 28

[30] D. Anderson, M. Desaix, M. Lisak, and M. L. Quiroga-Teixeiro. **Wave breaking in nonlinear-optical fibers**. *J. Opt. Soc. Am B*, **9**(8):1358–1361, 1992. 28

[31] A. Hasegawa and F. Tappert. **Transmission of stationary nonlinear optical pulses in dispersive dielectric fibers. I. Anomalous dispersion**. *Appl. Phys. Lett.*, **23**(142), 1973. 29

[32] P. Harper, F. M. Knox, P.N.Kean, L. Zhang, N. J. Doran, and I. Benniori. **Soliton Transmission Over 2700Km Using An Im- Fibre Bragg Grating Filter To Give Gordon-Hatjs Jitter Reduction**. *in Proc. CLEO/Europe'96*, **CThF3**, 1996. 29

[33] P. Harper, I S . Penketh, S. Alleston, and N.J. Doran. **200000 km 10 Gbit/s soliton propagation exploiting periodic saturable absorption**. *in Proc. ECOC'98*, **1**:107–108, 1998. 29

[34] P. Harper, A. E. El-Taher, H. Wang, M. Alcon-Camas, V. Karalekas, and J.D Ania-Castanon. **True soliton transmission through ultra-long laser links**. *in Proc. ECOC'08*, **1**(Mo.3.F.2):61–62, 2008. 29

[35] M. Shtaif. **Analytical description of cross-phase modulation in dispersive optical fibers**. *Optics Express*, **23**(15):1191–1193, 1998. 29

[36] T. Ogata, Y. Aoki, T. Koga, and L. Matsuoka. **Observation of bit-error-rate impairment due to dynamic cross-phase modulation in 2.5 Gbit/s WDM transmission systems with standard fiber**. *in Proc. OFC'96*, **TD**(Tul2), 1996. 29

[37] L. Rapp. **Experimental investigation of signal distortions induced by cross-phase modulation combined with dispersion**. *IEEE Photon. Technol. Lett.*, **9**(12):1592–1594, 1997. 29

[38] L. E. Nelson, A. H. Gnauck, R. M. Jopson, and A. R. Chraplyvy. **Cross-phase modulation resonances in wavelength-division-multiplexed lightwave transmission**. *in Proc. ECOC'98*, **1**:309–310, 1998. 29

[39] C. V. Raman. **A new class of spectra due to secondary radiation**. *Indian J. Phys*, **2**(387):399 – 419, 1928. 29

[40] G. P. Agraval. *Nonlinear Fiber Optics*, **Ch. 8**. Academic Press, 4th edition, 2007. 29, 30

[41] B. G. Saar, C. W. Freudiger, J. Reichman, C. M. Stanley, G. R. Holtom, and X. S. Xie. **Video-Rate Molecular Imaging in Vivo with Stimulated Raman Scattering**. *Science Translational Medicine*, **330**:1368–1370, 2010. 30

[42] M. Ji, D. A. Orringer, C. W. Freudiger, S. Ramkissoon, X. Liu, D. Lau, A. J. Golby, I. Norton, M. Hayashi, N. Y. R. Agar, G. S. Young, C. Spino, S. Santagata, S. C. Piragua, K. L. Ligon, O. Sagher, and X. S. Xie. **Rapid, Label-Free Detection of Brain Tumors with Stimulated Raman Scattering Microscopy**. *Science Translational Medicine*, **5**(201), 2013. 30

[43] Z. Yusoff, J. H. Lee, W. Belardi, T. M. Monro, P. C. Teh, and D. J. Richardson. **Raman effects in a highly nonlinear holey fiber: amplification and modulation**. *Optics Letters*, **27**(6):424–426, 2002. 30

[44] R. Claps, D. Dimitropoulos, V. Raghunathan, Y. Han, and B. Jalali. **Observation of stimulated Raman amplification in silicon waveguides**. *Optics Express*, **11**(15):1731–1739, 2003. 30

[45] R. Claps, V. Raghunathan, D. Dimitropoulos, and B. Jalali. **Influence of nonlinear absorption on Raman amplification in Silicon waveguides**. *Optics Express*, **12**(12):2774–2780, 2004. 30

[46] J. P. Dakin and D. J. Pratt. **Distributed optical fibre raman temperature sensor using a semiconductor light source and detector**. *Electronics Letters*, **21**(13), 1985. 31

[47] Yan Feng Luke, R. Taylor, and D. B. Calia. **150 W highly-efficient Raman fiber laser**. *Optics Express*, **17**(26):23678–23683, 2009. 31

[48] Chinlon Lin and Rogers H. Stolen. **Backward Raman amplification and pulse steepening in silica fibers**. *Appl. Phys. Lett.*, **29**(428), 1976. 31, 35

[49] Clifford Headley and Govind P. Agrawal. *Raman Amplification In Fiber Optical Communication Systems*. Academic Press, 2005. 31, 35

[50] Mohammad N. Islam. *Raman Amplifiers for Telecommunications 1*. Springer, 2003. 31, 35

[51] Mohammad N. Islam. *Raman Amplifiers for Telecommunications 2*. Springer, 2004. 31, 35

[52] G. P. Agraval. *Nonlinear Fiber Optics*, **Ch. 10**. Academic Press, 4th edition, 2007. 31, 32

[53] Chinlon Lin, W. A. Reed, A. D. Pearson, and H.T. Shang. **Phase matching in the minimum-chromatic-dispersion region of single-mode fibers for stimulated four-photon mixing**. *Optics Letters*, **6**(10):493–495, 1981. 32

[54] A. R. Chraplyvy. **Limitations on Lightwave Communications Imposed by Optical-Fiber Nonlinearities**. *Journal of Lightwave Technology*, **8**(10):1548–1557, 1990. 32, 61

[55] E. Snitzer and J. W. Hicks. **Optical Wave-Guide Modes in Small Glass Fibers, I Theoretical**. *J. Opt. Soc. Am*, **49**:1128, 1959. 33

[56] H. Osterberg, E. Snitzer, M. Polanyi, and R. Hilberg. **Optical Wave-Guide Modes in Small Glass Fibers, II Experimental**. *J. Opt. Soc. Am*, **49**:1128, 1959. 33

[57] E. Snitzer. **Optial MASER Action of Nd+3 in a barium Crown Glass**. *Physical Review Letters*, **7**(12):444–446, 1961. 33

[58] Charles J. Koester and Elias Snitzer. **Amplification in a Fiber Laser**. *Applied Optics*, **3**(10):1182–1186, 1964. 33

[59] S. B. Poole, D. N. Payne, and M. E. Fermann. **Fabrication of low-loss optical fibres containing rare-earth ions**. *Electronics Letters*, **21**:737–738, 1985. 33

[60] D. N. Payne and L. Reekie. **Rare-Earth Doped Fibre Lasers and Amplifiers**. *in Proc. ECOC'87*, 1987. 33

[61] R. S. Quimby. **Output saturation in a 980-nm pumped erbium-doped fiber amplifier**. *Applied Optics*, **30**(18):2546–2552, 1991. 33, 38

[62] R. Paschotta, J. Nilsson, A. C. Tropper, and D. C. Hanna. **Ytterbium-Doped Fiber Amplifiers**. *IEEE J. Quantum Electron*, **33**(7), 1997. 33

[63] M. J. Connelly. *Semiconductor Optical Amplifiers*. Springer, 2002. 34

[64] P. S. Cho and J. B. Khurgin. **Suppression of Cross-Gain Modulation in SOA Using RZ-DPSK Modulation Format**. *IEEE Photon. Technol. Lett.*, **15**(1):162–164, 2003. 34

[65] A. R. Chraplyvy and R. W.Tkach. **Narrowband Tunable Optical Filter For Channel Selection In Densely Packed Wdm Systems**. *Electronics Letters*, **22**(20):1084–1085, 1986. 34

[66] R. H. Stolen and J. E. Bjorkholm. **Parametric Amplification and Frequency Conversion in Optical Fibers**. *IEEE J. Quantum Electronics*, **QE-18**(7):1062–1072, 1982. 34

[67] M. E. Marhic, N. Kagi, T. K. Chiang, and L. G. Kazovsky. **Broadband fiber optical parametric amplifiers**. *Optics Letters*, **21**(8):573–575, 1996. 34

[68] J. A. Levenson, I. Abram, and Th. Rivera. **Reduction of quantum noise in optical parametric amplification**. *J. Opt. Soc. Am B*, **10**(11):2233–2238, 1993. 35

[69] W. Imajuku and A. Takada. **Noise Figure of Phase-Sensitive Parametric Amplifier Using a Mach–Zehnder Interferometer With Lossy Kerr Media and Noisy Pump**. *IEEE J. Quantum Electronics*, **39**(6):799–812, 2003. 35

[70] S. Olonkins, V. Bobrovs, and G. Ivanovs. **Investigation of Fiber Optical Parametric Amplifier Performance in DWDM Transmission Systems**. *Elektronika ir Elektrotechnika*, **20**(1), 2014. 35

[71] Jake Bromage. **Raman Amplification for Fiber Communications Systems**. *Journal of Lightwave Technology*, **22**(1):79–93, 2004. 35, 41, 42

[72] M. L. Dakss and P. Melman. **Two-channel fibre Raman amplification for wavelength division multiplexed systems**. *Optoelectronics, IEE Proceedings J*, **135**(2), 1988. 35

[73] G. P. Agraval. *Fiber-Optic Communication Systems*, **Ch. 6**. A John Wiley and Sons, 2002. 35

[74] R. Olshansky. **Noise Figure For Erbium-Doped Optical Fibre Amplifiers**. *Electronics Letters*, **24**(22):1663–1665, 1988. 36, 39

[75] R. I. Laming, M. N. Zervas, and D. N. Payne. **Erbium-Doped Fiber Amplifier with 54 dB. Gain and 3.1 dB Noise Figure**. *IEEE Photon. Technol. Lett.*, **4**(12):1345–1347, 1992. 36, 39

[76] J. Hansryd, P. A. Andrekson, M. Westlund, J. Li, and P. O. Hedekvist. **Fiber-Based Optical Parametric Amplifiers and Their Applications**. *IEEE J. Of Selected Topics in Quantum Electronics*, **8**(3), 2002. 36

[77] A. Klekamp, R. Dischler, and W. Idler. **"DWDM and single channel fibre nonlinear thresholds for 43 Gb/s ASK and DPSK formats over various fibre types"**. *in Proc. OFC'06*, **OFD5**, 2006. 36

[78] T. Horiguchi, T. Sato, and Y. Koyamada. **Stimulated Raman Amplification of 1.6-um-Band Pulsed Light in Optical Fibers**. *IEEE Photon. Technol. Lett.*, **4**(1):64–66, 1992. 36

[79] H. A. Haus and J. A. Mullen. **Quantum Noise in Linear Amplifiers**. *Physical Review*, **128**(5):2407–2413, 1962. 36

[80] C. M. Caves. **Quantum limits on noise in linear amplifiers**. *Physical Review D*, **26**(8):1817–1839, 1982. 36

[81] R. Hui and M. O'Sullivan. *Fiber Optic Measurement Techniques*, **Ch. 3**. Academic Press, 4th edition, 2009. 36, 37, 43

[82] M. Shimizu, M. Yamada, M. Horiguchi, T. Takeshita, and M. Okayasu. **Erbium-Doped Fibre Amplifiers With An Extremely High Gain Coefficient of 11dB/mW**. *Electronics Letters*, **26**(20), 1990. 38, 80

[83] R. I. Laming, D. N. Payne, L. Reekie, and P. R. Morkel. **Erbium-doped Fibre Amplifiers Operating at 1.5m**. *in Proc. OCTIMA*, **388**, 1989. 38

[84] J. M. P Delavaux and J. A. Nagel. **Multi-Stage Erbium-Doped Fiber Amplifier Designs**. *Journal of Lightwave Technology*, **13**(5):703–720, 1995. 39

[85] P. F. Wysocki, J. B. Judkins, R. P. Espindola, M. Andrejco, and A. M. Vengsarkar. **Broad-Band Erbium-Doped Fiber Amplifier Flattened Beyond 40 nm Using Long-Period Grating Filter**. *IEEE Photon. Technol. Lett.*, **9**(10):1343–1345, 1997. 39

[86] P. F. Wysocki, N. Park, and D. DiGiovanni. **Dual-stage erbium-doped, erbium/ytterbium-codoped fiber amplifier with up to +26-dBm output power and a 17-nm flat spectrum**. *Optics Letters*, **21**(21):1744–1746, 1996. 39

[87] M. Yamada, A. Mori, K. Kobayashi, H. Ono, T. Kanamori, K. Oikawa, Y. Nishida, and Y. Ohishi. **Gain-Flattened Tellurite-Based EDFA with a Flat Amplification Bandwidth of 76 nm**. *IEEE Photon. Technol. Lett.*, **10**(9):1244–1246, 1998. 39

[88] M. Yamada, M. Shimizu, M. Okayasu, T. Takeshita, M. Horiguchi, Y. Tachikawa, and E. Sugita. **Noise Characteristics of Er3+-Doped Fiber Amplifiers Pumped by 0.98 and 1.48 um Laser Diodes**. *IEEE Photon. Technol. Lett.*, **2**(3):205–207, 1990. 39

[89] R. Morkel and R. I. Laming. **Theoretical modeling of erbium-doped fiber amplifiers with excited-state absorption**. *Optics Letters*, **14**(19):1062–1064, 1989. 40

[90] C. R. Giles and E. Desurvire. **Modeling Erbium-Doped Fiber Amplifiers**. *Journal of Lightwave Technology*, **9**(2):271–283, 1991. 40

[91] R. M. Jopson and A. A. M. Saleh. **Modeling of gain and noise in erbium-doped fibre amplifiers**. *in Proc. of SPIE'91*, **1581**:114–119, 1991. 40

[92] S.A.E. Lewis, S. V. Chernikov, and J. R. Taylor. **Gain and saturation characteristics of dual-wavelength-pumped silica-fibre Raman amplifiers**. *Electronics Letters*, **35**(14):1178 – 1179, 1999. 40, 48, 74

[93] H. A. Fevrier and M. W. Chbat. **Raman amplification technology for bandwidth extension**. *IEEE, LEOS*, **1**:344–345, 2001. 40

[94] H. Kidorf, K. Rottwitt, M. Nissov, M. X. Ma, and E. Rabarijaona. **Pump interactions in a 100-nm bandwidth Raman amplifier**. *IEEE Photon. Technol. Lett.*, **11**(5):1041–1135, 1999. 40, 48, 74

[95] Y. Hadjar, N. J. Traynor, and S. Gray. **Noise Figure Tilt Reduction in Ultrawide-Band WDM Through Second-Order Raman Amplification**. *IEEE Photon. Technol. Lett.*, **16**(4):1200–1202, 2004. 40, 50

[96] P.M. Krummrich, R.E. Neuhauser, H. Bock, W. Fischler, and C. Glingener. **System performance improvements by codirectional Raman pumping of the transmission fiber**. *in Proc. ECOC'01*, **Tu.A.1.4**:114–115, 2001. 40

[97] M.X. Ma, H. D. Kidorf, K. Rottwitt, F. W. Kerfoot, and C. R. Davidson. **240-km repeater spacing in a 5280-km WDM system experiment using 8 x 2.5 Gb/s NRZ transmission**. *IEEE Photon. Technol. Lett.*, **10**(6):893 – 895, 1998. 40, 67

[98] H. Bissessur. **Amplifier Technologies for Unrepeatered links, Submarine Transmissions**. *in Proc. OFC'13*, **OTh4C.3**, 2013. 40

[99] J. Ma, C. Jiang, and J. Wu. **Optimal design of ultrabroadband tellurite fiber Raman amplifier for wavelength-division multiplexing transmission systems**. *Optical Engineering*, **47**(4), 2008. 40

[100] K. Mochizuki, N. Edagawa, and Y. Iwamoto. **Amplified Spontaneous Raman Scattering in Fiber Raman Amplifiers**. *Journal of Lightwave Technology*, **LT-4**(9):1328–1333, 1986. 41

[101] N. A. Olsson and J. Hegarty. **Noise Properties of a Raman Amplifier**. *Journal of Lightwave Technology*, **LT-4**(4):396–399, 1986. 41

[102] Clifford Headley and Govind P. Agrawal. *Raman Amplification In Fiber Optical Communication Systems*, **Ch. 2.2.1**. Academic Press, 2005. 41

[103] N. A. Olsson. **Lightwave systems with optical amplifiers**. *Journal of Lightwave Technology*, **7**(7):1071 – 1082, 1989. 41

[104] M. L. Dakss and P. Melman. **Amplified Spontaneous Raman Scattering and Gain Fiber Raman Amplifiers**. *Journal of Lightwave Technology*, **LT-3**(4):806–813, 1985. 41

[105] P. B. Hansen, L. Eskildsen, A. J. Stentz, T. A. Strasser, J. Judkins, J. J. DeMarco, R. Pedrazzani, and D. J. DiGiovanni. **Rayleigh Scattering Limitations in Distributed Raman Pre-Amplifiers**. *IEEE Photon. Technol. Lett.*, **10**(1):159–161, 1998. 41, 42

[106] M. O. van Deventer. **Polarization Properties of Rayleigh Backscattering in Single-Mode Fibers**. *Journal of Lightwave Technology*, **11**(12):1895–1899, 1993. 42

[107] J. Bromage, P. J. Winzer, and R.-J. Essiambre. **Multiple path interference and its impact on system design**. *in Raman Amplifiers for Telecommunciations 2*, **15**, 2004. 42

[108] R. J. Essiambre, P. Winzer, J. Bromage, and C. H. Kim. **Design of Bidirectionally Pumped Fiber Amplifiers Generating Double Rayleigh Backscattering**. *IEEE Photon. Technol. Lett.*, **14**(7):914–916, 2002. 42, 68

[109] G. Bolognini and A. Bononi. **Reduction of double Rayleigh scattering noise in distributed Raman amplifiers employing higher-order pumping**. *Optics Express*, **17**(9):6996–7003, 2009. 42

[110] G. P. Agraval. *Fibre-Optic Communication Systems*, **Ch. 3**. John Wiley & Sons, 2002. 43

[111] C. R. S. Fludger, V. Handerek, and R. J. Mears. **Pump to Signal RIN Transfer in Raman Fiber Amplifiers**. *Journal of Lightwave Technology*, **19**(8):1140–1148, 2001. 43, 44

[112] M. D. Mermelstein, K. Brar, and C. Headley. **RIN Transfer Suppression Technique for Dual-Order Raman Pumping Schemes**. *IEEE Photon. Technol. Lett.*, **15**(10):1354–1356, 2003. 45

[113] S. Faralli, G. Bolognini, G. Sacchi, S. Sugliani, and F. Di Pasquale. **Bidirectional Higher Order Cascaded Raman Amplification Benefits for 10-Gb/s WDM Unrepeated Transmission Systems**. *Journal of Lightwave Technology*, **23**(8):2427–2433, 2005. 45

[114] M. Alcón-Camas and J. D. Ania-Castañón. **RIN transfer in 2nd-order distributed amplification with ultralong fiber lasers**. *Optics Express*, **18**(23):23569–23575, 2010. 45, 54

[115] E. Desurvire. **Erbium-Doped Fiber Amplifiers**. *Wiley*, pages 624–626, 1994. 46

[116] J. D. Ania-Castañón. **In private e-mail**. 2012. 46

[117] H. A. Luther and H. P. Konen. **Some Fifth-Order Classical Runge-Kutta Formulas**. *SIAM Review*, **7**(4):551–558, 1965. 47

[118] K. Rottwitt and H. D. Kidorf. **A 92 nm Bandwidth Raman Amplifier**. *in Proc. OFC'98*, **PD**(PD6):448–451, 1998. 48

[119] Y. Emori and S. Namiki. **100 nm bandwidth flat gain Raman amplifiers pumped and gain-equalized by 12-wavelength-channel WDM high power laser diodes**. *in Proc. OFC'99*, **PD19**, 1999. 48, 74

[120] J.C. Boutciller, K. Brar, S. Radic, J. Bromage, Z. Wang, and C. Headley. **Dual-order Raman pump providing improved noise figure and large gain bandwidth**. *in Proc. OFC'02*, **PD**(FB3), 2002. 48

[121] J. C. Bouteiller, K. Brar, J. Bromage, S. Radic, and C. Headley. **Dual-Order Raman Pump**. *IEEE Photon. Technol. Lett.*, **15**(2):212–214, 2003. 48, 50

[122] S. Faralli, G. Bolognini, G. Sacchi, S. Sugliani, and F. D. Pasquale. **Bidirectional Higher Order Cascaded Raman Amplification Benefits for 10-Gb/s WDM Unrepeated Transmission Systems**. *Journal of Lightwave Technology*, **23**(8):2427–2433, 2005. 50

[123] S.B. Papernyi, V.B. Xvnnov, Y.Koyanoand, and H. Yamamoto. **Sixth-Order Cascaded Raman Amplification**. *in Proc. OFC'05*, **4**(OThF4), 2005. 50

[124] K. Zang, C. Yu, X. Xin, J. Yuan, W. Xie, and Y. Wang. **Optimization on bandwidth in the third-order pumped distributed fiber Raman amplifier**. *SPIE Optical Engineering*, **52**(7), 2013. 50

[125] Y. Hadjar and N. J. Traynor. **Quantitative analysis of second order distributed Raman amplification**. *in Proc. OFC'02*, **ThB**(ThB1), 2002. 50

[126] J. D. Ania-Castañón, T. J. Ellingham, R. Ibbotson, X. Chen, L. Zhang, and S. K. Turitsyn. **Ultralong Raman Fiber Lasers as Virtually Lossless Optical Media**. *Physical Review Letters*, **96**(2), 2006. 50, 66

[127] J. D Ania-Castañón, V. Karalekas, P. Harper, and S. K. Turitsyn. **Simultaneous spatial and spectral transparency in ultralong fiber lasers**. *Physical Review Letters*, **101**(12), 2008. 50

[128] S. A. Babin, V. Karalekas, E. V. Podivilov, V. K. Mezentsev, P. Harper, J. D. Ania-Castanon, and S. K. Turitsyn. **Characterization of Ultra-Long Raman Fibre Lasers**. *in Proc. of SPIE'08*, **6873**, 2008. 50

[129] J.D. Ania-Castañón and S.K. Turitsyn. **Unrepeatered transmission through ultra-long fiber laser cavities**. *Optcs Communications*, **281**:5760–5763, 2008. 50, 66

[130] P. Rosa, P. Harper, N. Murray, and J. D. Ania-Castanon. **Unrepeatered 8 x 40Gb/s transmission over 320km SMF-28 using ultra-long Raman fibre based amplification**. *in Proc. ECOC'12*, **P4.04**, 2012. 58, 67, 79, 90, 102

[131] S. R. Bickham. **Ultimate Limits of Effective Area and Attenuation for High Data Rate Fibers**. *in Proc. OFC'11*, **OWA5**, 2011. 61

[132] Y. Yamamoto, M. Hirano, and T. Sasaki. **A New Class of Optical Fiber to Support Large Capacity Transmission**. *in Proc. OFC'11*, **OWA6**, 2011. 61

[133] J. D. Downie, J. Hurley, S. Ten, C. Towery, M. Sharma, Y. Mauro, C. Malouin, B. Zhang, J. Bennike, T. Schmidt, and R. Saunders. **Performance of 1200 km 40G DPSK systems over NZ-DSF with no in-line compensation**. *in Proc. OECC'10*, **9B1-4**:750–751, 2010. 61

[134] J.D. Downie, M. Sauer, and J. Hurley. **1500 km transmission over NZ-DSF without in-line or post-compensation of dispersion for 38 x 10.7 Gbit/s channels**. *Electronics Letters*, **42**(11), 2006. 61

[135] P. Harper. **Dispersion slope measurements**. *Aston Institute of Photonic Technologies*, 2007. 61

[136] N. Shibata, R. P. Braun, and R. G. Waarts. **Phase-Mismatch Dependence of Efficiency of Wave Generation Through Four-Wave Mixing in a Single-Mode Optical Fiber**. *IEEE J. Quantum Electron*, **QE-23**(7):1205–1210, 1987. 61

[137] R.E. Neuhauser, P.M. Krummrich, H. Bock, and C. Glingener. **Impact of nonlinear pump interactions on broadband distributed Raman amplification**. *in Proc. OFC'01*, **MA4-1**, 2001. 61

[138] L. Leng, B. Zhu, S. Stulz, L. Nelson, J. Bauteiiler, P. Kristensen, and L. Gmer-Nielsen. **Experimental Investigation of**

the Impact of NZDF Zero-Dispersion Wavelength on Broadband Transmission In Raman-Enhanced Systems. *in Proc. OFC'03*, **1**(WE4):330–332, 2003. 61

[139] J. C. Bouteiller, L. Leng, and C. Headley. **Pump–Pump Four-Wave Mixing in Distributed Raman Amplified Systems**. *Journal of Lightwave Technology*, **22**(3):723– 732, 2004. 61

[140] M. C. Ho, C. J. Chen, W. S. Wong, and H. K. Lee. **Parametric Interactions Between Pumps and Signals in a Copumped Raman Amplifier**. *in Proc. CLEO'02*, **CThJ6**:481–482, 2002. 62

[141] J. Bromage, L.E. Nelson, P.J. Winzer, and C.J. McKinstrie. **Raman-enhanced pump-signal four-wave mixing in bidirectionally-pumped Raman amplifiers**. *in Proc. OAA'02*, **OWA**(OWA5), 2002. 62

[142] F. D. Pasquale and F. Meli. **New Raman Pump Module for Reducing Pump–Signal Four-Wave-Mixing Interaction in Co-Pumped Distributed Raman Amplifiers**. *Journal of Lightwave Technology*, **21**(8):1742–1748, 2003. 62

[143] J. Bromage, J. C. Bouteiller, H. J. Thiele, K.Brar, L. E. Nelson, S. Stulz, C. Headley, J. Kim, A. Klein, G.Baynham, L.V. Jergensen, L. Griiner-Nielsen, R.L. Lingle Jr, and D. J. DiGiovanni. **High co-directional Raman gain for 200-km spans, enabling 40 x 10.66 Gb/s transmission over 2400 km**. *in Proc. OFC'03*, **PD24-1**, 2003. 68

[144] S. A. Babin, V. Karalekas, P. Harper, E. V. Podivilov, V. K. Mezentsev, J. D. Ania-Castañón, and S. K. Turitsyn. **Experimental demonstration of mode structure in ultralong Raman fiber lasers**. *Optics Express*, **32**(9):1135–1137, 2007. 70

[145] K. Rottwitt, A. Stentz, T. Nielsen, P. Hansen, K. Feder, and K. Walker. **Transparent 80km bi-directionally pumped distributed Raman amplifier with second order pumping**. *in Proc. ECOC'99*, **2**(144), 1999. 70

[146] J. D. Ania-Castañón. **Joint publication**. 2013. 71, 77

[147] M. Vasilyev, B. Szalabofka, S. Tsuda, J. M. Grochocinski, and A.F. Evans. **Reduction of Raman MPI and noise figure in dispersion-managed fibre**. *Electronics Letters*, **38**(6), 2002. 74, 79

[148] D. Dahan and G. Eisenstein. **The properties of amplified spontaneous emission noise in saturated fiber Raman amplifiers operating with CW signals**. *Optics Communications*, **236**:279–288, 2004. 76, 79

[149] S. Wang and C. Fan. **Distributed fiber Raman amplifers: analytical expression of noise characteristics under complex conditions**. *Optics Communications*, **198**:65–70, 2001. 79

[150] E. Desurvire. **Analysis of Distributed Erbium-Doped Fiber Amplifiers with Fiber Background Loss**. *IEEE Photon. Technol. Lett.*, **3**(7):625–628, 1991. 80

[151] G. Keiser. *Optical Fiber Communications*, **Ch. 11 p.438-440**. McGraw-Hill Education (India) Pvt Limited, 4th edition, 2008. 80

[152] L. Helczynski and A. Berntson. **Comparison of EDFA and Bidirectionally Pumped Raman Amplifier in a 40-Gb/s RZ Transmission System**. *IEEE Photon. Technol. Lett.*, **13**(7):669–671, 2001. 84

[153] T. Xu and B. J. Maxum. **Improved transmission performance by hybrid optical amplification in DWDM systems**. *Optical Engineering*, **42**(3):882–885, 2003. 84

[154] H. Bissessur, P. Bousselet D. A. Mongardien, and I. Brylski. **Ultra-long 10 Gb/s Unrepeatered WDM Transmission up to 601 km**. *in Proc. OFC'10*, **OTuD6**, 2010. 84

[155] V. V. Gainov, N. V. Gurkin, S. N. Lukinih, S. G. Akopov, S. Makovejs, S. Y. Ten, O. E. Nanii, and V. N. Treshchikov. **Record 500 km unrepeatered 100 Gb s-1 transmission**. *Laser Phys. Lett.*, **10**, 2013. 84

[156] D. Mongardien, P. Bousselet, O. Bertran-Pardo, P. Tran, and H. Bissessur. **2.6Tb/s (26 x 100Gb/s) Unrepeatered Transmission Over 401km Using PDM-QPSK with a Coherent Receiver**. *in Proc. ECOC'09*, **6.4.3**, 2009. 84

[157] J. D. Downie, J. Hurley, J. Cartledge, S. Ten, S. Bickham, S. Mishra, X. Zhu, and A. Kobyakov. **40 112 Gb/s Transmission over an Unrepeatered 365 km Effective Area-Managed Span Comprised of Ultra-Low Loss Optical Fibre**. *in Proc. ECOC'10*, **We.7.C.5**, 2010. 84

[158] Tsuyoshi Yamamoto. **High-Speed Directly Modulated Lasers**. *in Proc. OFC'12*, **OTh3F**(OTh3F.5), 2012. 86

[159] J. H. Song, M. Rensing, C. L. L. M. Daunt, P. O'Brien, and F. H. Peters. **Directly Modulated Laser Diode Module Exceeding 10 Gb/s Transmission**. *IEEE Transactions on Components, Packaging, and Manufacturing Technology*, **1**(6):975–980, 2011. 86

[160] Y. Yu, R. Lewen, S. Irmscher, U.Westergren, and L. Thylen. **80 Gb/s ETDM transmitter with a traveling-wave electroabsorption modulator**. *in Proc. OFC'05*, **OWE1**, 2005. 86

[161] D. Feng, S. Liao, H. Liang, J. Fong, B. Bijlani, R. Shafiiha, B. J. Luff, Y. Luo, J. Cunningham, A. V. Krishnamoorthy, and M. Asghari. **High speed GeSi electro-absorption modulator at 1550 nm wavelength on SOI waveguide**. *Optics Express*, **20**(20):22224–22232, 2012. 86

[162] P. J. Winzer and R. J Essiambre. **Advanced Modulation Formats for High-Capacity Optical Transport Networks**. *Journal of Lightwave Technology*, **24**(12):4711–4728, 2006. 86

[163] X. Xiao, H. Xu abd X. Li, Z. Li, T. Chu, Y. Yu, and J. Yu. **High-speed, low-loss silicon Mach–Zehnder modulators with doping optimization**. *Optics Express*, **21**(4):4116–4125, 2013. 86

[164] L. Liao, D. Samara-Rubio, M. Morse, A. Liu, D. Hodge, D. Rubin, U. Keil, and T. Franck. **High speed silicon Mach-Zehnder modulator**. *Optics Express*, **13**(8):3129–3135, 2005. 86

[165] J. Li, C. Schubert, R. H. Derksen, R. E. Makon, V. Hurm, A. Djupsjöbacka, M. Chacinski, U. Westergren, H. G. Bach, G. G. Mekonnen, A. G. Steffan, R. Driad, H. Walcher, and J. Rosenzweig. **112 Gb/s Field Trial of Complete ETDM System Based on Monolithically Integrated Transmitter and Receiver Modules for Use in 100GbE**. *in Proc. ECOC'10*, **P4.03**, 2010. 86

[166] S. Walklin and J. Conradi. **Effect of Mach–Zehnder Modulator DC Extinction Ratio on Residual Chirp-Induced Dispersion in 10-Gb/s Binary and AM-PSK Duobinary Lightwave Systems**. *IEEE Photon. Technol. Lett.*, **9**(10):1400–1402, 1997. 87

[167] S. D. Personick. **Receiver Design for Digital Fiber Optic Communication Systems, II**. *The Bell System Technical Journal*, **52**(6), 1973. 87

[168] Y. Miyamoto, A. Hirano, K. Yonenaga, A. Sano, H. Toba, K. Murata, and O. Mitomi. **320Gbit/s (8 x 40 Gbit/s) WDM transmission over 367 km with 120km repeater spacing using carrier-suppressed return-to-zero format**. *Electronics Letters*, **35**(23):2041–2042, 1999. 88

[169] B. Bakhshi, M. Vaa, E. A. Golovchenko, W. W. Patterson, R. L. Maybach, and N. S. Bergano. **Comparison of CRZ, RZ and NRZ modulation formats in a 64 x 12.3 Gb/s WDM transmission experiment over 9000 km**. *in Proc. OFC'01*, **WF4**, 2001. 88

[170] H. Haunstein and R. Schlenk. **Control Of Delay Line Interferometer**. *Unated States Patents*, **US 7266311 B2**, 2007. 90

[171] P. A. Humblet and M. Azizoglu. **On the bit error rate of lightwave systems with optical amplifiers**. *Journal of Lightwave Technology*, **9**(11):1576 – 1582, 1991. 90

[172] J. M. Kahn and K. P. Ho. **Spectral Efficiency Limits and Modulation/Detection Techniques for DWDM Systems**. *IEEE J. Of Selected Topics in Quantum Electronics*, **10**(2):259–272, 2004. 90, 93, 102

[173] S. R. Chinn, D. M. Boroson, and J. C. Livas. **Sensitivity of optically preamplified DPSK receivers with Fabry-Perot filters**. *Journal of Lightwave Technology*, **14**(3):370–376, 1996. 90

[174] X. Liu, C. Xu, and X. Wei. **Nonlinear phase noise in pulse-overlapped transmission based on return-to-zero differential-phase-shift-keying**. *in Proc. ECOC'02*, **4**, 2002. 90

[175] C. Xu, X. Liu, L. F. Mollenauer, and X. Wei. **Comparison of Return-to-Zero Phase Shift Keying and On-Off Keying in Long Haul Dispersion Managed Transmissions**. *in Proc. OFC'03*, **2**(ThE3), 2003. 90

[176] K. Ishida, T. Kobayashi, J. Abe, K. Kinjo, S. Kuroda, and T. Mizuochi. **A Comparative Study of 10 Gb/s RZ-DPSK and RZ-ASK WDM Transmission Over Transoceanic Distances**. *in Proc. OFC'03*, **15**(ThE2), 2003. 90

[177] T. Mizuochi, K. Ishida, T. Kobayashi, J. Abe, K. Kinjo, K. Motoshima, and K. Kasahara. **A Comparative Study of DPSK and OOK WDM Transmission Over Transoceanic Distances and Their Performance Degradations Due to Nonlinear Phase Noise**. *Journal of Lightwave Technology*, **21**(9):1993–, 2003. 90

[178] G. Vareille, L. Becouarn, P. Pecci, P. Tran, and J. F. Marcerou. **8370 km with 22 dB spans ULH transmission of 185x10.709 Gbit/s RZ-DPSK channels**. *in Proc. OFC'03*, **3**(PD20):1–3, 2003. 90

[179] J. X. Cai, D. G. Foursa, C. R. Davidson, Y. Cai, G. Domagala, H. Li, L. Liu, W. Patterson, A. Pilipetskii, M. Nissov, and N. Bergano. **A DWDM demonstration of 3.73Tb/s over 11,000km using 373 RZ-DPSK channels at 10Gb/s**. *in Proc. OFC'03*, **PD3**(PD22), 2003. 90

[180] L. Becouarn, G. Vareille, P. Pecci, and J. F. Marcerou. **3 Tbit/s transmission (301 DPSK channels at 10.709 Gb/s) over 10 270 km with a record efficiency of 0.65(bit/s)/Hz**. *in Proc. ECOC'03*, **PD**(Th4.3.2), 2003. 90

[181] T. Tsuritani, K. Ishida, A. Agata, K. Shimomura, I. Morita, T. Tokura, H. Taga, T. Mizuochi, and N. Edagawa. **70GHz-spaced 40 x 42.7Gbit/s transmission over 8700km using CS-RZ DPSK signal, all-Raman repeaters and symmetrically dispersion-managed fiber span**. *in Proc. OFC'03*, **PD3**(PD23), 2003. 90

[182] B. Zhu, L. E. Nelson, S. Stulz, A. H. Gnauck, C. Doerr, J. Leuthold, L. Gruner-Nielsen, M. O. Pedersen, J. Kim, R. Lingle, Y. Emori, Y. Ohki, N. Tsukiji, A. Oguri, and S. Namiki. **6.4-Tb/s (160 x 42.7 Gb/s) transmission with 0.8 bit/s/Hz spectral efficiency over 32 x 100 km of fiber using CSRZ-DPSK format**. *in Proc. OFC'03*, **PD3**(PD19), 2003. 90

[183] A.H. Gnauck, G.Raybon, S. Chandrasekhar, J. Leuthold, C. Doerr, L. Stulz, and E. Burrows. **25 x 40-Gb/s Copolarized DPSK Transmission Over 12 x 100-km NZDF With 50-GHz Channel Spacing**. *IEEE Photon. Technol. Lett.*, **15**(3):467–469, 2003. 90

[184] C. J. Rasmussen, T. Fjelde, J. Bennike, F. Liu, S. Dey, B. Mikkelsen, P. Mamyshev, P. Serbe, P. van der Wagt,

Y. Akasaka, D. Harris, D. Gapontsev, V. Ivshin, and P. Reeves-Hall. **DWDM 40G transmission over trans-Pacific distance (10,000km) using CSRZ-DPSK, enhanced FEC and all-Raman amplified 100km UltraWave™ fiber spans**. *in Proc. OFC'03*, **PD3**(PD18), 2003. 90

[185] A. Kanno, T. Sakamoto, A. Chiba, T. Kawanishi, K. Higuma, M. Sudou, and J. Ichikawa. **166 Gb/s PDM-NRZ-DPSK Modulation Using Thin-LiNbO3-Substrate Modulator**. *in Proc. NFOEC*, **JWA**(JWA40), 2010. 90

[186] R. Griffin and A.C. Carter. **Optical differential quadrature phase-shift key (oDQPSK) for high capacity optical transmission**. *in Proc. OFC'02*, **WX**(WX6), 2002. 92

[187] R. A. Griffin, R. I. Johnstone, R. G. Walker, J. Hall, S. D. Wadsworth, K. Berry, A. C. Carter, M. J. Wale, J. Hughes, P. A. Jerram, and N. J. Parsons. **10 Gb/s Optical Differential Quadrature Phase Shift Key (DQPSK) Transmission using GaAs/AlGaAs Integration**. *in Proc. OFC'02*, **FD**(FD6), 2002. 92

[188] C. Wree, J. Leibrich, and W. Rosenkranz. **RZ-DQPSK Format with High Spectral Efficiency and High Robustness Towards Fiber Nonlinearities**. *in Proc. ECOC'02*, **Paper 9.6.6**, 2002. 92

[189] H. Kim and P. J. Winzer. **Robustness to Laser Frequency Offset in Direct-Detection DPSK and DQPSK Systems**. *Journal of Lightwave Technology*, **21**(9):1887, 2003. 92

[190] G. Kramer, A. Ashikhmin, A. J. van Wijngaarden, and X. Wei. **Spectral Efficiency of Coded Phase-Shift Keying for Fiber-Optic Communication**. *Journal of Lightwave Technology*, **21**(10):2438–, 2003. 93

[191] P. J. Winzer, G. Raybon, H. Song, A. Adamiecki, S. Corteselli, A. H. Gnauck, D. A. Fishman, C. R. Doerr, S. Chandrasekhar, L. L. Buhl, T. J. Xia, G. Wellbrock, W. Lee, B. Basch, T. Kawanishi, K. Higuma, and Y. Painchaud. **100-Gb/s DQPSK Transmission: From Laboratory Experiments to Field Trials**. *Journal of Lightwave Technology*, **26**(20):3388–3402, 2008. 93

[192] L. Marazzi, P. Parolari, P. Martelli, R. Siano, P. Boffi, M. Ferrario, A. Righetti, M. Martinelli, V. Pusino, P. Minzioni, I. Cristiani, V. Degiorgio, C. Langrock, and M. M. Fejer. **Real-time 100-Gb/s POLMUX RZ-DQPSK Transmission over Uncompensated 500 km of SSMF by Optical Phase Conjugation**. *in Proc. NFOEC*, **JWA**(JWA44), 2009. 93

[193] C. Fürst, H. Wernz, M. Camera, P. Nibbs, J. Pribil, R. Iskra, and G. Parsons. **43Gb/s RZ-DQPSK Field Upgrade Trial in a 10Gb/s DWDM Ultra-Long-Haul Live Traffic System in Australia**. *in Proc. OFC'08*, **NTuB2**, 2008. 93

[194] C. Fürst, M. Camera, H. Wernz, and H. Griesser. **Experimental Experiences in High Speed DQPSK Transmission**. *in Proc. OFC'09*, **OMT5**, 2009. 93

[195] H. Wernz, S. Herbst, S. Bayer, H. Griesser, E. Martins, C. Furst, B. Koch, V. Mirvoda, R. Noe, A. Ehrhardt, L. Schurer, S. Vorbeck, M. Schneiders, D. Breuer, and R. P. Braun. **Nonlinear Behaviour of 112 Gb/s Polarisation-Multiplexed RZ-DQPSK with Direct Detection in a 630 km Field Trial**. *in Proc. ECOC'09*, **p3.4.3**, 2009. 93

[196] E. M. Ip and J. M. Kahn. **Fiber Impairment Compensation Using Coherent Detection and Digital Signal Processing**. *Journal of Lightwave Technology*, **28**(4):502–519, 2010. 93

[197] S. J. Savory, G. Gavioli, R. I. Killey, and P. Bayvel. **Transmission of 42.8Gbit/s Polarization Multiplexed NRZ-QPSK over 6400km of Standard Fiber with no Optical Dispersion Compensation**. *in Proc. OFC'07*, **OTuA1**, 2007. 93, 95

[198] E. Ip and J. M. Kahn. **Compensation of Dispersion and Nonlinear Impairments Using Digital Backpropagation**. *Journal of Lightwave Technology*, **26**(20):3416–3425, 2008. 93

[199] Rafique D, M. Mussolin, M. Forzati, J. Martensson, M. N. Chugtai, and A. D. Ellis. **Compensation of intra-channel nonlinear fibre impairments using simplified digital back-propagation algorithm**. *Optics Express*, **19**(10):9453–9460, 2011. 93

[200] F. Yaman and G. Li. **Nonlinear Impairment Compensation for Polarization-Division Multiplexed WDM Transmission Using Digital Backward Propagation**. *IEEE Photonics Journal*, **1**(2):144–152, 2009. 93

[201] M. Mussolin, M. Forzati, J. Martensson, A. Carena, and G. Bosco. **DSP-based compensation of non-linear impairments in 100 Gb/s PolMux QPSK**. *in Proc. ICTON'10*, **We.D1.2**, 2010. 93

[202] J. R. Barry and J. M. Kahn. **Carrier Synchronization for Homodyne and Heterodyne Detection of Optical Quadriphase-Shift Keying**. *Journal of Lightwave Technology*, **10**(12):1939–1951, 1992. 94

[203] R. J. Essiambre, G. Foschini, P. Winzer, and G. Kramer. **Capacity Limits of Fiber-Optic Communication Systems**. *in Proc. OFC'09*, **OThL1**, 2009. 95

[204] R. J. Essiambre, G. Kramer, P. Winzer, G. Foschini, and B. Goebel. **Capacity Limits of Optical Fiber Networks**. *Journal of Lightwave Technology*, **28**(4), 2010. 95

[205] W. Shieh and C. Athaudage. **Coherent optical orthogonal frequency division multiplexing**. *Electronics Letters*, **42**(10), 2006. 95

[206] G. Gavioli, E. Torrengo, G. Bosco, A. Carena, V. Curri, V. Miot, P. Poggiolini, M. Belmonte, F. Forghieri, C. Muzio, S. Piciaccia, A. Brinciotti, A. La Porta, C. Lezzi, S. Savory, and S. Abrate. **Investigation of the Impact of Ultra-Narrow Carrier Spacing on the Transmission of a 10-Carrier 1Tb/s Superchannel**. *in Proc. OFC'10*, **OThD3**, 2010. 95, 96

[207] J. X. Cai, Y. Cai, C. R. Davidson, D. G. Foursa, A. Lucero, O. Sinkin, W. Patterson, A. Pilipetskii, G. Mohs, and N. S. Bergano. **Transmission of 96x100G pre-filtered PDM-RZ-QPSK channels with 3004,368km**. *in Proc. OFC'10*, **PDPB10**, 2010. 95

[208] E. Torrengo, R. Cigliutti, G. Bosco, G. Gavioli, A. Alaimo, A. Carena, V. Curri, F. Forghieri, S. Piciaccia, M. Belmonte, A. Brinciotti, A. La Porta, S. Abrate, and P. Poggiolini. **Transoceanic PM-QPSK Terabit Superchannel Transmission Experiments at Baud-Rate Subcarrier Spacing**. *in Proc. ECOC'10*, **We.7.C.2**, 2010. 95

[209] W. Shieh, H. Bao, and Y. Tang. **Coherent optical OFDM: theory and design**. *Optics Express*, **16**(2):841–859, 2008. 96

[210] Y. Ma, Q. Yang, Y. Tang, S. Chen, and W. Shieh. **1 Tb/s per Channel Coherent Optical OFDM Transmission with Subwavelength Bandwidth Access**. *in Proc. OFC'09*, **PDPC1**, 2009. 96

[211] S. Chandrasekhar, X. Liu, B. Zhu, and D. W. Peckham. **Transmission of a 1.2-Tb/s 24-Carrier No-Guard-Interval Coherent OFDM Superchannel over 7200-km of Ultra-Large-Area Fiber**. *in Proc. ECOC'09*, **PD2.6**, 2009. 96

[212] G. Bosco, A. Carena, V. Curri, P. Poggiolini, and F. Forghieri. **Performance Limits of Nyquist-WDM and CO-OFDM in High-Speed PM-QPSK Systems**. *IEEE Photon. Technol. Lett.*, **22**(15):1129–1131, 2010. 96

[213] G. Bosco, V. Curri, A. Carena, P. Poggiolini, and F. Forghieri. **On the Performance of Nyquist-WDM Terabit Superchannels Based on PM-BPSK, PM-QPSK, PM-8QAM or PM-16QAM Subcarriers**. *Journal of Lightwave Technology*, **29**(1):53–61, 2011. 96

[214] K. Igarashi, Y. Mori, K. Katoh, and K. Kikuchi. **Bit-error Rate Performance of Nyquist Wavelength-Division Multiplexed Quadrature Phase-Shift Keying Optical Signals**. *in Proc. OFC'11*, **OMR6**, 2011. 96

[215] Z. Dong, J. Yu, Z. Jia, H. C. Chien, X. Li, and G. K. Chang. **7224 Gb/s/ch Nyquist-WDM Transmission Over 1600-km SMF-28 Using PDM-CSRZ-QPSK Modulation**. *IEEE Photon. Technol. Lett.*, **24**(13):1157–1159, 2012. 96

[216] Z. Dong. **100 Gbit/s Nyquist-WDM PDM 16-QAM Transmission over 1200 km SMF-28 with Ultrahigh Spectrum Efficiency**. *ZTE Communications*, **10**(3):22–27, 2012. 96

[217] G. Bosco. **Spectrally Efficient Transmission: a Comparison between Nyquist-WDM and CO-OFDM Approaches**. *Signal Processing in Photonic Communications*, **SpW3B.1**, 2012. 96

[218] Z. Jia, J. Yu, H. C. Chien, Z. Dong, and D. Huo. **Field Transmission of 100G and Beyond: Multiple Baud Rates and Mixed Line Rates Using Nyquist-WDM Technology**. *ZTE Communications*, **10**(3):28–38, 2012. 97

[219] B. Bakhshi, L. Richardson, and E.A. Golovchenko. **Ultimate Capacity Limitations in Repeater-less WDM Transmission up to 505 km**. *in Proc. OFC'09*, **OThC4**, 2009. 97

[220] P. Bousselet, H. Bissessur, J. Lestrade, M. Salsi, L. Pierre, and D. Mongardien. **High Capacity (64 x 43 Gb/s) Unrepeatered Transmission over 440 km**. *in Proc. OFC'11*, **OMI2**, 2011. 97

[221] H. Bissessur, P. Bousselet, D. Mongardien, G. Boissy, and J. Lestrade. **4 x 100Gb/s Unrepeatered Transmission over 462km Using Coherent PDM-QPSK Format and Real-Time Processing**. *in Proc. ECOC'11*, **Tu.3.B.3**, 2011. 97

[222] Optolex Corporation. **http://www.optoplex.com**. *DPSK Demodulator / Delay Line Interferometer*, 2013. 99

[223] SHF Communication Technologies. **http://www.shf.de**. *Broadband Bit Error Rate Tester*, 2013. 99

[224] R. J. S. Pedersen, B. F. Jorgensen, M. Nissov, and H. Yongqi. **10Gbit/s repeaterless transmission over 250km standlard fibre**. *Electronics Letters*, **32**(23), 1996. 102

[225] Y. Cai. **Coherent Detection in Long-Haul Transmission Systems**. *in Proc. OFC'08*, **OTuM1**, 2008. 105

[226] E. Lach and W. Idler. **Modulation formats for 100G and beyond**. *Optical Fibre Technology*, **17**(5):377–386, 2011. 106

[227] M. Salsi, H. Mardoyan, P. Tran, C. Koebele, E. Dutisseuil, G. Charlet, and S. Bigo. **155100Gbit/s coherent PDM-QPSK transmission over 7,200km**. *in Proc. ECOC'09*, 2009. 106

[228] G. Charlet, J. Renaudier, H. Mardoyan, P. Tran, O. B. Pardo, F. Verluise, M. Achouche, A. Boutin, F. Blache, J. Y. Dupuy, and S. Bigo. **Transmission of 16.4Tbit/s Capacity over 2,550km using PDM QPSK Modulation Format and Coherent Receiver**. *in Proc. OFC'08*, **PDP3**, 2008. 106

[229] P. J. Winzer, A. H. Gnauck, G. Raybon, M. Schnecker, and P. J. Pupalaikis. **56-Gbaud PDM-QPSK: Coherent Detection and 2,500-km Transmission**. *in Proc. ECOC'09*, **PD 2.7**, 2009. 106

[230] A. H. Gnauck, P. J. Winzer, G. Raybon, M. Schnecker, and P. J. Pupalaikis. **10 x 224-Gb/s WDM Transmission of 56-Gbaud PDM-QPSK Signals Over 1890 km of Fiber**. *IEEE Photon. Technol. Lett.*, **22**(13):954–956, 2010. 106

[231] M. Birk, P. Gerard, R. Curto, L. E. Nelson, X. Zhou, P. Magill, T. J. Schmidt, C. Malouin, B. Zhang, E. Ibragimov, S. Khatana, M. Glavanovic, R. Lofland, R. Marcoccia, R. Saunder, Gary Nicholl, M. Nowell, and F. Forghieri. **Coherent 100 Gb/s PM-QPSK Field Trial**. *IEEE Communications Magazine*, **48**(7):52–60, 2010. 106

[232] J. D. Downie, J. Hurley, D. Pikula, and X. Zhu. **Ultra-long-haul 112 Gb/s PM-QPSK transmission systems using longer spans and Raman amplification**. *Optics Express*, **10**(9):10353–10358, 2012. 106

[233] Oclaro Inc. **http://www.oclaro.com**. *DWDM Transponder Modules and Transceivers*, 2013. 107

[234] R. Wu, V. R. Supradeepa, C. M. Long, D. E. Leaird, and A. M. Weiner. **Generation of very flat optical frequency combs from continuous-wave lasers using cascaded intensity and phase modulators driven by tailored radio frequency waveforms**. *Optics Letters*, **35**(19):3234–3236, 2010. 109

[235] S. J. Savory. **Digital filters for coherent optical receivers**. *Optics Express*, **16**(2):804–817, 2008. 111, 112

[236] A. J. Viterbi and A. M. Viterbi. **Nonlinear Estimation of PSK-Modulated Carrier Phasewith Application to Burst Digital Transmission**. *IEEE Transactions On Information Theory*, **IT-29**(4):543–551, 1983. 111